

UNIVERSITI MALAYA

**ORIGINAL LITERARY WORK DECLARATION**

Name of Candidate: **TAN SAY MIN**

(I.C/Passport No:

Registration/Matric No: **KGA 090043**

Name of Degree: **MASTER OF ENGINEERING SCIENCE**

Title of Project Paper/Research Report/Dissertation/Thesis ("this Work"):

**PREPARATION AND CHARACTERIZATION OF PEO-PMMA-LiClO<sub>4</sub>-EC-MnO<sub>2</sub> NANOCOMPOSITE POLYMER ELECTROLYTES**

Field of Study: **Nanotechnology**

I do solemnly and sincerely declare that:

- (1) I am the sole author/writer of this Work;
- (2) This Work is original;
- (3) Any use of any work in which copyright exists was done by way of fair dealing and for permitted purposes and any excerpt or extract from, or reference to or reproduction of any copyright work has been disclosed expressly and sufficiently and the title of the Work and its authorship have been acknowledged in this Work;
- (4) I do not have any actual knowledge nor do I ought reasonably to know that the making of this work constitutes an infringement of any copyright work;
- (5) I hereby assign all and every rights in the copyright to this Work to the University of Malaya ("UM"), who henceforth shall be owner of the copyright in this Work and that any reproduction or use in any form or by any means whatsoever is prohibited without the written consent of UM having been first had and obtained;
- (6) I am fully aware that if in the course of making this Work I have infringed any copyright whether intentionally or otherwise, I may be subject to legal action or any other action as may be determined by UM.

Candidate's Signature

Date

Subscribed and solemnly declared before,

Witness's Signature

Date

Name:

Designation:

## Abstract

Polymer electrolytes are of great interest for solid-state-electrochemical devices especially in fuel cells and battery. There have been many studies that carried out to improve the ionic conductivity in polymer electrolytes which include polymer blending, incorporating plasticizers and filler additives in the electrolytes system. This thesis describes the combined effect of incorporating the nano-sized  $\text{MnO}_2$  filler and the EC plasticizer on the ionic conductivity enhancement of the polymer blend PMMA-PEO- $\text{LiClO}_4$  electrolyte. Maximum conductivity has been achieved by optimizing the compositions of the plasticizer and the filler. Conduction characteristics of the polymer electrolyte system are investigated. Free standing flexible electrolyte films of composition 13.68 wt% PEO, 54.72 wt% PMMA, 7.59 wt%  $\text{LiClO}_4$ , 19 wt% EC and 5 wt%  $\text{MnO}_2$  are prepared by solution casting method. A combination of X-ray diffraction (XRD), UV-Vis spectroscopy, Fourier-transform infrared (FTIR) spectroscopy, Field Emission Scanning Electron Microscopy (FESEM), thermal gravimetric analysis (TGA) and differential scanning calorimetry (DSC) studies have indicated enhancement in the amorphous phase of polymer system due to the polymer blend, plasticizer addition and filler addition. Further, a reduction in the glass transition temperature and optical band gap has inferred increase in the flexibility of the polymer chains. Ionic conductivity studies are carried out as a function of chemical composition and temperature using impedance spectroscopy. The conductivity values are presented and results are discussed.

## Abstrak

Elektrolit polimer begitu mendapat perhatian dalam peranti keadaan pepajal elektrokimia terutamanya sel fuel dan bateri. Terdapat banyak kajian yang telah dijalankan untuk meningkatkan kekonduksian ionik dalam elektrolit polimer. Ini termasuklah pemaduan polimer, penambahan agen plastik dan pengisi dalam sistem elektrolit polimer. Tesis ini melaporkan kesan pada elektrolit polimer PMMA-PEO-LiClO<sub>4</sub> apabila pengisi MnO<sub>2</sub> yang bersaiz nano ditambahkan dalam elektrolit polimer yang telah dipadukan dua polimer yang berlainan dan ditambahkan agen plastic, EC. Kekonduksian ionik maksimum telah dicapai apabila komposisi pengisi dan agen plastik yang optimum telah ditambahkan ke dalam sistem elektrolit polimer. Sifat-sifat kekonduksian elektrolit polimer telah dikaji dan dibincang. Filem kukuh elektrolit yang mengandungi komposisi 13.68 wt% PEO, 54.72 wt% PMMA, 7.59 wt% LiClO<sub>4</sub>, 19 wt% EC dan 5 wt% MnO<sub>2</sub> disediakan dengan keadaan “solution casting”. Kombinasi kajian XRD, optik, FTIR, FESEM dan DSC telah membuktikan fasa amorfus elektrolit polimer. Tambahan lagi, penurunan suhu peralihan gelas dan jurang jalur optik telah menjelaskan peningkatan kelenturan rantai polimer yang menyebabkan peningkatan kekonduksian ionik. Kajian kekonduksian ionik telah dikaji dengan fungsi komposisi kimia dan suhu dengan menggunakan mesin EIS. Nilai kekonduksian yang diperolehi juga dibincangkan.

## **ACKNOWLEDGEMENT**

I would like to express my deepest appreciation and thanks to my respectable supervisor, Dr. Mohd Rafie Johan for his invaluable guidance, advice and encouragement throughout this whole project. He always assists and guides me patiently in solving various kinds of problems.

I would like to extend my sincere gratitude to Ms Alya and Ms Sue who had kindly granted me the permission to do various tests and studies in Advanced Materials Laboratory, University of Malaya (UM) and Science Laboratory, University Teknologi MARA (Uitm). My sincere appreciation also goes to Ms. Ng Meng Nee, my beloved senior for her invaluable help in guiding me in my research.

I would like to show my great gratitude to my lovely family and my fellow course mates. Without their understanding, continuous support, concern and encouragement, I wouldn't have completed the whole study smoothly. In short, I'm wish to thanks all that have been kind to offer their assistance to help me to accomplish my final year project.



## Table of content

ORIGINAL LITERARY WORK DECLARATION .....	ii
Abstract .....	iii
Abstrak .....	iv
ACKNOWLEDGEMENT .....	v
Table of content.....	vi
List of Tables.....	viii
List of Figures .....	ix
LIST OF PAPERS PUBLISHED AND CONFERENCE PROCEEDING .....	xiv
LIST OF ABBREVIATIONS .....	xv
CHAPTER ONE .....	1
INTRODUCTION .....	1
1.1 Background.....	1
1.2 Importance Research Problem .....	4
1.3 Significance of Research .....	6
1.4 Research Objectives.....	6
1.5 Scope of Research.....	7
CHAPTER TWO .....	9
LITERATURE REVIEW.....	9
2.1 Classification of polymer electrolyte .....	9
2.2 Ion conduction mechanism in electrolytes.....	13
2.3 PEO/PMMA blend polymer electrolytes .....	19
2.4 Solvent .....	22
2.5 Salts.....	26
2.6 Plasticizer .....	29
2.7 Filler.....	31
2.8 Dielectric properties of polymer electrolytes.....	33
2.9 Thermal stability of polymer electrolytes .....	36
2.10 Optical properties of electrolytes .....	38
CHAPTER THREE.....	40
3.1 Materials .....	40
3.2 Preparation of polymer blend electrolyte .....	41
3.3 Characterization Techniques .....	46
CHAPTER FOUR.....	77

RESULTS AND DISCUSSION .....	77
4.1 Structural Studies .....	77
4.2 Conductivity Studies .....	97
4.3 Dielectric Studies .....	108
4.4 Thermal Studies .....	113
4.4 Optical Studies .....	126
CHAPTER FIVE.....	131
CONCLUSION AND FUTURE RECOMMENDATIONS .....	131
References .....	134
Appendix .....	143

## List of Tables

Table 2.1 Some selected polymer host and their chemical formulae	15
Table 2.2 Properties of various polymer electrolyte solvents	24
Table 2.3 Examples of plasticizers commonly used in polymer electrolytes	29
Table 3.1 Materials and chemicals used in preparation of polymer electrolyte	40
Table 3.2 Samples with various composition of PMMA-PEO blend films	42
Table 3.3 Composition of PMMA-PEO-LiClO <sub>4</sub> with manipulated salt content	43
Table 3.4 Composition of PMMA/PEO/ LiClO <sub>4</sub> with various plasticizer contents	44
Table 3.5 Composition of PMMA/PEO/LiClO <sub>4</sub> /EC with various filler contents	45
Table 3.6: Equipments used in characterization of solid polymer electrolytes	46
Table 3.7 List of some simple chromophores and their light absorption characteristics	74
Table 4.1 Crystallite size of pure PEO and pure PMMA in comparison with the various composition of PMMA/PEO polymer blend system	84
Table 4.2 Crystallite sizes for various composition of filler MnO <sub>2</sub> in plasticized polymer electrolyte	85
Table 4.3 Thermal properties of PMMA/PEO blends	113
Table 4.4 Thermal properties of PMMA/PEO/LiClO <sub>4</sub> polymer electrolyte systems	114
Table 4.5 Thermal properties of PMMA/PEO/LiClO <sub>4</sub> /EC polymer electrolyte system	115
Table 4.6 Thermal properties of PMMA/PEO/LiClO <sub>4</sub> /EC/MnO <sub>2</sub> polymer electrolyte system	116
Table 4.7 Initial and decomposition temperatures and percentage of total weight loss for various solid polymer electrolyte systems	125
Table 4.8 Optical band gap for both direct and indirect of different polymer electrolyte systems	130

## List of Figures

Figure 2.1 Schematic illustration of lithium ion transport in polyether media	16
Figure 3.1 Solution-casting for thin films	41
Figure 3.2 HIOKI HiTESTER machine	47
Figure 3.3 Complex impedance spectra of polymer electrolytes	50
Figure 3.4 X-ray diffraction machine	51
Figure 3.5 Diffraction of X-ray by planes of atoms	52
Figure 3.6 Diffraction of X-ray pattern of 80 wt% PMMA and 20 wt% PEO.	53
Figure 3.7 Placement of TEM grids on the gravimetric filter holder	55
Figure 3.8 Typical TEMs workings principal	56
Figure 3.9 TEM machine	58
Figure 3.10 Schematic diagram of light microscope (LM), transmission electron microscope (TEM) and field emission scanning electron microscope (FESEM)	61
Figure 3.11 Field Emission Scanning Electron Microscope (FESEM)	62
Figure 3.12 Spectrum FTIR Spectrometer dual system	65
Figure 3.13 Differential scanning calorimetry (DSC)	67
Figure 3.14 Transgravimetric analysis machine	70
Figure 3.15 Electronic excitation of organic molecules	73
Figure 3.16 Cary 50 UV-Visible spectrophotometer	76
Figure 4.1 TEM image of MnO <sub>2</sub> nanoparticles	78
Figure 4.2 Histogram of particle size distribution of MnO <sub>2</sub> nanoparticles	78
Figure 4.3 (a) shows the XRD pattern for pure PMMA	79
Figure 4.3 (b) shows the XRD pattern for pure PEO.	80
Figure 4.4 (a) XRD pattern for 90:10 wt% of PMMA/PEO blend	80
Figure 4.4 (b) XRD pattern for 80:20 wt% of PMMA/PEO blend	81
Figure 4.4 (c) XRD pattern for 70:30 wt% of PMMA/PEO blend	81
Figure 4.4 (d) XRD pattern for 60:40 wt% of PMMA/PEO blend	82

Figure 4.4 (e) XRD pattern for 50:50 wt% of PMMA/PEO blend	82
Figure 4.4 (f) XRD pattern for 40:50 wt% of PMMA/PEO blend	83
Figure 4.5 XRD patterns for polymer electrolytes with various weight percent of MnO <sub>2</sub> nanofiller : a)54.7PMMA:13.4PEO:7.6LiClO <sub>4</sub> :19EC:5MnO <sub>2</sub> ; b)51.9PMMA:13PEO:7.2LiClO <sub>4</sub> :18EC:10MnO <sub>2</sub> ; c)48.9PMMA:12.2PEO:6.8LiClO <sub>4</sub> :17EC:15MnO <sub>2</sub> ; d)46.1PMMA:11.5PEO:6.4LiClO <sub>4</sub> :16EC:20MnO <sub>2</sub> ; e) 43.2PMMA:10.8PEO:6LiClO <sub>4</sub> :15EC:25MnO <sub>2</sub>	87
Figure 4.6 XRD pattern for (a)80PMMA:20PEO (b) 72PMMA:18PEO:10LiClO <sub>4</sub> (c) 57.6PMMA:14.4PEO:8LiClO <sub>4</sub> :20EC; (d)54.7PMMA:13.4PEO:7.6LiClO <sub>4</sub> :19EC:5MnO <sub>2</sub>	88
Figure 4.7 FTIR spectra for (a) pure PEO ; (b) pure PMMA (c) 80PMMA:20PEO polymer blend; (d)72PMMA:18PEO:10LiClO <sub>4</sub> polymer electrolyte; (e) 57.6PMMA:14.4PEO:8Li:20EC plasticized polymer electrolyte	90
Figure 4.7 (f) FTIR spectra for 54.7PMMA:13.4PEO:7.6LiClO <sub>4</sub> :19EC:5MnO <sub>2</sub> composite polymer electrolye.	90
Figure 4.8 FTIR spectra for the optimum concentration of polymer electrolytes with various weight percent of MnO <sub>2</sub> nanofiller: (a) 54.7PMMA:13.4PEO:7.6LiClO <sub>4</sub> :19EC:5MnO <sub>2</sub> (b) 51.9PMMA:13PEO:7.2LiClO <sub>4</sub> :18EC:10MnO <sub>2</sub> (c) 48.9PMMA:12.2PEO:6.8LiClO <sub>4</sub> :17EC:15MnO <sub>2</sub> (d) 46.1PMMA:11.5PEO:6.4LiClO <sub>4</sub> :16EC:20MnO <sub>2</sub> (e) 43.2PMMA:10.8PEO:6LiClO <sub>4</sub> :15EC:25MnO <sub>2</sub>	93
Figure 4.9 FESEM images for (a) 80PMMA:20PEO, (b) 72PMMA:18PEO:10 LiClO <sub>4</sub> , (c) 57.6PMMA:14.4PEO:8 LiClO <sub>4</sub> :20EC,	

(d) 54.72 PMMA:13.68PEO:7.6 LiClO <sub>4</sub> :19EC:5MnO <sub>2</sub>	96
--	----

Figure 4.10 (a) Complex impedance spectra of polymer electrolytes at various weight percent of PMMA/PEO blend: (a) 90:10 (b) 80:20 (c) 70:30 (d) 60:40 (e) 50:50 (f) 40:60	98
--	----

Figure 4.10 (b) Variation of conductivity for different weight percent of PMMA/PEO	98
--	----

Figure 4.11 (a) Complex impedance spectra of polymer electrolytes 80:20 wt% of PMMA/PEO at various LiClO <sub>4</sub> : (a) 2.5 wt%; (b) 5 wt%; (c) 7.5 wt%; (d) 10 wt% (e) 12.5 wt%	99
--	----

Figure 4.11 (b) Variation of conductivity for 80:20 wt% PMMA-PEO with different wt % of LiClO <sub>4</sub>	100
--	-----

Figure 4.12 (a) Complex impedance spectra for PMMA/PEO/LiClO <sub>4</sub> polymer electrolytes at various EC plasticizer: (a) 5 wt% (b) 10 wt% (c) 15 wt% (d) 20 wt% (e) 25 wt%	101
---	-----

Figure 4.12 (b) Variation of ionic conductivity for PMMA/PEO/LiClO <sub>4</sub> with different weight percent of EC.	102
--	-----

Figure 4.13 (a) Complex impedance spectra for 80:20:10:20 wt% of PMMA/PEO/LiClO <sub>4</sub> /EC polymer electrolytes at various MnO <sub>2</sub> filler: (a) 5 wt% (b) 10 wt% (c) 15 wt% (d) 20 wt% (e) 25 wt%	103
---	-----

Figure 4.13 (b) Variation of ionic conductivity 80:20:10:20 wt% of PMMA/PEO/LiClO <sub>4</sub> /EC polymer electrolyte with respect to filler content at room temperature	104
---	-----

Figure 4.14 (a) Temperature dependence of ionic conductivity for various weight percent of PMMA: PEO blend polymer electrolyte systems: 90:10; (b) 80:20; (c) 50:50; (d) 60:40; (e) 50:50; (f) 40:60	106
--	-----

Figure 4.14 (b) Temperature dependence of ionic conductivity for PMMA/PEO blend at various weight percent of LiClO <sub>4</sub> salt: (a) 2.5 wt% (b) 5 wt%	
---	--

(c) 7.5 wt% (d) 10 wt% (e) 12.5 wt%	106
Figure 4.14 (c) Temperature dependence of ionic conductivity for PMMA/PEO/LiClO <sub>4</sub> at various weight percent of EC plasticizer:	
(a) 5 wt% (b) 10 wt% (c) 15 wt% (d) 20 wt% (e) 25 wt%	107
Figure 4.14 (d) Temperature dependence of ionic conductivity for PMMA/PEO/LiClO <sub>4</sub> /EC at various weight percent of MnO <sub>2</sub> filler:	
(a) 5 wt% (b) 10 wt% (c) 15 wt% (d) 20 wt% (e) 25 wt%	107
Figure 4.15 Variation of real part of dielectric constant of (a) PMMA-PEO, (b) PMMA-PEO-LiClO <sub>4</sub> , (c) PMMA-PEO-LiClO <sub>4</sub> -EC and (d) PMMA-PEO-LiClO <sub>4</sub> -EC-MnO <sub>2</sub> at room temperature.	108
Figure 4.16 Variation of imaginary part of dielectric constant of (a) PMMA-PEO, (b) PMMA-PEO-LiClO <sub>4</sub> , (c) PMMA-PEO-LiClO <sub>4</sub> -EC and (d) PMMA-PEO-LiClO <sub>4</sub> -EC-MnO <sub>2</sub> at room temperature.	109
Figure 4.17 Variation of tan $\delta$ for (a) PMMA-PEO, (b) PMMA-PEO-LiClO <sub>4</sub> , (c) PMMA-PEO-LiClO <sub>4</sub> -EC and (d) PMMA-PEO-LiClO <sub>4</sub> -EC-MnO <sub>2</sub> at room temperature.	111
Figure 4.18 DSC thermograms for PMMA/PEO blend at various weight percent:	
(a) 90:10; (b) 80:20 ; (c) 70:30; (d) 60:40; (e) 50:50; (f) 40:60	118
Figure 4.19 DSC thermograms for PMMA/PEO polymer electrolyte system at various weight percent of LiClO <sub>4</sub> : (a) 2.5 wt% ; (b) 5 wt%; (c) 7.5 wt%; (d) 10 wt%; (e) 12.5 wt%	119
Figure 4.20 DSC thermograms for PMMA/PEO/LiClO <sub>4</sub> polymer electrolyte system at various weight percent of EC : (a) 5 wt% ; (b) 10 wt% ; (c) 15 wt%; (d) 20 wt%; (e) 25 wt%	120
Figure.4.21 DSC thermograms for PMMA/PEO/LiClO <sub>4</sub> /EC polymer electrolyte system at various weight percent of MnO <sub>2</sub> filler: (a) 5 wt% MnO <sub>2</sub> (b) 10 wt% MnO <sub>2</sub> (c) 15 wt% MnO <sub>2</sub> (d) 20 wt% MnO <sub>2</sub>	

(e) 25 wt% MnO <sub>2</sub>	121
Figure 4.22 TGA-DTG curves for 80:20 wt% of PMMA/PEO blend	122
Figure 4.23 TGA-DTG curves for 72PMMA:18PEO:10Li polymer electrolytes	123
Figure 4.24 TGA-DTG curves for 57.6PMMA:14.4PEO:8Li:20EC polymer electrolytes	123
Figure 4.25 TGA-DTG curves for 54.7PMMA:13.4PEO:7.6LiClO <sub>4</sub> :19EC:5MnO <sub>2</sub> polymer electrolytes	124
Figure 4.26 Optical absorption spectra for optimum polymer electrolytes: a) PEO- PMMA b) PEO-PMMA-LiClO <sub>4</sub> c) PEO-PMMA-LiClO <sub>4</sub> -EC d) PEO-PMMA-LiClO <sub>4</sub> -EC- MnO <sub>2</sub>	127
Figure 4.27 Plot of $(\alpha h\nu)^2$ against E <sub>g</sub> (photon energy) for the optimum polymer electrolytes : a) PEO- PMMA b) PEO-PMMA-LiClO <sub>4</sub> c) PEO-PMMA-LiClO <sub>4</sub> -EC d) PEO-PMMA-LiClO <sub>4</sub> -EC- MnO <sub>2</sub>	128
Figure 4.28 Plots of $(\alpha h\nu)^{1/2}$ against E <sub>g</sub> (photon energy) for the optimum polymer electrolytes: a) PEO- PMMA b) PEO-PMMA-LiClO <sub>4</sub> c) PEO-PMMA-LiClO <sub>4</sub> -EC d) PEO-PMMA-LiClO <sub>4</sub> -EC MnO <sub>2</sub>	129



**LIST OF PAPERS PUBLISHED  
AND  
CONFERENCE PROCEEDING**

- Tan Say Min, M. R. Johan, Effects of MnO<sub>2</sub> nano- particles on the conductivity of PMMA-PEO-LiClO<sub>4</sub>-EC polymer electrolytes, Ionics 17 (2011) 485-490 (ISI-Cited Publication)
  
- Tan Say Min, M. R. Johan, Effect of MnO<sub>2</sub> nano-sized filler in ionic conductivity of PEO/PMMA based polymer electrolytes, Proceeding of International Conference on NanoElectronics, Taiwan (2011)
  
- Tan Say Min, M. R. Johan, Electrical and optical properties of PMMA-PEO-LiClO<sub>4</sub>-EC-MnO<sub>2</sub>, Ionics (2011) under revision [Manuscript No: IONICS-2011-0126].

## LIST OF ABBREVIATIONS

Abbreviation	Phrase
AgNO <sub>3</sub>	Silver nitrate
DBP	Dibutyl phthalate
DMP	Dimethyl phthalate
DSC	Differential Scanning Calorimetry
EC	Ethylene carbonate
EIS	Electrochemical Impedance Spectroscopy
IS	Impedance Spectroscopy
LPB	Lithium Polymer Batteries
Li <sup>+</sup>	Lithium ion
LiTf	Lithium triflate
LiBF <sub>4</sub>	Lithium-boron-tetrafluoride
LiBr	Lithium bromide
LiCF <sub>3</sub> SO <sub>3</sub>	Lithium triflate
LiClO <sub>4</sub>	Lithium perchlorate
LiNO <sub>3</sub>	Lithium nitrate
LiPF <sub>6</sub>	lithium hexafluorophosphate
LPB	Lithium Polymer Batteries
MnO <sub>2</sub>	Manganese Dioxide
PEO	Poly (ethylene oxide)
PC	Propylene carbonate

PMMA	Poly(methyl methacrylate)
PVC	Polyvinyl chloride
SPEs	Solid polymer electrolytes
T <sub>g</sub>	Glass transition temperature
T <sub>m</sub>	Melting temperature
TEM	Transmission Electron Microscope
wt %	Weight Percentage
XRD	X-Ray Diffraction

# CHAPTER ONE

## INTRODUCTION

This chapter covers the introduction of present work, objectives and scope of this research. This report is made up of five chapters and the organization has been discussed.

### 1.1 Background

The development of polymer electrolytes has drawn the attention of many researchers in the last two decades as they find applications not only in lithium batteries, but also in other electrochemical devices such as super capacitors, electrochromic devices and sensors etc. Such systems based on conventional poly (ethylene oxide) (PEO) matrix offer room temperature conductivities generally of the order of  $10^{-5} \text{ S cm}^{-1}$  (Fenton *et al*, 1973). which preclude their utility in practical devices. Poly (methyl methacrylate) PMMA, on the other hand, demonstrated to form highly conducting gel electrolytes ( $10^{-3} \text{ S cm}^{-1}$ ) at room temperature (Croce *et al*, 1993).

However, the ionic conductivity of such polymer electrolyte at ambient temperature is rather low. Thus, in order to enhance the room temperature ionic conductivity of the polymer electrolytes, several strategies have been developed that include incorporating organic solvents (plasticizer) to form plasticized or gel polymer electrolyte (Qian *et al*, 2002), doped with inorganic fillers to make composite polymer electrolyte (Nan *et al*, 2003) and synthesizing new polymer (Ali *et al*, 2006). Plasticization is an effective way to improve the ionic conductivity of polymer electrolyte, and among

a number of plasticizers, the most used plasticizers are low molecular weight organic solvents such as propylene carbonate (PC), ethylene carbonate (EC), dimethyl carbonate (DMC), and diethyl carbonate (DEC) (Qian *et al*, 2002). Plasticizers reduce the glass transition temperature,  $T_g$ , of the polymer electrolyte which helps to increase the segmental motion of the polymer backbone and generate free volume. Therefore, the ions can migrate easily through the void resulting in ionic conductivity enhancement. Besides that, the high dielectric constant and low viscosity of plasticizers also enable them to incorporate with the polymer host to facilitate the formation of dissociated ions. This approach leads to a high ambient conductivity but promotes deterioration of the electrolyte's mechanical properties and increases its reactivity toward the lithium metal anode (Nan *et al*, 2003).

Alternatively, the addition of inorganic filler, namely, ceramic filler to the polymer electrolytes has recently become an attractive approach due to the mechanical stability and enhanced ionic conductivity and to electrolyte-electrode interface stability (Qian *et al*, 2002). It has been well established that the addition of ceramic fillers improved the conductivity of polymer host and their interfacial properties in contact with the lithium electrode (Li *et al* , 2004). The concentration and the particles size of the inert solid particles play a significant role in improving these physical properties as the smaller the particles size is, the larger the conductivity enhancement will be. In part, because of this idea, nanocomposite polymer electrolyte (NCPE) in which dispersion of small fraction of low dimension particles in the conventional solid polymer complexes is presently the focus of many studies (Li *et al* , 2004). The addition of filler particles inhibit the crystallization of polymer chains and, hence, decrease the degree of crystallinity (or increase the proportion of amorphous phase) in polymer. This, in turn,

lowers the temperature of stabilization of the amorphous phase in the polymer electrolyte and, hence, increases the practical applicable range of conductivity of the electrolyte.

## 1.2 Importance Research Problem

The key factor to make a high performance polymer electrolytes are 1) high ionic conductivity, 2) chemically and electrochemically stable, 3) mechanically strong and flexible, 4) thermally stable, 5) environmentally safety (Oh & Kim, 1978). The high molecular weight of poly(ethylene oxide) (PEO) emerged as the best candidates to be used as polymer matrix because of their salvation power, complexion ability and ion transport mechanism (alkaline salt) (Pitawala *et al.*, 2007). However, the ionic conductivity of PEO–lithium salts (LiX) electrolytes at ambient temperature ( $10^{-7}$ – $10^{-6}$  Scm<sup>-1</sup>) is not sufficiently high for most practical applications. This main drawback however, can be overcome by polymer blending, addition of low molecular weight aprotic plasticizer, and addition of nanosized fillers (Qian *et al.*, 2002).

In polymer blending, two or more polymers are blended together to create a new polymer matrix with higher amorphousity compare to single polymer host. Following by that, salts are added to provide mobile ions into the system with minimum possible toxic by products. Furthermore, the use of plasticizers tends to increase the chain mobility of the polymer yet decrease the mechanical strength of electrolytes, particularly at a high degree of plasticization. As a result, the inorganic fillers are used to improve the electrochemical and mechanical characteristics. In spite of that, there are no reports that reveal the best selection and optimum composition of filler in polymer electrolytes that give the maximum ionic conductivity and high mechanical stability.

In this work, PMMA/PEO-LiClO<sub>4</sub>-EC-MnO<sub>2</sub> nanocomposite polymer electrolytes were prepared, in which MnO<sub>2</sub> filler were first ball-milled into nanosized

after  $\text{LiClO}_4$  salt and EC plasticizer were added in the polymer blend network. The objective of this work is to determine the optimum composition and to study the combined effect of salt, plasticizer and nanosized filler on the chemical interaction, morphology, structure, thermal stability, and ionic conductivity of PMMA/PEO polymer blend electrolyte system.



### **1.3 Significance of Research**

The production of high ionic conductivity of polymer electrolytes is always the main objective. To the best of our knowledge, there are no studies with regard to the use of nano-sized manganese dioxide ( $\text{MnO}_2$ ) as filler in polymer electrolytes. Therefore, this study is a very significance and important either towards the fundamental aspect of polymer electrolyte or their applications in the industry.

### **1.4 Research Objectives**

The objectives of this research are listed below:

- To formulate the optimum miscibility of PMMA/PEO polymer blend as a host polymer in a plasticized composite polymer electrolytes.
- To investigate the effects of lithium salt ( $\text{LiClO}_4$ ), plasticizer ethylene carbonate (EC) and nanofiller manganese dioxide ( $\text{MnO}_2$ ) on the PMMA/PEO polymer blend
- To determine the optimum composition of salt, plasticizers and filler in PMMA/PEO blend with respect to the ionic conductivity

## **1.5 Scope of Research**

There have been several reviews with regard to the lithium polymer batteries technology from various perspectives since the inception of lithium ion technology (Blomgren, 1999; Fry and Wiley, 1989). Seeing that electrolytes interact closely with both cathode and anode materials during the operation, their effect on cell performance has been discussed in most reviews. However, attention has always focused on electrode materials, especially the anodes and yet electrolytes as an important component of the cell have not been comprehensively treated in any of the dedicated reviews.

This research tends to invalidate the deficit by improving the development of electrolytes of lithium-based batteries. Since lithium ion chemistry is the only apparent successful commercialized rechargeable lithium-based technology, emphasis will be placed on the electrolytes developed for this system. The integration and the characterization of polymer blend electrolytes will taken as the dominant stage, and the scope of the review will include their ionic conductivity, effect of nano-size filler and plasticizer, thermal stability, chemical stability, thermal properties and performance at elevated temperatures, compatibility in lithium battery and safety characterizations.

Unfortunately, the exact electrolyte compositions in commercialized devices are usually proprietary knowledge, but publications from the affiliated researchers normally disclose sufficient information to reveal the skeletal electrolyte components employed. However, a great effort has been done based on such open literature to postulate the fundamental of lithium polymer electrolyte battery. Although comprehensive coverage was attempted, it is essentially impossible to embrace every aspect in an exhaustive

manner. The selection of references and the organization of the content is based on the point of view of the author only.

## CHAPTER TWO

### LITERATURE REVIEW

This chapter begins with the fundamentals of lithium-ion polymer battery and follows by the introduction of polymer electrolytes as well as classification of various polymer electrolytes. Type of solvent, effect of plasticizer and filler are briefly discussed. Finally, temperature behavior of polymer electrolytes is concisely discussed.

#### 2.1 Classification of polymer electrolyte

Generally there are three main types of polymer electrolytes which are solid polymer electrolytes, gelled polymer electrolytes and composite electrolytes. Gelled polymer electrolytes and composites electrolytes are developed later to compromise the drawback of solid polymer electrolytes.

Solid polymer electrolytes (SPE) are solvent of polar macromolecules that dissolve salts like  $\text{LiClO}_4$ ,  $\text{LiBF}_4$ ,  $\text{LiPF}_6$ ,  $\text{LiAsF}_6$  and etc. Since this system does not possess any organic liquid and thus the polymer host is used as mechanical matrix to support process ability. The very first example of “dry solid” polymer electrolyte is the poly (ethylene oxide) (PEO) based systems that showed very low ambient temperature conductivities of the order of  $10^{-8} \text{ S cm}^{-1}$  (Fenton *et al*, 1973). However, the cycling performance of this dry solid polymer electrolyte with lithium metal electrodes was not satisfactory due to the decomposition of lithium dendrites and high degree of crystallization of PEO. The poor performance of the cells was attributed to poor ionic conductivity of the electrolytes.

Furthermore, ionic conductivity is not the only obstacle in developing SPEs in electrochemical devices. In 1994, Anderman (1994) questioned almost all of the previously projected advantages from the viewpoint of cell design and engineering. He argued that: (1) The flexibility that a polymer electrolyte could not offer obvious advantage to cell design, since the current cell components (i.e., electrodes coated on substrates and a separator based on polyolefin films) already possess sufficient flexibility. The limitations on the geometric shapes of lithium cells do not come from the rigidity of electrolytes but rather from the terminals/connectors as well as economical considerations; (2) The low reactivity of a polymer toward an electrode would very likely be counteracted by the micrometer thickness of such polymer materials (the necessity for thin films arises from the poor ion conductivities of such electrolyte); (3) The safety of polymer electrolyte-based cells would be further challenged by technical difficulties, since it would be almost impossible to manufacture a polymer film of micrometer thickness in large scale and pinhole free; and (4) there would be hardly any improvement in the tolerance against mechanical abuse for the polymer electrolytes, since they do not offer superior mechanical strength to that of the presently used polyolefin separators. In addition to the criticisms from Anderman (1994), a further challenge to the application of SPEs comes from their interfacial contact with the electrode materials, which presents a far more severe problem to the ion transport than the bulk ion conduction does.

In liquid electrolytes, the electrodes are well wetted and soaked, so that the electrode/electrolyte interface is well extended into the porosity structure of the electrode. Hence, the ion path is little affected by the tortuosity of the electrode materials. However, the solid nature of the polymer would make it impossible to fill

these voids with SPEs that would have been accessible to the liquid electrolytes, even if the polymer film is cast on the electrode surface from a solution. Hence, the actual area of the interface could be close to the geometric area of the electrode, that is, only a fraction of the actual surface area that contact between electrode and electrolyte. Since the porous structure is present in both electrodes in a lithium ion cell, the effect of interfacial impedances associated with SPEs would become more pronounced (Song *et al*, 1998)

However, the second category of polymer electrolyte called “gel polymer electrolyte” (SPE) or “plasticized polymer electrolyte” are much closer to the actual applications because they inherited the major properties from the bulk liquid electrolytes, including ion conduction, electrochemical stability on both carbonaceous anode and various metal oxide cathode materials, safety, and tolerance against mechanical and electric abuses (Song *et al*, 1998). In GPEs, the major solvents are small organic molecules that help in solvating the salts and also act as conducting medium. While only small percentage of polymer are added in GPEs to provide mechanical stability by increasing the viscosity of electrolytes (Sekhon *et al*, 1998). Since the small amount of polymer only serves as the skeleton providing dimensional integrity, the ether linkage of polymer is no longer the sole choice of building block for its chemical structure. Thus eliminating potential concerns over the electrochemical stability that might arise from the oxidative or reductive degradations of polymer segments in a lithium or lithium ion cell environment. Certainly, the concomitant consequence of the low polymer presence in GPEs is the poorer mechanical strength as compared with the cases of the pure SPEs, and either chemical or physical cross-linking is frequently necessary for the dimensional stability of such gel materials.

Composite electrolyte on the other hand, is a subset of polymer electrolytes with an idea of incorporating electrochemically inert fillers in to polymer matrices (Croce *et al*, 1998). Generally, high surface area particulate fillers such as  $\text{ZrO}_2$ ,  $\text{TiO}_2$ ,  $\text{Al}_2\text{O}_3$  and hydrophobic fumed silica were incorporated in to the polymer matrices and are called “composite polymer electrolytes” or “composite ceramic electrolytes”. The advantages of incorporating the fillers are two-fold. One is the enhancement in ionic conductivity at low temperatures and the other one is to improve the stability at the interface with electrodes. The increase in conductivity is generally attributed either to the formation of a new kinetic path via a thin interphase layer along the interface itself, or to a concentration enhancement due to space charges in the sub interface region (Liang 1973; MacCallum and Vincent 1987, 1989; Maier, 1989; Wagner, 1989).

## 2.2 Ion conduction mechanism in electrolytes

The ability to conduct ion is the basic function of electrolytes. This would determine how fast the energy stored in the electrodes can be delivered. In liquid electrolytes, the transport of ions is realized via two-step process: (1) the solvation and dissociation of ionic compounds (usually crystalline salts) by polar solvent molecules and (2) the migration of these solvated ions through the solvent media. During the solvation, the stability of the salt crystal lattice is energetically compensated by the coordination of solvent dipoles with the isolated ions. Therefore these ions should always migrate with a “solvation sheath” around them, which consists of a certain number of oriented solvent molecules (Ue, 1994).

Ion conduction in the solid polymer electrolyte is fundamentally different from the conventional ion-hopping conduction observed in aqueous electrolyte. The ion conduction of polymer electrolyte below glass transition temperature,  $T_g$  is usually described by a simple Arrhenius expression:

$$\sigma = \sigma_0 e^{-E_a/RT} \quad (2.1)$$

where  $\sigma_0$  is a constant,  $R$  is the gas constant,  $T$  is the absolute temperature and  $E_a$  is the activation energy for the thermally activated process.



However, at temperature above  $T_g$ , the ionic conductivity amorphous polymer electrolytes is decidedly non-Arrhenius, that is, a plot of the logarithm of the conductivity versus the reciprocal temperature is markedly curved. These conductivity data is said to show Vogel-Tamman-Fulcher (VTF) profile. According to VTF, viscosity ( $\eta$ ) of the polymer electrolyte system at high temperature start to take place of reaction rate where polymer segmental motion is faster than the classical ion hopping rates which explain the non-Arrhenius behaviour. Conceptually, the local segmental motion of the conductive polymer is often characterized by the glass transition temperature ( $T_g$ ) of the polymer, as exemplified by the VTF form of temperature-dependent conductivity.

$$\sigma = \sigma_0 T^{\frac{-1}{2}} \exp\left(-\frac{B}{T-T_0}\right) \quad (2.2)$$

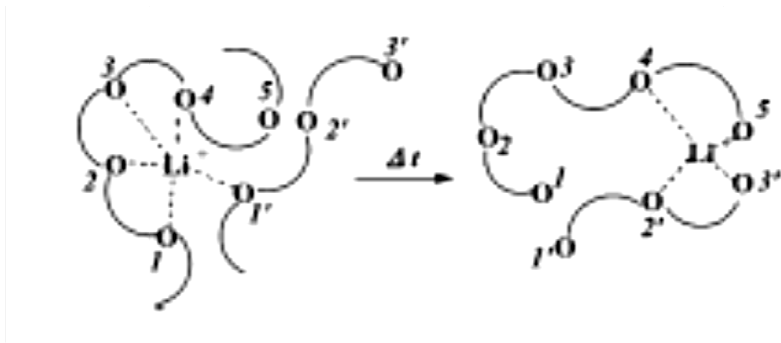
where  $T_0$  is the equilibrium glass transition temperature below which all segmental motion is frozen and  $B$  is the pseudoactivation energy. Knowledge of the structural properties of the ion-conducting amorphous phase is, however limited. Consequently, the mechanism of ion conduction at the molecular level is still not fully understood. However in general, polymers which are suitable to act as a matrix in polymer electrolytes are those with low enough  $T_g$  to remain rubbery at room temperature while preserving the lithium ion conductivities similar to those of the typical ionic liquid systems. In spite of that, as the  $T_g$  of polymer is getting lowered, the mechanical strength of these polymers approaches “liquidlike” state, thus conflicting with the fundamental reason polymer electrolytes are desired (Stephan, 2005). Table 2.1 show some selected polymer host and their chemical formulae.

Table 2.1 Some selected polymer host and their chemical formule ( Stephan, 2005)

Polymer host	Repeat unit	Glass transition temperature, $T_g$ (°C)	Melting point, $T_m$ (°C)
Poly(ethylene oxide)	$-(CH_2CH_2O)_n-$	-64	65
Poly(propylene oxide)	$-(CH(-CH_3)CH_2O)_n-$	-60	-
Poly(acrylonitrile)	$-(CH_2-CH(-CN))_n-$	125	317
Poly(methyl methacrylate)	$-(CH_2C(-CH_3)(-COOCH_3))_n-$	105	-
Poly(vinyl chloride)	$-(CH_2-CHCl)_n-$	85	-
Poly(vinylidene fluoride)	$-(CH_2-CF_2)_n-$	-40	171
Poly(vinylidene fluoride-hexafluoropropylene)	$-(CH_2-CH)$	-90	135

Apparently, the ion conduction in polymer electrolytes was close associated with certain local structural relaxations related to glass transition of the polymer. Poly(ethylene oxide) (PEO) is a commonly used example of ether-based polymer which can dissolve inorganic salts and exhibit ion conduction at room temperature. Wright and co-workers were the first group of researchers to discover that the ether-based polymer poly(ethylene oxide) (PEO) was able to dissolve inorganic salts and exhibit ion conduction at room temperature (Fenton *et al*, 1973). The ion conduction of PEO and other similar polyether-based media mainly occurred in the amorphous phases.

A generally accepted model described a microscopic sequence in which lithium ions were coordinated by the ether oxygen atoms on the segments of a polymeric chain in a similar way to their complexation by crown ethers or other oligoether-based solvents (Armand *et al*, 1980). A continuous segmental rearrangement accompanied by the gradual replacement of the ligands in the solvation sheath of lithium ions, hence, resulted in the long-range net displacement of lithium ions, as shown in Figure 1.



polyether media

Ion conduction actually consists of the oriented movement of ion/solvent complexes of both charges. Ionic conductivity  $\sigma$ , which quantifies the ion conduction ability, reflects the influence of these two aspects, that is, solvation/dissociation and the subsequent migration, in terms of the free ion number  $n_i$  and the ionic mobility  $u_i$ , where  $Z_i$  is the valence order of ionic species  $i$ , and  $e$  is the unit charge of electrons as expressed in the equation below:

$$\sigma = \sum_i n_i \mu_i Z_i e \quad (2.3)$$

The mobility of an ion is known to vary inversely with its solvation radius  $r_i$  according to the Stokes-Einstein relation (Robinson & Stokes, 1959):

$$\mu = \frac{1}{6\pi\eta r_i} \quad (2.4)$$

where  $\eta$  is the viscosity of the media. This approach seems to be useful in increasing the cation mobility when the cation species are kept constant. In spite of that, very few attempts are realized at improving ion conductivity via the salt approach due to limited choice of suitable anions for lithium electrolyte solute. Instead, solvent composition tailoring has been the main tool for manipulating electrolyte ion conductivity (Bockris and Reddy, 2000). From Equation (2.4), it is known that the most important bulk properties of the solvents which determine the charge carrier number ( $n_i$ ) and ion mobility ( $\mu_i$ ) are dielectric constant  $\epsilon$  and viscosity  $\eta$ .

In order for a solvated ion to migrate under an electric field, it must prohibit from forming close ion pairs with its counterions by the solvating solvent. The ability of the solvent molecule in shielding the interionic coulombic attraction is closely related with its dielectric constant. The critical distance for the ion pair formation  $q$  is given by Bjerrum's treatment,

$$q = \frac{|Z_i Z_j| e^2}{8\pi \epsilon_0 \epsilon kT} \quad (2.5)$$

where  $z$ ,  $\epsilon_0$ ,  $k$ , and  $T$  are the valence orders of ions, the dielectric constant of vacuum, Boltzmann's constant, and temperature, respectively (Bockris and Reddy, 2000; Robinson and Stokes, 1959). Apparently, in a solvent with a higher dielectric constant, ions would have a higher probability of staying free at a given salt concentration and ion association would be less likely to occur.

Solvents of low viscosity have always been considered the ideal candidates for electrolyte application. However, their actual use was restricted because most of these

solvents have low dielectric constants and cannot dissociate ions effectively enough to prevent ion pairing (Jasinski, 1968). Since a high dielectric constant and low viscosity usually cannot be integrated into a single solvent, usually binary or mixture of selected components with optimum viscosity and dielectric was used to formulate electrolytes for lithium batteries (Bockris and Reddy, 2000). Extensive studies have been carried out on the effects of salt concentration, solvent composition, and temperature on ionic conductivity in different electrolyte systems (Xu and Angell, 2001; Ding *et al*, 2001; Chen *et al*, 2000). The most meticulous work among these research by Ding et al. (2001) and Chen et al. (2000). They developed a series of binary systems pertinent in lithium ion cells. This trend allows the tailoring of salt concentration and solvent composition to maximize ion conductivity at a given temperature for practical interests.

### 2.3 PEO/PMMA blend polymer electrolytes

A macromolecule is simply a molecule with a large relative molecular mass,  $M_r$ . A polymer electrolyte must have high ionic conductivity. The main criteria for the selection of polymer as a host in the polymer electrolyte are polymer must contain polar groups which can act as electron donors in order to form a dative bond with the cations of the incorporating salts. Other than that, the polymer must have low glass transition temperature,  $T_g$  and high dielectric constant,  $\epsilon$ . Glass transition temperature,  $T_g$  constitutes the most important mechanical property for all polymers. Upon synthesis of a new polymer, the glass transition temperature is among the properties measured. The glass transition temperature,  $T_g$  is the temperature at which the amorphous phase of the polymer is converted between rubbery and glassy state. Above  $T_g$  polymer is in rubbery state, the polymer is soft and flexible; below  $T_g$  polymer is in glassy state, the polymer is hard and rigid.

PEO-based electrolyte is the earliest and the most extensively studied system. This system usually refers to the solvent-free PEO-salt complexes. The electrolytes commonly exhibit conductivities which range from  $10^{-8}$  to  $10^{-4}$  S cm<sup>-1</sup> at temperatures between 40 and 100 °C, which excludes practical applications at ambient temperature. This obstacle originates from, first, the high degree of crystallinity which is unfavourable for ionic conduction in these complexes and, second, the low solubility of salt in the amorphous phase. However, their high viscosities even near its melting point allow a very thin electrolyte layers. Therefore, many valuable investigations and evolution have therefore focused primarily on the PEO-based electrolytes via various approaches such as using blends (Borkowska *et al*, 1993; Wieczorek *et al*, 1995),

copolymers (Wieczorek and Stevens, 1997), combbranch polymers (Booth *et al*, 1989) and cross-linked 'networks' (LeNest *et al*, 1985). All these enhancements have been achieved either by reducing the crystallinity of polymers or by lowering the glass-transition temperature.

On the other hand, Iijima and Toyoguchi (1985) found that poly (methyl methacrylate) (PMMA) could be used as gelating agent in polymer electrolytes. The influence of concentration of polymer in the gelled electrolytes and the conductivity and viscosity of gel electrolytes comprising of PMMA-LiClO<sub>4</sub> and PC have been reported (Iijima *et al*, 1985). At ambient temperature the ionic conductivity was found to decrease with increasing amount of polymer and was in the range of  $10^{-3}$ – $10^{-5}$  S cm<sup>-1</sup> (Bohnke *et al*, 1993). In low concentrations of PMMA, the gelatinized electrolyte was considered as a liquid electrolyte encaged in a polymer matrix. However, the decrease in ionic conductivity and an increase in activation energy at high concentration were attributed to some interactions created between the polymer chain and the conducting electrolytes. In addition, they have been shown to possess higher Li<sup>+</sup> transference numbers than PEO and good compatibility with lithium (Iijima *et al*, 1985). However, though PMMA have better conductivity and compatibility with lithium electrodes, their practical application is offset due to their poor mechanical strength.

Consequently, a new attempt has been achieved to provide a powerful route to engineering new properties in materials using available polymers - polymer blending. Blending of polymers generally increase the amorphousity of the electrolyte and inhibit crystallinity thus leading to conductivity mechanical strength enhancement. From polymer blending it is possible to produce a range of materials with properties that are

superior to that of each individual component polymers (Rhoo *et al*, 1997; Oh and Kim, 1999; Pielichowski, 1999; Stephen *et al*, 2000; Tang and Liao, 2000; Pielichowski and Amerton, 2000). The main advantages of the blended systems are simplicity of preparation and ease of control of physical properties by compositional changes (Acosta and Morales, 1996; Rocco *et al.*, 2001) and also it usually requires little or no extra expenditure compared to new polymer synthesis. However, the miscibility between the constituents of polymer mixture on molecular scale is responsible for material with superior properties (Rajulu *et al*, 1999).

Miscibility between the components in the polymer blend determines the polymer electrolyte performance. Miscibility may arise from specific interactions, such as dipole-dipole forces (Aubin *et al*, 1983) and charge transfer complexes (Ohno and Kumanotani, 1979) for homopolymer mixtures or segment-segment repulsion inside the blends. The breakage and formation of new bond between the polymers in miscible polymer blend require less applied thermal energy to produce chain mobility which increases ionic conductivity of the polymer electrolyte. In general, miscible blend of two polymers have the properties somewhere between or more superior than those of the two unblended polymers.



## 2.4 Solvent

Generally, the solvent in liquid electrolytes is used to allow facile ion transports that determine the performance of device. The solvent in conventional liquid electrolyte remain in the system but however, the solvent that used in polymer electrolyte system does not remain in the system but evaporated after the formation of polymer electrolytes. Solvent in polymer electrolytes does not contribute much in faster ion transport but is used to dissociate and stabilized the ions in the system and prevent ion agglomeration. The ionic conductivity of polymer electrolytes is due to local segmental motion of polymer mainly. Conspicuously, local relaxation of the polymer chain explains the ion conduction in the system.

The solvent used to dissolve polymer, salts, plasticizer and filler must possesses high dielectric constant,  $\epsilon$  to ensure complete dissociation of ions to allow possible interactions between the components that give rise to superior properties. An ideal solvent should meet the following minimal criteria: (1) It should be able to dissolve salts to sufficient concentration. In other words, it should have a high dielectric constant ( $\epsilon$ ). (2) It should be fluid (low viscosity  $\eta$ ), so that facile ion transport can occur. (3) It should remain inert to all cell components, especially the charged surfaces of the cathode and the anode, during cell operation. (4) It should remain liquid in a wide temperature range. In other words, its melting point ( $T_m$ ) should be low and its boiling point ( $T_b$ ) is high. (5) It should also be safe (high flash point  $T_f$ ), nontoxic, and economical (Xu 2004). In addition, polymer electrolyte solvents which are only organic molecules must be able to dissolve sufficient amounts of lithium salt as well. Therefore,

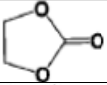
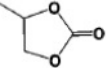

only those with polar groups such as carbonyl (C=O), nitrile (C≡N), sulfonyl (S=O), and ether-linkage (-O-) merit consideration.

In 1958 it was observed that lithium could be electrodeposited from a solution of LiClO<sub>4</sub> in PC, and PC became the immediate focus of investigation (Jasinski and Kirkland, 1963). However, it was soon discovered that PC solvent offered poor cycling efficiency and the potential hazards that make people turned to ethers for improved lithium morphology (Jasinski, 1967; Selim and Bro, 1974; Raul and Brummer, 1977). The formation of dendrite lithium in ether based solvents seemed to be sufficiently suppressed even at high charge rates (Koch *et al*, 1982). However, efforts to incorporate ether-based electrolytes in lithium cells were still troubled by the poor capacity retention and prolonged cycling (>100 cycles) of the cells still produced dendrite deposition which terminated the cells by creating shorts, despite the improved lithium morphology observed in the short term (Abraham *et al*, 1984)

Compared with PC, EC has comparable viscosity and slightly higher dielectric constant, which are favorable merits for a solvent candidate. However, because of its high melting point (36 °C), it was never favored as an ambient-temperature electrolyte solvent in the early days of lithium battery research. In early 1970s, Scrosati and Pistoia (1970) reported that the suppression of the melting point of EC could be done by addition of small percentage (9%). Further investigation found that the electrolytes based on EC as compared with PC demonstrated improvements, not only in bulk ion conductivity but also in interfacial properties such as lower polarization on various cathode surfaces (Pistoia *et al*, 1970)

On the other hand, acetonitrile is a colourless liquid with simplest organic nitrile. It is produced mainly as a byproduct of acrylonitrile manufacture. It is used as a medium-polarity solvent that is miscible with water and has a convenient liquid range in laboratory with a dipole moment of 3.84 D, Acetonitrile is widely used in the battery applications because of its relatively high dielectric constant and ability to dissolve electrolytes (*Internet reference 29/12/2009*). Its low viscosity and low chemical reactivity make it a popular choice for solvent. However, the role of the solvent molecules is not fully understood, since thermodynamic salvation dissociation considerations are involved in addition to dynamic mass-transport effects.

Table 2.2 Properties of various polymer electrolyte solvents (*Internet Reference 29/12/2009*)

Solvent	Molecular structure	M <sub>w</sub>	T <sub>m</sub> / °C	T <sub>b</sub> / °C	Viscosity, η	Dielectric constant, ε (25°C)	Dipole moment/ debye	Density/ g cm <sup>-3</sup> , 25°C
EC		88	36.4	248	1.9	89.78 (40°C)	4.61	1.321
PC		102	-48.8	242	2.53	64.92	4.81	1.200
Aceto-nitrile	$\text{H}_3\text{C}-\text{C}\equiv\text{N}$	41	-45.0	82	0.352	36.00	3.84	0.7767
THF		72.11	-108.4	66	0.48	7.58	1.75	0.8892

In spite of that, Tetrahydrofuran (THF) appears to be the preferable solvent in the laboratory when a moderately higher-boiling ethereal solvent is required and its water miscibility is not an issue. THF is a colourless, water-miscible organic liquid with low viscosity at standard temperature and pressure. This heterocyclic compound has the chemical formula (CH<sub>2</sub>)<sub>4</sub>O. As one of the most polar ethers with a wide liquid range, it is a useful solvent (*Internet reference 18/09/2011*). The oxygen center of ethers in THF

can coordinate to Lewis acids such as  $\text{Li}^+$ ,  $\text{Mg}^{2+}$ , and boranes. THF appear as a better option to dissolve polymer due to the THF is considered a relatively nontoxic solvent, with the median lethal dose comparable to that for acetone and acetonitrile. Table 2.2 shows the properties of various polymer electrolyte solvents.

## 2.5 Salts

An ideal electrolyte solute for rechargeable polymer lithium batteries should meet the following minimal requirements: (1) It should have large anions and low dissociation energy so that it easily dissociates. (2) The anion should be stable against oxidative decomposition at the cathode. (3) The anion should be inert to electrolyte solvents. (4) Both the anion and the cation should remain inert toward the other cell components such as separator, electrode substrate and cell packaging materials. (5) The anion should be nontoxic and remain stable against thermally induced reactions with electrolyte solvents and other cell components. Apparently, the available choice of lithium salts that are suitable for electrolyte application is rather limited when compared to the wide spectrum of aprotic organic compounds that could make possible electrolyte solvents (Kang, 2004).

In spite of that,  $\text{LiClO}_4$  has been a popular electrolyte solute owing to its satisfactory solubility and high conductivity ( $9.0 \text{ mS cm}^{-1}$  in EC/DMC at  $20^\circ\text{C}$ ) as well as its high anodic stability (Tarascon *et al*, 1994). Recent studies found that solid electrolytes interface (SEI) films formed in  $\text{LiClO}_4$  electrolytes, on both lithium and carbonaceous anode surfaces, are of lower impedance than those formed in  $\text{LiPF}_6$  or lithium tetrafluoroborate ( $\text{LiBF}_4$ ) electrolytes due to the absence of hydrogen fluoride (HF) (Aurbach *et al*, 1995). It is believed that HF will react with either alkyl carbonate or  $\text{Li}_2\text{CO}_3$  and forms the highly resistive lithium fluoride (LiF) (Aurbach *et al*, 1995). Compared with other lithium salts,  $\text{LiClO}_4$  also has the merits of being relatively less hygroscopic and is stable to ambient moisture. However, the high oxidation state of chlorine (VII) in perchlorate makes it a strong oxidant, which readily reacts with most

organic species in violent ways under certain conditions such as high temperature and high current charge (Jasinski and Carroll, 1970). Actually, back in the 1970s it had already been realized that  $\text{LiClO}_4$  was impractical as an electrolyte solute for industry purposes (Jasinski and Carroll, 1970). Nevertheless, it is still frequently used as a salt of convenience in various laboratory tests because it is easy to handle and economical.

In general,  $\text{LiAsF}_6$  was a superior salt to  $\text{LiClO}_4$  as an electrolyte solute for lithium batteries (Rauh *et al*, 1978). However, the electrochemical reduction of As(V) would raise concern about the safety of using  $\text{LiAsF}_6$  in a commercial battery where arsenate in its oxidation state of As(III) and As(0) are particularly toxic. In spite of that, the combination of cathodic and anodic stability would have made  $\text{LiAsF}_6$  a very promising candidate salt for both lithium and lithium ion batteries yet the toxicity not been a source of concern (Jasinski and Carroll, 1970). Like  $\text{LiAsF}_6$ ,  $\text{LiBF}_4$  is a salt based on an inorganic superacid anion and has moderate ion conductivity in nonaqueous solvents. It was out of favouring in the early days of lithium battery research because the ether-based electrolytes containing it were found to result in poor lithium cycling efficiencies, which decayed rapidly with cycle number (Koch *et al*, 1978). However, later it was found that the multiple advantages of  $\text{LiBF}_4$  as compared with other salts which include less toxicity than  $\text{LiAsF}_6$  and higher safety than  $\text{LiClO}_4$ , but its moderate ion conductivity has been a major obstacle to its application (Ue, 1994).

Among the numerous salts vying for lithium/lithium ion batteries,  $\text{LiPF}_6$  was the obvious winner and was eventually commercialized. The success of  $\text{LiPF}_6$  was not achieved by any single outstanding property but, rather by the combination of a series of well- balanced properties with concomitant compromises and restrictions. For example,

in the commonly used carbonate solvent mixtures it has a lower conductivity than  $\text{LiAsF}_6$  (Walker *et al* 1996), a lower ionic mobility than  $\text{LiBF}_4$  (Ue, 1994), a lower thermal stability than most of the other salts (Methlie *et al*, 1969), a lower anodic stability than  $\text{LiAsF}_6$  and  $\text{LiSbF}_6$  (Takeda *et al*, 1997) and a lower chemical stability toward ambient moisture than  $\text{LiClO}_4$ ,  $\text{LiIm}$ , and  $\text{LiTf}$ . However, none of these other salts could meet all these multifaceted requirements simultaneously as well as  $\text{LiPF}_6$  does.  $\text{LiPF}_6$  was proposed as an electrolyte solute for lithium-based batteries in the late 1960s.

With a cell thickness measuring as little as one millimeter (0.039 inches), dry polymer electrolytes enable equipment designers to create designs with their own imagination in terms of form, shape and size. Since then, it is possible to have part of a protective housing in the shape of a mattress that can be rolled up, or are even embedded into a carrying case or piece of clothing. Unfortunately, the dry Li-polymer suffers from poor conductivity. Internal resistance is too high which cause them unsuitable in the commercial application.

## 2.6 Plasticizer

Plasticizers are additives that increase the plasticity or fluidity of a material. There are many types of plasticizers for various applications such as plasticizer for plastics, concrete, gypsum wallboard production and plasticizer for energetic materials. In polymer electrolytes, plasticizer for plastics is used to further increase the ionic conductivity of polymer electrolyte system. Plasticizers work by embedding themselves between the chains of polymers, spacing them apart (increasing the free volume and thus significantly lowering the glass transition temperature).

Table 2.3 Examples of plasticizers commonly used in polymer electrolytes (Nogueira *et al*, 2004).

Plasticizer	Dielectric constant	Viscosity / mPa.s (at 25°C)
Ethylene carbonate (EC)	89.6	1.86
Propylene carbonate (PC)	64.4	2.53
Dimethyl sulfoxide	46.8	2.0
Diethyl carbonate (DEC)	2.82	0.748
Dimethyl carbonate (DMC)	3.12	0.585
Dimethylacetamide (DMA)	37.8	1.937

Plasticizer that used in polymer electrolytes must possesses high dielectric constant and good miscibility with polymer-salt to help in dissociating the salts, thereby increasing the number of mobile ions which leads to conductivity enhancement. Other



than that, it must have low viscosity and volatility to help to increase the mobility of the conducting ions. Plasticizer with high boiling temperature and low freezing temperature is important as it can be used to reduce the crystallinity of the host polymer and decrease the viscosity of the polymer electrolytes. Some plasticizers are able to assist in dissolution and dissociation of salts that further lower down the glass transition temperature,  $T_g$  and provide new pathways for the ion migrations which increase the ionic mobility. (Cao *et al*, 1995; Biancardo *et al*. 2006). Table 2.3 shows the examples of plasticizers commonly used in polymer electrolytes (Nogueira *et al*, 2004).

From Table 2.2, it is obvious that ethylene carbonate (EC) is most suitable to be used as plasticizer as EC has the highest dielectric constant and lowest viscosity among other plasticizers. In addition, the essence of plasticizer addition is to enhance the conductivity of solid polymer electrolytes using low molecular weight and high dielectric constant additives such as propylene carbonate (PC), ethylene carbonate (EC), polyethylene glycol (PEG) etc. (Kumar and Sekhon , 2002; Tsutsumi *et al*, 1998). These additives increase the amorphous content of the polymer matrix and tend to dissociate ion-pairs into free cations and anions thereby leading to an overall enhancement in conductivity. Therefore, by incorporating substantial amount of plasticizer, improved ionic conductivity of polymer electrolytes have been attained. By increasing the polymer segmental mobility, plasticizers can result in greater ion dissociation which allows greater numbers of charge carriers for ionic transport.

## 2.7 Filler

Fillers are particles that added in polymer electrolytes to form composite polymer electrolytes. Fillers are able to improve the ionic conductivity without degrading mechanical and interfacial properties of polymer electrolyte. Examples of fillers that used in polymer electrolytes are oxide ceramics including  $\text{Al}_2\text{O}_3$ ,  $\text{TiO}_2$ , and  $\text{ZrO}_2$ , treated  $\text{SiO}_2$ , molecular sieves or zeolite, rare-earth ceramics, carbon, and ferroelectric materials (Maier *et al*, 1989). Inorganic or ceramic fillers are most commonly used type of filler in polymer electrolyte system. However, the particle size and the characteristics of the fillers play vital roles in the electrochemical properties of the electrolytes (Srun Jung *et al*, 2009).

In a polymer electrolyte, relaxation and segmental motion of the polymer chains are regarded as the key factors in enabling ion transport, suggesting that a sufficient conductivity obtained only when the polymer is over its amorphous state. The addition of fillers to a polymer was found to improve the ionic conductivity by reducing the crystallization tendency. Upon filler addition into polymer electrolyte, filler particles compete with  $\text{Li}^+$  to coordinate with polymer chain segment. Such coordination prevents polymer host from crystallizing and releases more free  $\text{Li}^+$  ions. These two modes of coordination produce more dissociated lithium ions as charge carriers and more amorphous region for the carriers to transfer and finally enhance the conductivity of the polymer electrolytes (Maier *et al*, 1989).

Most of the studies have focused on the synthesis of nanosized fillers because the mechanical strength and the electrochemical performance of the electrolytes increase with the decreasing size of fillers. Having nanosized of filler with greater surface charges increase the ionic charge carrier concentration at the interface and create the presence of a high conductivity path at the interface. This help in developing connectivity or ‘percolation’ at a certain composition threshold of the dispersoid. Introducing ceramic powders with nanometer-sized grains to a polymer electrolyte may improve mechanical strength as well. At the electrode/electrolyte interface, certain ceramic fillers are found to suppress the growth of resistive layers (Scrosati and Vincent, 2000). The addition of these solid fillers to the polymer electrolyte significantly increases the properties of the electrolytes in terms of ionic conductivity, mechanical stability, thermal and chemical stability, and stability of the interface between the electrolytes and lithium electrodes.

## 2.8 Dielectric properties of polymer electrolytes

Dielectrics are insulating materials which have very tightly bound electrons to the nuclei in their atoms. Accordingly they have very few free electrons to flow the current and their electrical conductivity is very low. Most of the polymers (or plastics) are typical dielectrics. Irradiation of polymers with gamma rays, neutrons, protons or other heavy ions produces structural changes in the polymer matrix. Such changes have been studied in recent past by many workers (Singh *et al.*, 2005, Surinder Singh 2006, Martinez-Pardo *et al.*, 1998)

The most important property of a dielectric is to get polarized under the action of applied electric field. As the relationship between electric displacement vector  $\vec{D}$ , electric field vector  $\vec{E}$ , polarization vector  $\vec{P}$  and the dielectric constant (or relative permittivity)  $\epsilon_r$  is given by

$$\vec{D} = \epsilon_0 \vec{E} + \vec{P} = \epsilon_r \epsilon_0 \vec{E} = \epsilon \vec{E} \quad (2.6)$$

where  $\epsilon_0$  is the permittivity of free space, a measurement of dielectric constant,  $\epsilon_r$  gives significant insight to the modification of the bulk properties responsible for the dielectric response. Such studies will give better understanding of track formation mechanism on the basis of microstructures so formed due to passage of heavy ions through polymers (or plastics).

The study of changes in dielectric response of solids also provides information about orientation and translational adjustment of mobile charges present in the dielectric

medium in response to an applied electric field. The energy transferred to an alternating field is a function not only of the field but also depends on physical characteristic of the material. The dependence of contributions of different components of dielectric polarization (viz. the electric polarization, ionic polarization and orientational polarization) on frequency of applied ac field is responsible for the changes in the value of dielectric constant.

The dielectric constant (or relative permittivity) of a dielectric solid, placed in an alternating electric field of angular frequency  $\omega$ , is a complex quantity because the orientational polarization lags behind the polarizing electric field as the frequency of the applied field is increased. The complex dielectric constant can be written in the form

$$\epsilon_{r(\omega)} = \epsilon'_{r(\omega)} - i\epsilon''_{r(\omega)} \quad (2.7)$$

where  $\epsilon'_{r(\omega)}$  is the real dielectric constant and characterizes the most important electrical property of the dielectric material. The imaginary part  $\epsilon''_{r(\omega)}$  characterizes the dissipation of energy of electric oscillation in a dielectric subjected to the action of an alternating electric field. In this way there is a phase lag between the electric displacement vector  $\vec{D}$ , and the electric field vector  $\vec{E}$  because at high frequencies the dipoles do not faithfully follow the rapidity of the applied alternating field.

This phase lag is described by the so-called dielectric loss tangent or dissipation factor given by

$$\tan \delta = \frac{\epsilon''_{r(\omega)}}{\epsilon'_{r(\omega)}} \quad (2.8)$$

The magnitude of real dielectric constant  $\epsilon'_{r(\omega)}$  of the polymer is determined by the chemical constitution, structure and composition. The parameters that

characterize the dielectric loss depend upon the specific features of molecular motion in polymers; hence, on changes in their chemical constitution and structure. Real polymeric dielectrics are commonly described by a spectrum of relaxation times. In their case relaxation spectra appear due to presence of long polymeric chains and specific inter-molecular interactions. However, the expression for  $\epsilon_r(\omega)$  assume the simplest form in the case of relaxation process characterized by a single relaxation time (Perpechko, 1997). If we introduce a relaxation time  $\tau$ , for the process to go from one equilibrium state to another equilibrium state, i.e., from absorption to dissipation,

$$\epsilon'_r(\omega) = A + \frac{B}{1+\omega^2\tau^2} \quad (2.9)$$

$$\epsilon''_r(\omega) = \frac{B}{1+\omega^2\tau^2} \quad (2.10)$$

where A and B are constants and  $\omega$  is the angular frequency.

On the other hand, dielectric constant was calculated from the measured capacitance using the relation (Perpechko, 1997)

$$\epsilon_r = \frac{C_p}{C_o}, \quad C_o = \frac{\epsilon_0 A}{d} \quad (2.11)$$

Here,  $\epsilon_0$  is the permittivity of vacuum or free space, A is the cross-sectional area and d is the thickness of the sample film.  $C_p$  is the capacity of the condenser filled with the dielectric (plastic).

## 2.9 Thermal stability of polymer electrolytes

Polymer electrolytes that exhibit fast ion transport at elevated temperatures are essential especially in electrochemical devices that operating in the 100-200°C range. For instance, the used of polymer electrolytes in fuel cell at elevated temperature has several advantages. It increases the kinetic rates for the fuel cell reactions, it reduces problems of catalyst poisoning by absorbed carbon monoxide in the 150±200°C range, it reduces the use of expensive catalysts, and it minimizes problems due to electrode flooding. Thus, the thermal stability of polymer electrolyte is a very important.

Generally, it is very difficult to increase the thermal stability of polymer electrolytes owing to the chemical instability of electrolytes in the organic solvents at elevated temperature and the difficulty of replacing it with new lithium salts. Xu et al. (2002) and Jow et al. (2003) showed that LiPF<sub>6</sub>-based cells suffer obvious permanent capacity loss when operate at temperatures up to 70 °C. They believed that reactive decomposition products such as HF and PF<sub>5</sub> confer upon the electrolyte stable performance at elevated temperatures. On the other hand, Zhang et al. (2002) reported that electrolytes based on LiBF<sub>4</sub> could allow the lithium ion cells to cycle at temperatures up to 70 °C. Irreversible reactions occurred at temperatures above 80 °C, and the cells lost capacity rapidly, which was accompanied by the rise of cell impedance simultaneously.

Principally, thermal stabilities of polymer electrolyte were studied by heating samples in a TGA and DSC and analyze the resulting residues by elemental analysis.

The glass transition temperature, melting point and the thermal stability of the polymer electrolyte membrane are all important parameters resulting from the microstructure and morphology of the system. These parameters will affect the overall properties of the electrolyte. The glass transition temperature ( $T_g$ ) is one of the most important parameters of the amorphous phase for the flexibility of the polymer at room temperature. The volume of amorphous phase in polymer electrolyte system can be calculated using relative percentage of crystallinity. By assuming that PMMA-PEO-LiClO<sub>4</sub>-EC as comparison, the relative percentage of crystallinity ( $X_c$ ) was calculated based on the following equation with the DSC data. The degree of crystallinity ( $\chi_c$ ) of the MnO<sub>2</sub> fraction in the matrix is calculated from the equation.:

$$\chi_c (\text{filler}) = \frac{\Delta H_{m, \text{MnO}_2}}{\Delta H_{m, \text{PMMA-PEO-LiClO}_4\text{-EC}}} \quad (2.12)$$

Where  $\Delta H_{m, \text{PMMA-PEO-LiClO}_4\text{-EC}} = 198.45 \text{ J g}^{-1}$  is the melting enthalpies per gram of solid polymer electrolyte system without filler (Cosaerr *et al*, 2002) and  $\Delta H_{m, \text{MnO}_2}$  is the melting enthalpies per gram of solid polymer electrolyte system with filler. The apparent enthalpies of melting ( $\Delta H_m$ ) are derived from the area under the endothermic peaks respectively.



## 2.10 Optical properties of electrolytes

It is known that optical absorption studies have been particularly useful to understand the band structure and energy gap of crystalline and amorphous materials. The band structure, direct and indirect transition, as well as the absorption edge of amorphous and crystalline materials can be determined from optical absorption results, which illustrate the energy band structure. Insulators/semiconductors are generally classified into two types; (a) direct band gap and (b) indirect band gap. The top of the valence band and the bottom of the conduction band both correspond to zero crystal momentum in direct band gap semiconductors. It is a different case for indirect band gap semiconductors, whereby the bottom of the conduction band does not correspond to zero crystal momentum. In indirect band gap materials, the transition from valence to conduction band is associated with a phonon of the right magnitude of crystal momentum.

Davis and Shalliday (Davis and Shalliday, 1960) reported that near the fundamental band edge, both direct and indirect transitions occur and can be observed by plotting  $\alpha^{1/2}$  and  $\alpha^2$  as a function of energy ( $h\nu$ ) as in Equation (2.15) and (2.16) (Davis and Shalliday, 1960 ; Thutpalli and Tomlin, 1976) :

$$(h\nu n \alpha)^2 = C_1 (h\nu - E_{gd}) \quad (2.15)$$

$$(h\nu n \alpha)^{1/2} = C_2 (h\nu - E_{gi}) \quad (2.16)$$

where  $h\nu$  is the photon energy,  $E_{gd}$ , the direct band gap,  $E_{gi}$ , the indirect band gap,  $n$ , the refractive index,  $\alpha$ , the absorption coefficient and  $C_1$ ,  $C_2$  are constants. These

expressions can be applied to both direct and indirect transitions and are helpful in the determination of the band structure of materials. When a direct band gap exists, the absorption coefficient has the following dependence on the energy of the incident photon as in Equation (2.17) (Davis and Shalliday, 1960 ; Thutpalli and Tomlin, 1976)

$$\alpha h\nu = C(h\nu - E_g)^{1/2} \quad (2.17)$$

where  $E_g$  is the band gap,  $C$ , is a constant dependent on the specimen structure,  $\alpha$  is the absorption coefficient,  $\nu$  is the frequency of the incident light, and  $h$ , the Planck's constant. To determine the nature and width of the band gap,  $\alpha$ ,  $(\alpha h\nu)^2$ ,  $(\alpha h\nu)^{1/2}$  were plotted as a function of photon energy ( $h\nu$ ) and the absorption edge values were obtained by extrapolating the linear portions of the curves to zero absorption value. For indirect transitions, which require photon assistance, the absorption coefficient has the following dependence on the photon energy (Davis and Shalliday, 1960 ; Thutpalli and Tomlin, 1976).

$$\alpha h\nu = A[h\nu - E_g + E_p]^2 + B[h\nu - E_g - E_p]^2 \quad (2.18)$$

where  $E_p$  is the energy of the photon associated with the transition and  $A$  and  $B$  are constants depending on the band structure.

## CHAPTER THREE

This chapter outlines the experimental procedures for the sample preparation and the list of materials and equipments that have been used for characterizations.

### 3.1 Materials

The materials used are listed in Table 3.1 below.

Table 3.1 Materials and chemicals used in preparation of polymer electrolyte

Chemical	Molecular Formula	Source
Poly (ethylene oxide) (M.W. = 600,000)	$C_2H_4O$	ACROS
Poly(methyl methacrylate) (PMMA) (M.W.=35,000)	$(C_5O_2H_8)_n$	ACROS
Tetrahydrofuran (THF)	$C_4H_8O$	Fisher Scientific
Lithium perchlorate (M.W.= 106.39)	$LiClO_4$	ACROS
Ethylene carbonate (EC) (M.W.= 88.06)	$C_3H_4O_3$	ACROS
Manganese (VI) Dioxide (M.W.= 86.94)	$MnO_2$	ACROS

## 3.2 Preparation of polymer blend electrolyte

### 3.2.1 Preparation of PMMA-PEO blend polymer electrolytes

PMMA and PEO were put in a vacuum oven respectively at 60 and 100°C for 24 hours. Desired amount of PMMA was dissolved in tetrahydrofuran and stirred for about 12 hours. Respective amount of PEO was dissolved in tetrahydrofuran and stirred for about 12 hours at 60°C. The two solutions were then mixture together and stirred for another 12 hours to get a homogeneous viscous mixture as shown in Figure 3.1. The solution obtained was cast as thin film on petri dishes and solvents were allowed to evaporate at room temperature. The samples were stored in desiccators until further use. Table 3.2 summarized the weight percent and mass of the prepared samples.



Figure 3.1 Solution-casting for thin films

Table 3.2 Samples with various composition of PMMA-PEO blend films

Sample	PMMA		PEO	
	Wt(%)	Mass (g)	Wt (%)	Mass (g)
90PMMA_10PEO	90	0.90	10	0.10
80PMMA_20PEO	80	0.80	20	0.20
70PMMA_30PEO	70	0.70	30	0.30
60PMMA_40PEO	60	0.60	40	0.40
50PMMA_50PEO	50	0.50	50	0.50
40PMMA_60PEO	40	0.40	60	0.60

### 3.2.2 Preparation of PMMA-PEO-LiClO<sub>4</sub> polymer electrolytes

Prior to the preparation of polymer electrolytes, LiClO<sub>4</sub> was dried at 100 °C for 24 hours in order to remove any trace of water present in the samples. Having optimized and confirmed the homogeneous blending of PMMA-PEO composition (80PMMA:20PEO) showed the highest conductivity, manipulated amount of salt were added into the solution and similar procedure as stated previously was carried out to produce thin film on Petri dishes. The total amount of salt was based on 100% by weight of the total polymer blend (PMMA-PEO). The samples were stored in the desiccators until further use. Table 3.3 summarized the weight percent and mass of the prepared sample.

Table 3.3 Composition of PMMA-PEO-LiClO<sub>4</sub> with manipulated salt content

Sample	PMMA	PEO	LiClO <sub>4</sub>	
	Mass (g)	Mass (g)	Wt (%)	Mass (g)
80PMMA:20PEO	0.80	0.20	0	0.0000
78PMMA:19.5PEO:2.5Li	0.80	0.20	2.5	0.0256
76PMMA:19PEO:5Li	0.80	0.20	5.0	0.0526
74PMMA:18.5PEO:7.5Li	0.80	0.20	7.5	0.0811
72PMMA:18PEO:10Li	0.80	0.20	10.0	0.1111
70PMMA:17.5PEO:12.5Li	0.80	0.20	12.5	0.1429

### 3.2.3 Preparation of PMMA-PEO-LiClO<sub>4</sub>-EC polymer electrolytes

In order to investigate the effect of plasticizers on the PMMA-PEO- salt electrolyte system, the highest conducting PMMA-PEO-salt sample (72PMMA:18PEO:10Li) was added with plasticizer which is ethylene carbonate (EC). The similar procedure as stated previously was carried out and various wt% of EC (plasticizer) were added to the homogeneous solution. The total amount of plasticizer was based on 100% by weight of the total polymer/ salt. In all of these samples, the amount of PMMA, PEO and salt were kept constant. The polymer solution was then cast as film on petri dishes and solvents were allowed to evaporate at room temperature. The samples were stored in desiccator until further use. Table 3.4 summarized the weight percent and mass of the prepared samples.

Table 3.4 Composition of PMMA/PEO/ LiClO<sub>4</sub> with various plasticizer contents

Sample	PMMA	PEO	LiClO <sub>4</sub>	EC	
	Mass (g)	Mass (g)	Mass (g)	Wt (%)	Mass (g)
72PMMA:18PEO:10Li	0.60	0.40	0.1111	0	0.0000
68.4PMMA:17.1PEO:9.5Li:5EC	0.60	0.40	0.1111	5	0.0585
64.8PMMA:16.2PEO:9Li:10EC	0.60	0.40	0.1111	10	0.1235
61.2PMMA:15.3PEO:8.5Li:15EC	0.60	0.40	0.1111	15	0.1961
57.6PMMA:14.4PEO:8Li:20EC	0.60	0.40	0.1111	20	0.2777
54PMMA:13.5PEO:7.5Li:25EC	0.60	0.40	0.1111	25	0.3704

### 3.2.4 Preparation of PMMA-PEO-LiClO<sub>4</sub>-EC- MnO<sub>2</sub> polymer electrolytes

To investigate the effect of fillers to the PMMA-PEO-salt-plasticizer samples, manganese dioxide (MnO<sub>2</sub>) ~ 10 nm were added to the highest conducting PMMA-PEO-salt-plasticizer sample (57.6PMMA:14.4PEO:8Li:20EC). The amounts of PMMA-PEO-salt-plasticizer were kept constant and the amount of filler was manipulated. MnO<sub>2</sub> was milled in a planetary ball mill for 36 hours in order to get the nanosize filler. The polymer solution was then cast as film on the Petri dishes and solvent were allowed to evaporate at room temperature. Due to the hygroscopic nature of the films, the samples were kept in desiccator for continuous drying before further characterizations were carried out. Table 3.5 summarizes the weight percent and mass of the prepared samples.

Table 3.5 Composition of PMMA/PEO/LiClO<sub>4</sub>/EC with various filler contents.

Sample	MnO <sub>2</sub>	
	Wt (%)	Mass (g)
57.6PMMA:14.4PEO:8LiClO <sub>4</sub> :20EC	0	0.0000
54.7PMMA:13.4PEO:7.6LiClO <sub>4</sub> :19EC:5MnO <sub>2</sub>	5	0.0731
51.9PMMA:13PEO:7.2LiClO <sub>4</sub> :18EC:10MnO <sub>2</sub>	10	0.1543
48.9PMMA:12.2PEO:6.8LiClO <sub>4</sub> :17EC:15MnO <sub>2</sub>	15	0.2451
46.1PMMA:11.5PEO:6.4LiClO <sub>4</sub> :16EC:20MnO <sub>2</sub>	20	0.3472
43.2PMMA:10.8PEO:6LiClO <sub>4</sub> :15EC:25MnO <sub>2</sub>	25	0.4629



### 3.3 Characterization Techniques

PMMA-PEO polymer blend based nano-composite polymer electrolytes were studied in detailed using several analytical techniques which include electrical and structural, mechanical as well as thermal properties. The studies were only performed on the films with the highest room temperature of conductivity systems. Some experiments (FTIR and XRD) were carried out to run on pure sample as a control set. The equipments used in these studies are shown in Table 3.6 below:

Table 3.6: Equipments used in characterization of solid polymer electrolytes.

Equipment	Model	Function
Impedance Spectroscopy (IS)	HIOKI 3531 Z Hi Tester	To investigate the electrical properties of polymer/salt at various composition of plasticizer and filler.
Fourier Transform Infrared Spectroscopy (FTIR)	FTIR ABB BOMEN MB104 IR	To study the characteristic band of polymer electrolytes
Transmission Electron Microscope (TEM)	LIBRA® 120	To study the size distribution of the filler nano-particles
X-Ray Diffraction (XRD)	Phillips X-pert MRD	To examine the crystallinity of SPEs.
Differential Scanning Calorimeter (DSC)		To measure glass transition and crystallization temperature of the composite electrolyte film
Field Emission Scanning Electron Microscope (FESEM)		To study the surface structure of electrolyte film

### 3.3.1 *Electrical Studies*

#### 3.3.1.1 Impedance Spectroscopy (IS)

Impedance spectroscopy is a powerful tool for the characterization of many electrical properties of material and their interface with electron conducting electrodes. Figure 3.2 show the picture of HIOKI HiTESTER machine. The impedance technique is extremely resourceful for determining the contribution of electrode or electrolyte processes because the detail contained in an impedance spectrum is quite significant. A single impedance spectrum can provide information about diffusion, charge transfer and adsorption / dissociation processes at the electrode / electrolyte interface as well as about the grain conductivity (intragrain) and grain boundary (intergrain) blocking in polycrystalline electrolytes (Cahn, 1994).



Figure 3.2 HIOKI HiTESTER machine

Impedance spectroscopy (IS) has been widely used to characterize the nature of lithium-ion electrode processes and interfacial properties, as well as for distinguishing individual contributions to overall cell impedance and resistivity. Impedance data is used to quantify changes that can be linked to electrode film formation and changes in the interfacial properties of the electrode. Also, by comparing impedance spectra at different states of discharge of an electrochemical cell, one can draw rough conclusions about phenomena such as film growth, diffusion resistance, etc. Comparing impedance data as a function of cell cycle life affords a measure of overall cell, as well as individual cell component, stability with time.

According to the theoretical analysis given by Watanabe and Ogata (Watanabe and Ogata, 1987), two semicircles should appear in the impedance spectrum for a symmetric cell, i.e., one at high frequencies corresponding to the bulk electrolyte impedance and the other at low frequencies related to the interfacial impedance. It has also been reported (Song *et al*, 1998; Abraham *et al*, 1995; Appetecchi *et al*, 1999) that the high-frequency semicircle does not appear in practical impedance plots for plasticized polymer and filler-added polymer electrolyte membranes. This feature indicates that the conductivity is mainly due to ions. (Watanabe and Ogata, 1987). The high-frequency intercept corresponds to the bulk resistance ( $R_b$ ) of the electrolyte and provides a measure of its bulk ionic conductivity (Monroe *et al*, 2004).

In the present work, the sample is in the form of thin film. The thickness of the sample films was controlled between the ranges of 1.9 to 2.1 mm. To measure the impedance of the films, the samples were palletized into a round shape that fit the size of the electrodes. The samples were then sandwiched between the two stainless steel

blocking electrodes with the contact area of 2.33 to 2.36 cm<sup>2</sup>. A HIOKI 3531 LCR bridge that has been interfaced with a computer was used to perform the impedance measurement for each polymer electrolyte film in the frequency of 50 Hz to 1 MHz and in the temperature range of room temperature (25°C) to elevated temperatures (60°C). The software for controlling the measurement can also calculate the real and imaginary impedance.

The conductivity-temperature studies were performed only on the films with the highest room temperature of conductivity from the (PMMA / PEO), (PMMA / PEO / LiClO<sub>4</sub>), (PMMA / PEO / LiClO<sub>4</sub> / EC), (PMMA / PEO / LiClO<sub>4</sub> / EC / MnO<sub>2</sub>) systems. The conductivity-temperature studies were carried out by placing the sample holder containing the sample in temperature controlled furnace in 25 to 100 °C temperature range in steps of 10°C.

Hence the conductivity ( $\sigma$ ) of the sample were then calculated using

$$\sigma = \frac{t}{R_b A} \quad (3.5)$$

where,  $t$  is the sample thickness (cm),  $A$  is the effective contact area of the electrode and the electrolyte (cm<sup>2</sup>) and  $R_b$  is the bulk resistance ( $\Omega$ ). The bulk resistance ( $R_b$ ) value was obtained from the plot of negative imaginary impedance versus real impedance. Figure 3.3 shows the complex impedance spectra of polymer electrolytes. On the other hand, the resistivity,  $\rho$  is the reciprocal value of conductivity:

$$\rho = \frac{1}{\sigma} \quad (3.6)$$

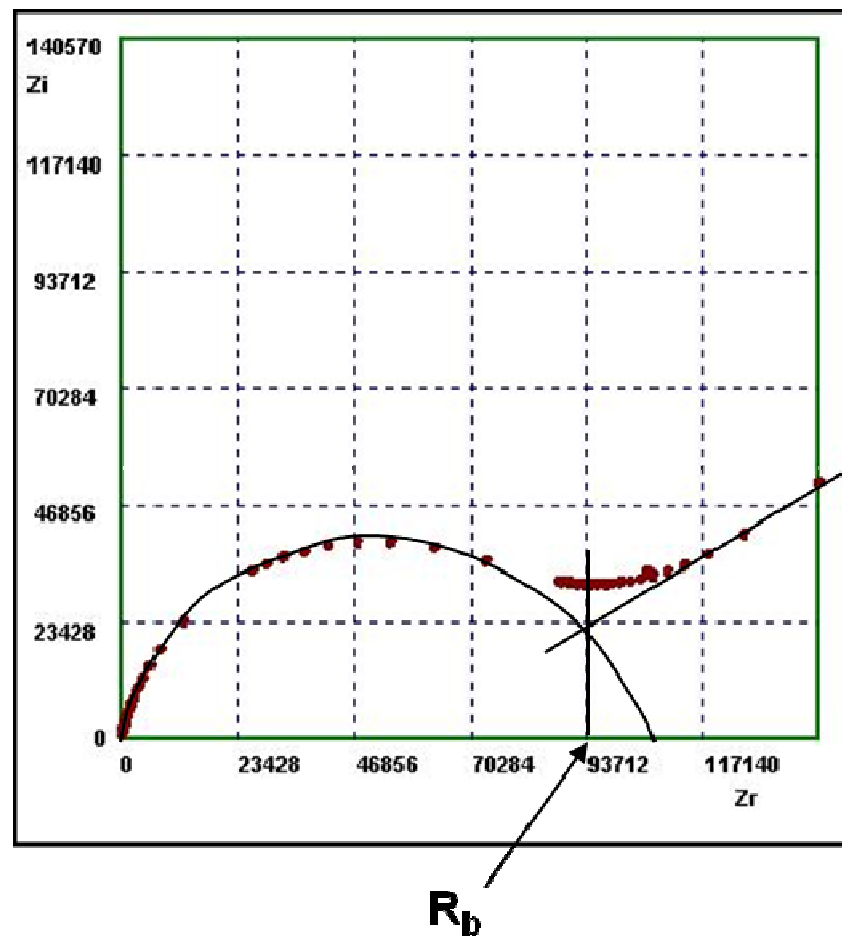


Figure 3.3 Complex impedance spectra of polymer electrolytes. (*Internet Reference 12/10/2009*)

### 3.3.3 *Structural Studies*

#### 3.3.3.1 X-Ray Diffraction (XRD)

X-ray diffraction is a powerful experimental tool which can be used to determine the main feature of the structure, for example the lattice parameter and type of structure, as well as other details such as the arrangement of different kinds of atoms in crystal. Figure 3.4 shows X-ray diffraction machine. The technique is also widely used in chemical identification and analysis due to the accurate intensity measurements which allows a quantitative estimate of the various elements in the sample to be made (Smallman, 1995 ; Shackleford, 2000).

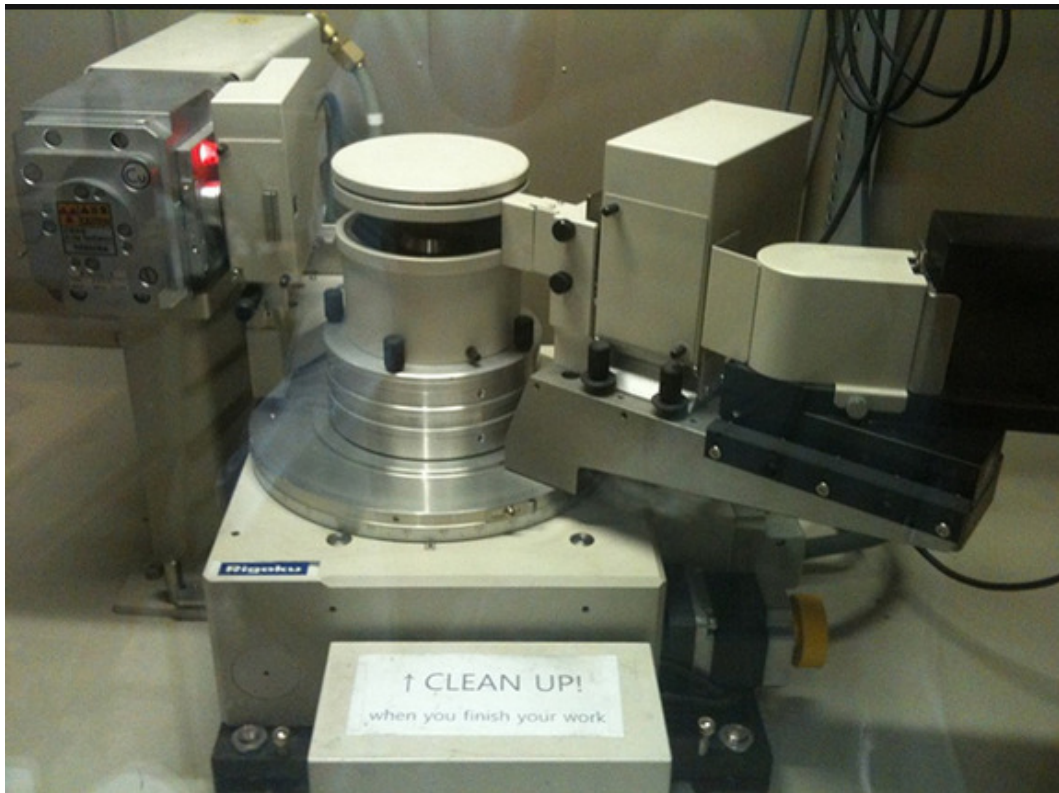


Figure 3.4: X-ray diffraction machine

As the sample rotates in XRD machines, the angle between the incident beam emitted and the normal to the film varies. The relationship of x-ray wavelength and interatomic spacing to the diffracted beam is clearly stated in Bragg's law (Shackleford, 2003):

$$2d \sin \Theta = n \lambda \quad (3.7)$$

Here  $d$  is the interplanar spacing,  $\Theta$  is the Bragg angle,  $n$  is the order of the reflection,  $\lambda$  is the X-ray wavelength. The samples were scanned with a beam of monochromatic  $\text{CuK}\alpha$ - X radiation of wavelength  $\lambda = 1.5406 \text{ \AA}$  between a  $2 \Theta$  angle of  $20^\circ$  to  $80^\circ$ . From the diffractograms, the crystallite size was calculated. The crystalline size can be obtained from the Scherrer equation (Shackleford, 2003):

$$L = 0.9 \lambda / \beta \cos \Theta \quad (3.8)$$

where,  $L$  is the crystalline size and  $\beta$  is the full width half maximum (FWHM) of the chosen peak. The chosen peaks must exist in the diffractogram of all samples prepared. An example of a XRD diffractogram is shown in Figure 3.5 (Calister, 2003) and Figure 3.6.

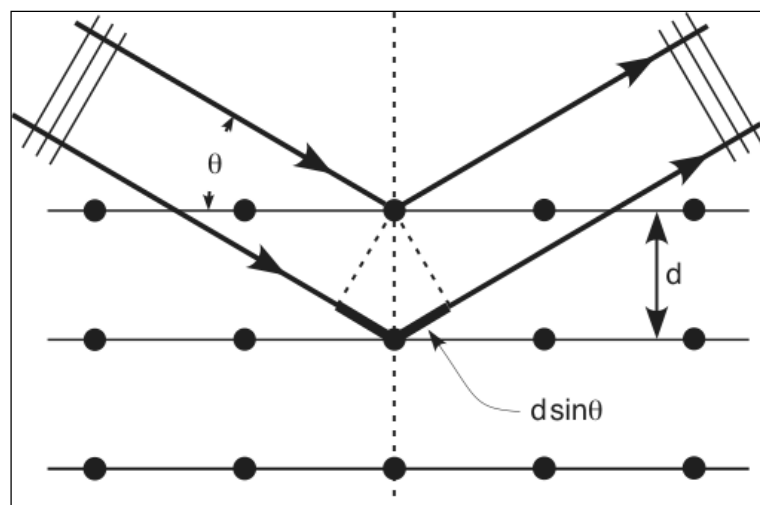


Figure 3.5 Diffraction of X-ray by planes of atoms (*Internet reference 08/04/2010*)

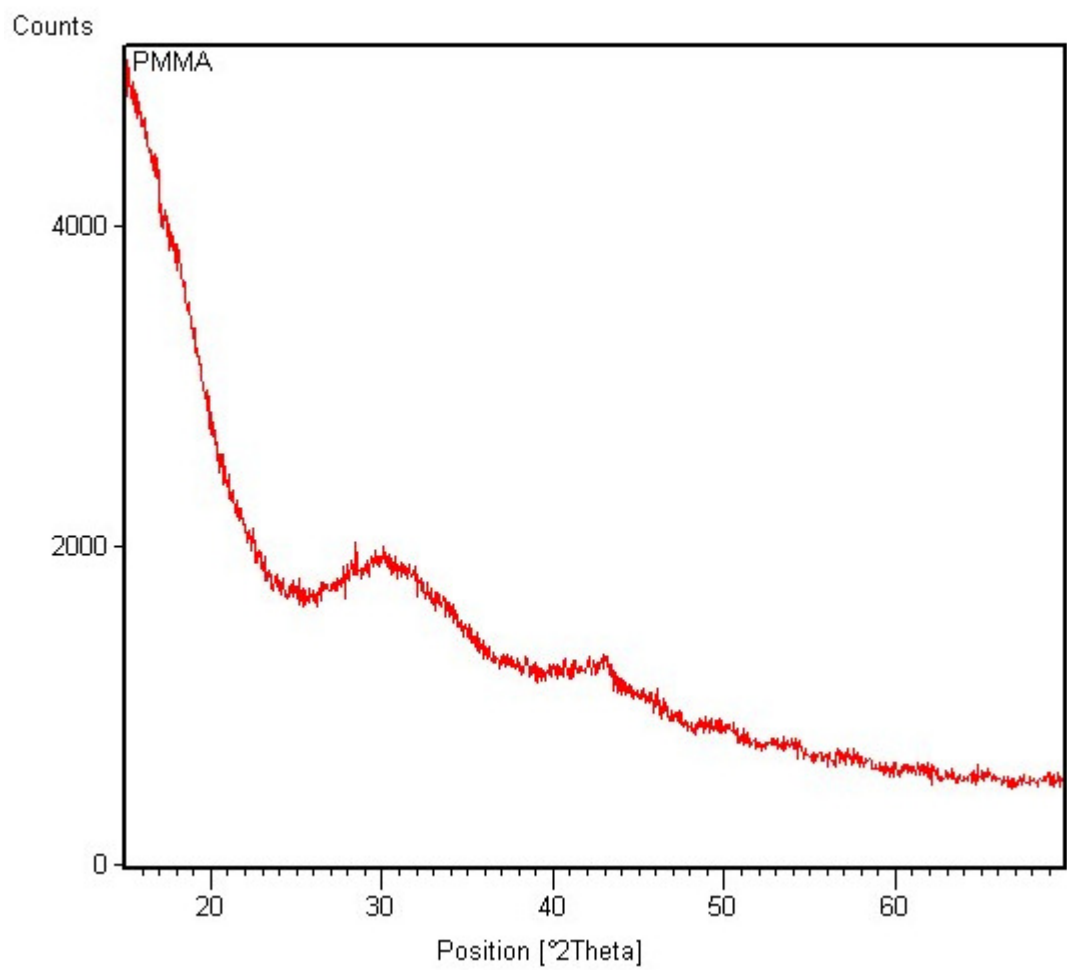


Figure 3.6 Diffraction of X-ray pattern of 80 wt% PMMA and 20 wt% PEO. (*Internet reference 08/09/2011*)



### 3.3.3.2 Transmission Electron Microscope (TEM)

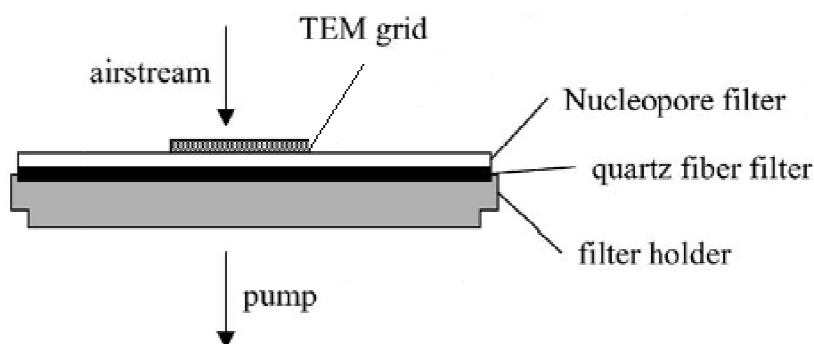
Transmission electron microscopy (TEM) is a microscopy technique whereby a beam of electrons is transmitted through an ultra thin specimen, interacting with the specimen as they pass through. An image is formed from the interaction of the electrons transmitted through the specimen, which is magnified and focused onto an imaging device, on a layer of photographic film, or to be detected by a sensor such as a CCD camera. TEM owing to the small de Broglie wavelength of electron enables the instrument to be able to examine fine detail of a sample. Alternate modes of use allow for the TEM to observe modulations in chemical identity, crystal orientation, electronic structure and sample induced electron phase shift as well as the regular absorption based imaging.

For TEM observations, thin samples are required due to the important absorption of the electrons in the material. High acceleration voltage reduces the absorption effects but can cause radiation damage (estimated at 170 kV for Al). At these acceleration tensions, a maximum thickness of 60 nm is required for TEM observations and quantifications. Therefore, prior to the analysis of TEM, the sample must be well prepared in order to obtain a clear resolution image. This can be achieved by the deposition of a dilute sample containing the specimen onto support grids or films.

In the present work, the composite filler, Manganese Oxide (MnO), after being ball milled for 36 hours were dispersed in the ethanol and sonicated for 60 minutes to prevent them from agglomeration on the copper grid later. The high dispersion of MnO nano-particles can be formed during the high-energy ball-milling process. A single drop of suspension was placed onto a 200 Cu Mech holey support film

and dried before it was sent to TEM analysis. Approximately 180 particles were randomly selected for image captured.

A schematic layout of the sampling set-up is given in Fig. 3.7. TEM-copper grids were taped on 47 mm diameter nucleopore polycarbonate membrane filters. Quartz fiber filters were used to support the nucleopore filters. The TEM (LIBRA® 120) was operated at an accelerating voltage of 120 kV. The resolution of point to point is 0.34 nm. For morphological analysis the TEM was operated in bright field mode (Mathis, 2004).



*'internet Resources,*

A TEM works much like a slide projector. A projector shines a beam of light through (transmits) the slide, as the light passes through it is affected by the structures and objects on the slide. These effects result in only certain parts of the light beam being transmitted through certain parts of the slide. This transmitted beam is then projected onto the viewing screen, forming an enlarged image of the slide. TEMs work the same

way except that they shine a beam of electrons (like the light) through the specimen (like the slide). Whatever part is transmitted is projected onto a phosphor screen for the user to see.

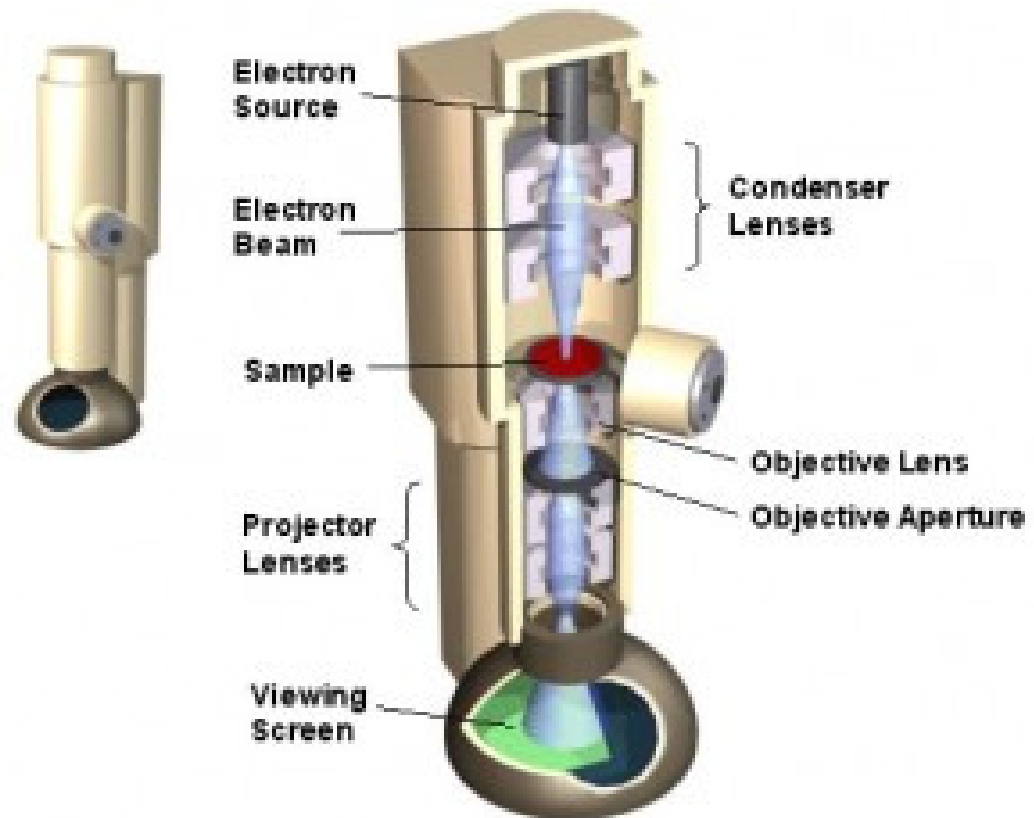


Figure 3.8 Typical TEMs workings principal (*Internet References*, 19/03/2009).

The "Virtual Source" at the top represents the electron gun, producing a stream of monochromatic electrons. This stream is focused to a small, thin, coherent beam by the use of condenser lenses 1 and 2. The first lens controlled by the "spot size knob" determines the "spot size"; the general size range of the final spot that strikes the sample while the second lens controlled by the "intensity or brightness knob" which changes the size of the spot on the sample by changing it from a wide dispersed spot to a pinpoint beam.

The beam is restricted by the condenser aperture, knocking out high angle electrons. The beam strikes the specimen and parts of it are transmitted. This transmitted portion is focused by the objective lens into an image. Optional Objective and Selected Area metal apertures can restrict the beam. In addition to that, the resolution of objective aperture can be contrasted by blocking out high-angle diffracted electrons whereas the selected area aperture allow the user to examine the periodic diffraction of electrons by ordered arrangements of atoms in the sample.

The image is passed down the column through the intermediate and projector lenses, being enlarged all the way. The image strikes the phosphor image screen and light is generated, allowing the user to see the image. The darker areas of the image represent those areas of the sample that fewer electrons were transmitted through (they are thicker or denser). The lighter areas of the image represent those areas of the sample that more electrons were transmitted through (they are thinner or less dense). Figure 3.9 show the TEM machine.



Figure 3.9 TEM machine

### 3.3.3.3 Field Emission Scanning Electron Microscope (FESEM)

FESEM is the abbreviation of Field Emission Scanning Electron Microscope. A FESEM is microscope that works with electrons (particles with a negative charge) instead of light. These electrons are liberated by a field emission source. The object is scanned by electrons according to a zig-zag pattern. FESEM is used to visualize very small topographic details on the surface or entire or fractioned objects. Researchers in biology, chemistry and physics apply this technique to observe structures that may be as small as 1 nanometer (= billion of a millimeter). The FESEM may be employed for example to study organelles and DNA material in cells, synthetical polymeres, and coatings on microchips.

In FESEM, electrons are liberated from a field emission source and accelerated in a high electrical field gradient. Within the high vacuum column these so-called primary electrons are focussed and deflected by electronic lenses to produce a narrow scan beam that bombards the object. As a result secondary electrons are emitted from each spot on the object. The angle and velocity of these secondary electrons relates to the surface structure of the object. A detector catches the secondary electrons and produces an electronic signal. This signal is amplified and transformed to a video scan-image that can be seen on a monitor or to a digital image that can be saved and processed further.

In standard electron microscopes electrons are mostly generated by heating a tungsten filament by means of a current to a temperature of about 2800°C. Sometimes electrons are produced by a crystal of lanthanumhexaboride ( $\text{LaB}_6$ ) that is mounted on a

tungsten filament. This modification results in a higher electron density in the beam and a better resolution than with the conventional device. In a field emission (FE) scanning electron microscope no heating but a so-called "cold" source is employed. An extremely thin and sharp tungsten needle (tip diameter  $10^{-7}$  –  $10^{-8}$  m) functions as a cathode in front of a primary and secondary anode. The voltage between cathode and anode is in the order of magnitude of 0.5 to 30 KV. Because the electron beam produced by the FE source is about 1000 times smaller than in a standard microscope, the image quality is markedly better. As field emission necessitates an extreme vacuum ( $10^{-8}$  Torr) in the column of the microscope, a device is present that regularly decontaminates the electron source by a current flash. In contrast to a conventional tungsten filament, a FE tip last theoretically for a lifetime, provided the vacuum is maintained stable.

The electron beam is focused by the electro-magnetic lenses (condenser lens, scan coils, stigmator coils and objective lens) and the apertures in the column to a tiny sharp spot. The current in the condenser determines the diameter of the beam: a low current results in a small diameter, a higher current in a larger beam. A narrow beam has the advantage that the resolution is better, but the disadvantage that the signal to noise ratio is worse. The situation is reversed when the beam has a large diameter. The condenser lens consists mostly out of two parts. The scan coils deflect the electron beam over the object according to a zig-zag pattern. The formation of the image on the monitor occurs in synchrony with this scan movement. The scan velocity determines the refreshing rate on the screen and the amount of noise in the image. The smaller the scanned region on the object, the larger the magnification becomes at a constant window size. Scan coils often consist of upper and lower coils, which prevent the formation of a circular shadow at low magnification.

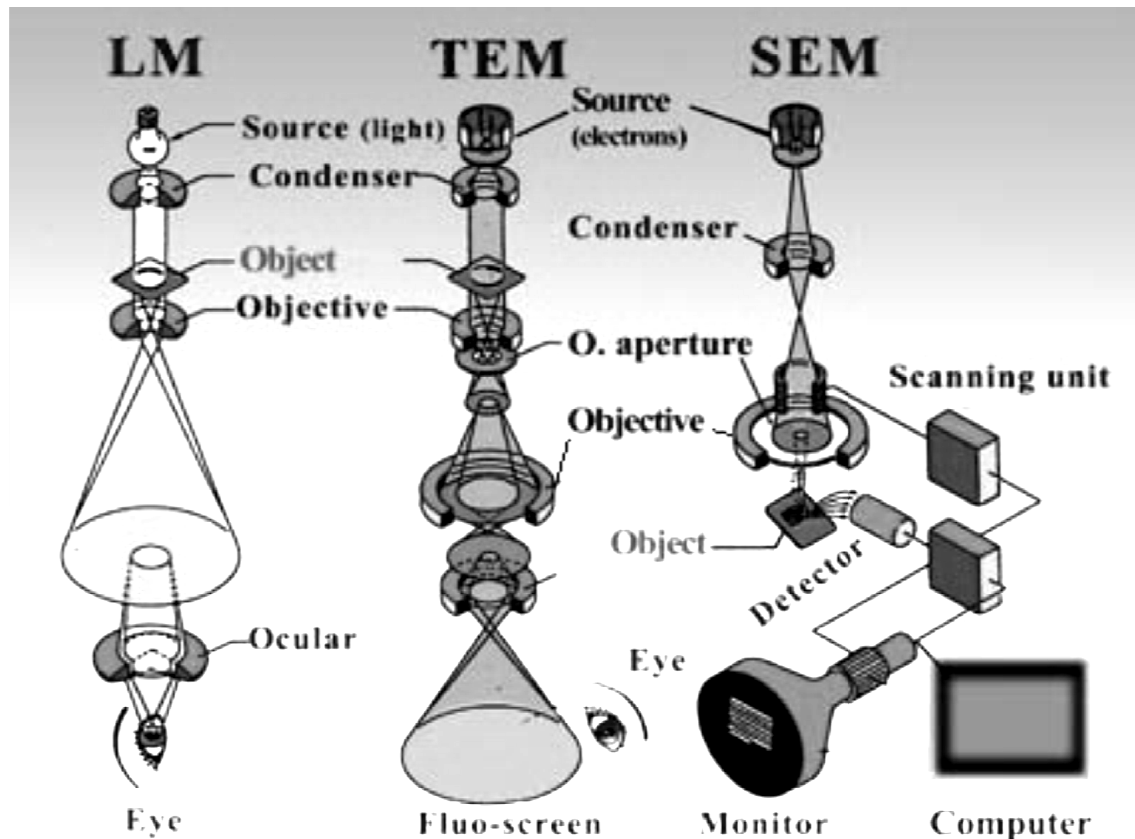


Figure 3.10 Schematic diagram of light microscope (LM), transmission electron microscope (TEM) and field emission scanning electron microscope (FESEM).  
(Internet Resources 08082011)

The objective lens is the lowest lens in the column. The objective focuses the electron beam on the object. At a short working distance the objective lens needs to apply a greater force to deflect the electron beam. The shortest working distance produces the smallest beam diameter, the best resolution, but also the poorest depth of field.. The stigmator coils are utilized to correct irregularities in the x and y deflection of the beam and thus to obtain a perfectly round-shaped beam. When the beam is not circular, but ellipsoidal, the image looks blurred and stretched.



After the object has been covered by a conductive layer, it is mounted on a special holder. The object is inserted through an exchange chamber into the high vacuum part of the microscope and anchored on a moveable stage. In the virtual FESEM the object can be moved in horizontal and vertical direction on the screen by operating the arrows in the particular box. In the real microscope the object can be repositioned in the chamber by means of a joy stick that steers in left right axis, or forward and backward. In addition, the object can be tilted (e.g. for stereo views), rotated and moved in Z direction. Figure 3.11 shows field emission scanning electron microscope connected to a computer.

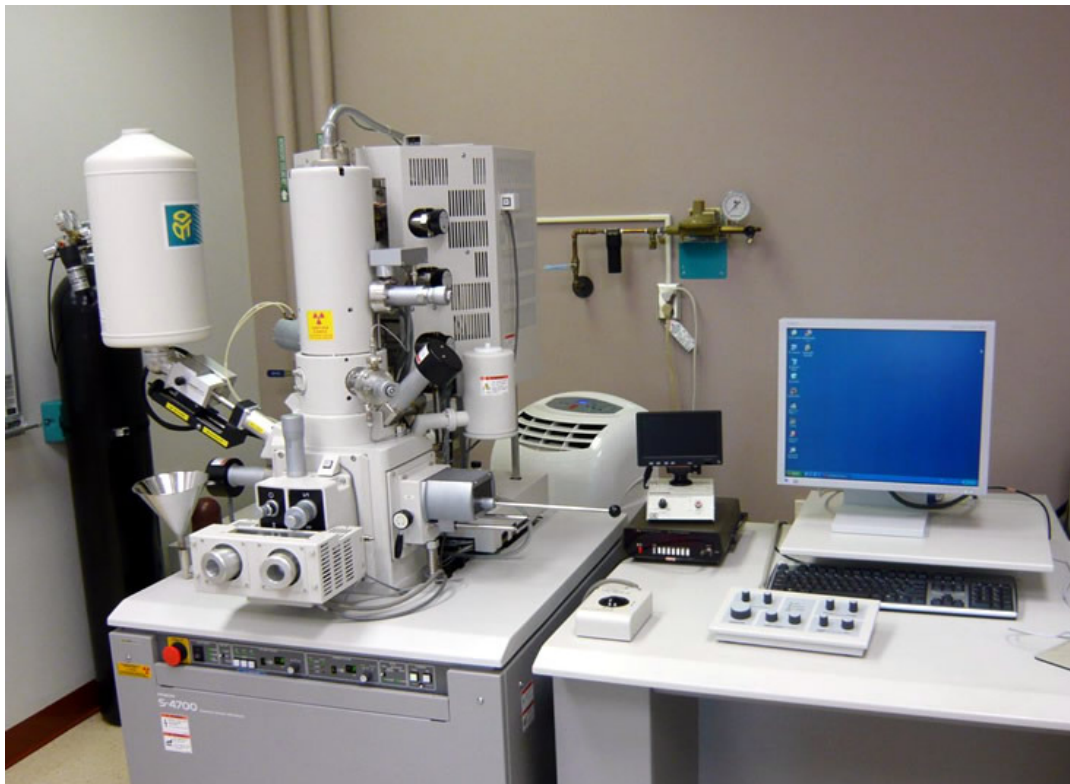


Figure 3.11 Field Emission Scanning Electron Microscope (FESEM)

On the other hand, the “secondary electron emission” detector (scintillator) is located at the rear of the object holder in the chamber. When the primary probe bombards the object, secondary electrons are emitted from the object surface with a certain velocity that is determined by the levels and angles at the surface of the object. The secondary electrons, which are attracted by the Corona, strike the scintillator (fluorescing mirror) that produces photons. The location and intensity of illumination of the mirror vary depending on the properties of the secondary electrons. The signal produced by the scintillator is amplified and transduced to a video signal that is fed to a cathode ray tube in synchrony with the scan movement of the electron beam. The contrast in the ‘real time’ image that appears on the screen reflects the structure on the surface of the object. Parallel to the analog image, a digital image is generated which can be further processed.

#### 3.3.3.4 Fourier Transform Infrared Spectroscopy (FTIR)

Fourier transform infrared spectroscopy (FTIR) is a technique which is used to obtain an infrared spectrum of absorption, emission, photoconductivity or Raman scattering of a solid, liquid or gas. An FTIR spectrometer simultaneously collects spectral data in a wide spectral range. This confers a significant advantage over a dispersive spectrometer which measures intensity over a narrow range of wavelengths at a time.

The term Fourier transform infrared spectroscopy originates from the fact that a Fourier transform (a mathematical algorithm) is required to convert the raw data into the actual spectrum. The goal of any absorption spectroscopy (FTIR, ultraviolet-visible ("UV-Vis") spectroscopy, etc.) is to measure how well a sample absorbs light at each wavelength. The most straightforward way to do this, the "dispersive spectroscopy" technique, is to shine a monochromatic light beam at a sample, measure how much of the light is absorbed, and repeat for each different wavelength. (This is how UV-Vis spectrometers work, for example.)

Fourier transform spectroscopy is a less intuitive way to obtain the same information. Rather than shining a monochromatic beam of light at the sample, this technique shines a beam containing many different frequencies of light at once, and measures how much of that beam is absorbed by the sample. Next, the beam is modified to contain a different combination of frequencies, giving a second data point. This process is repeated many times. Afterwards, a computer takes all these data and works backwards to infer what the absorption is at each wavelength.

The beam described above is generated by starting with a broadband light source one containing the full spectrum of wavelengths to be measured. The light shines into a certain configuration of mirrors, called a Michelson interferometer, that allows some wavelengths to pass through but blocks others (due to wave interference). The beam is modified for each new data point by moving one of the mirrors; this changes the set of wavelengths that pass through. As mentioned, computer processing is required to turn the raw data (light absorption for each mirror position) into the desired result (light absorption for each wavelength). The processing required turns out to be a common algorithm called the Fourier transform (hence the name, "Fourier transform spectroscopy"). The raw data is sometimes called an "interferogram".



Figure 3.12: Spectrum FTIR Spectrometer dual system

In this work, the FTIR spectra of the samples were recorded using Perkin Elmer FL Winlab FTIR spectrometer, equipped with an air-cooled rare earth oxide filament source, CSI beam splitter and DTGS detector, as shown in Figure 3.12. The instrument was set for ten scans at  $4\text{ cm}^{-1}$  resolution with cosine apodisation in the mid-IR region:  $4,000 - 400\text{ cm}^{-1}$ . No purging was carried out. The samples were placed into the sample holder made and contacted with a diamond stub.

### 3.3.4 Thermal Studies

#### 3.3.4.1 Differential scanning calorimetry (DSC)

Differential scanning calorimetry or DSC is a thermoanalytical technique in which the difference in the amount of heat required to increase the temperature of a sample and reference is measured as a function of temperature. Both the sample and reference are maintained at nearly the same temperature throughout the experiment. Generally, the temperature program for a DSC analysis is designed such that the sample holder temperature increases linearly as a function of time. The reference sample should have a well-defined heat capacity over the range of temperatures to be scanned. In this thesis, differential scanning calorimeter was used to measure the glass transition and crystallization temperature of the composite electrolyte films within the temperature range of -100 to 200°C at a scanning rate of 5°C per min. Figure 3.13 show the machine of DSC.

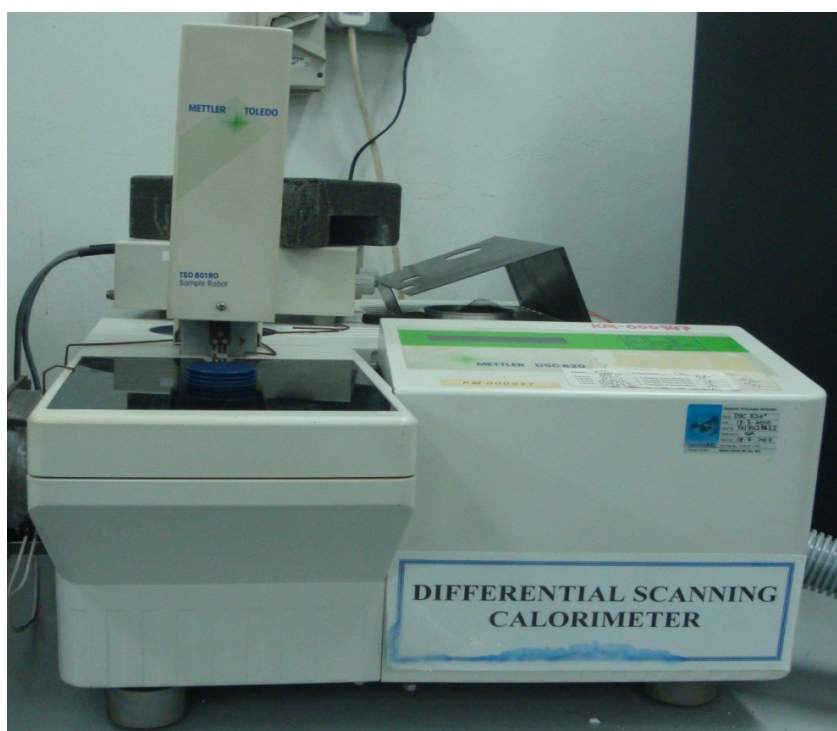


Figure 3.13: Differential scanning calorimetry (DSC)

The basic principle underlying this technique is that when the sample undergoes a physical transformation such as phase transitions, more or less heat will need to flow to it than the reference to maintain both at the same temperature. Whether less or more heat must flow to the sample depends on whether the process is exothermic or endothermic. For example, as a solid sample melts to a liquid it will require more heat flowing to the sample to increase its temperature at the same rate as the reference. This is due to the absorption of heat by the sample as it undergoes the endothermic phase transition from solid to liquid. Likewise, as the sample undergoes exothermic processes (such as crystallization) less heat is required to raise the sample temperature. By observing the difference in heat flow between the sample and reference, differential scanning calorimeters are able to measure the amount of heat absorbed or released during such transitions. DSC may also be used to observe more subtle phase changes, such as glass transitions. It is widely used in industrial settings as a quality control instrument due to its applicability in evaluating sample purity and for studying polymer curing.

DSC is used widely for examining polymers to check their composition. Melting points and glass transition temperatures for most polymers are available from standard compilations, and the method can show possible polymer degradation by the lowering of the expected melting point,  $T_m$ , for example.  $T_m$  depends on the molecular weight of the polymer, so lower grades will have lower melting points than expected. The percentage crystallinity of a polymer can be found from the crystallization peak of the DSC graph since the heat of fusion can be calculated from the area under an absorption peak. DSC can also be used to study thermal degradation of polymers.

Impurities in polymers can be determined by examining thermograms for anomalous peaks, and plasticisers can be detected at their characteristic boiling points.



### 3.3.4.2 Thermogravimetric analysis (TGA)

Thermogravimetric analysis or thermal gravimetric analysis (TGA) is a type of testing performed on samples that determines changes in weight in relation to change in temperature. Figure 3.14 show the machine of TGA. Such analysis relies on a high degree of precision in three measurements: weight, temperature, and temperature change. As many weight loss curves look similar, the weight loss curve may require transformation before results may be interpreted. A derivative weight loss curve can identify the point where weight loss is most apparent. Again, interpretation is limited without further modifications and deconvolution of the overlapping peaks may be required.



Figure 3.14: Transgravimetric analysis machine

TGA is commonly employed in research and testing to determine characteristics of materials such as polymers, to determine degradation temperatures, absorbed moisture content of materials, the level of inorganic and organic components in materials, decomposition points of explosives, and solvent residues. Simultaneous TGA-DTA/DSC measures both heat flow and weight changes (TGA) in a material as a function of temperature or time in a controlled atmosphere. Simultaneous measurement of these two material properties not only improves productivity but also simplifies interpretation of the results. The complementary information obtained allows differentiation between endothermic and exothermic events with no associated weight loss (e.g. melting and crystallization) and those that involve a weight loss (e.g. degradation).

The sample is placed in a small electrically heated oven with a thermocouple to accurately measure the temperature. The atmosphere may be purged with an inert gas to prevent oxidation or other undesired reactions. A computer is used to control the instrument. Analysis is carried out by raising the temperature of the sample gradually and plotting weight (percentage) against temperature. The temperature in many testing methods routinely reaches 1000°C or greater. After the data are obtained, curve smoothing and other operations may be done to find the exact points of inflection.

### **3.3.5 Optical Studies**

#### **3.3.5.1 Ultra-Violet Visible (UV-Vis) Spectroscopy**

Ultraviolet-visible spectroscopy (UV-Vis) refers to absorption spectroscopy or reflectance spectroscopy in the ultraviolet-visible spectral region. This means it uses light in the visible and adjacent (near-UV and near-infrared (NIR)) ranges. The absorption or reflectance in the visible range directly affects the perceived colour of the chemicals involved. In this region of the electromagnetic spectrum, molecules undergo electronic transitions. UV/Vis spectroscopy is routinely used in analytical chemistry for the quantitative determination of different analytes, such as transition metal ions, highly conjugated organic compounds, and biological macromolecules.

The functioning of this instrument is relatively straightforward. A beam of light from a visible and/or UV light source (colored red) is separated into its component wavelengths by a prism or diffraction grating. Each monochromatic (single wavelength) beam in turn is split into two equal intensity beams by a half-mirrored device. One beam, the sample beam (colored magenta), passes through a small transparent container (cuvette) containing a solution of the compound being studied in a transparent solvent. The other beam, the reference (colored blue), passes through an identical cuvette containing only the solvent. The intensities of these light beams are then measured by electronic detectors and compared. Over a short period of time, the spectrometer automatically scans all the component wavelengths in the manner described. The ultraviolet (UV) region scanned is normally from 200 to 400 nm, and the visible portion is from 400 to 800 nm.

The visible region of the spectrum comprises photon energies of 36 to 72 kcal/mole, and the near ultraviolet region, out to 200 nm, extends this energy range to 143 kcal/mole. Absorption spectroscopy carried out in this region is sometimes called "electronic spectroscopy". Various kinds of electronic excitation that may occur in organic molecules are shown in Figure 3.15. As a rule, energetically favoured electron promotion will be from the highest occupied molecular orbital (HOMO) to the lowest unoccupied molecular orbital (LUMO), and the resulting species is called an excited state. When sample molecules are exposed to light having an energy that matches a possible electronic transition within the molecule, some of the light energy will be absorbed as the electron is promoted to a higher energy orbital. An optical spectrometer records the wavelengths at which absorption occurs, together with the degree of absorption at each wavelength. The resulting spectrum is presented as a graph of absorbance (A) versus wavelength.

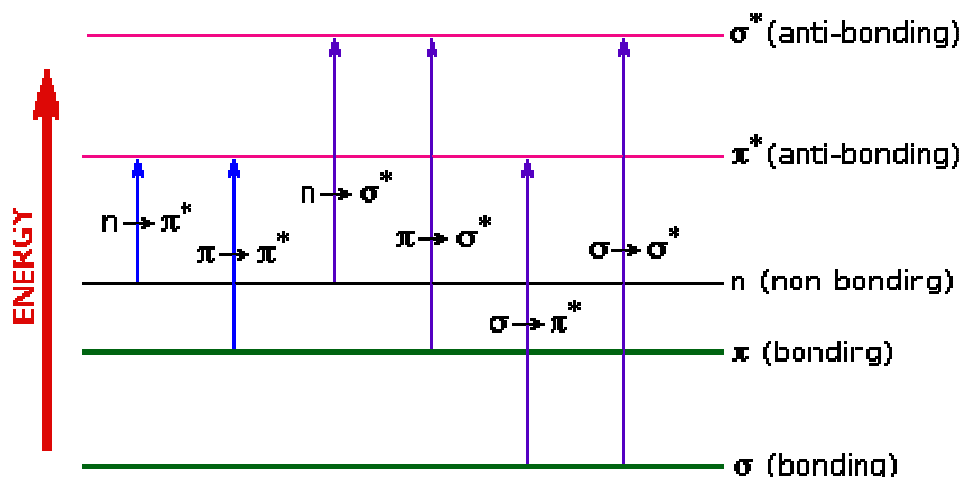


Figure 3.15 Electronic excitation of organic molecules

Because the absorbance of a sample will be proportional to the number of absorbing molecules in the spectrometer light beam (e.g. their molar concentration in the sample tube), it is necessary to correct the absorbance value for this and other operational factors. The corrected absorption value is called "molar absorptivity", and is particularly useful when comparing the spectra of different compounds and determining the relative strength of light absorbing functions (chromophores). Molar absorptivity ( $\epsilon$ ) is defined as in equation (3.9):

$$\epsilon = \frac{A}{cl} \quad (3.9)$$

where  $A$  is the absorbance,  $c$  is the sample concentration in moles/liter and  $l$  is length of light path through the sample in cm.

Table 3.7 List of some simple chromophores and their light absorption characteristics

Chromophore	Example	Excitation	$\lambda_{\text{max}}$ , nm	$\epsilon$	Solvent
C=C	Ethene	$\pi \rightarrow \pi^*$	171	15,000	hexane
C $\equiv$ C	1-Hexyne	$\pi \rightarrow \pi^*$	180	10,000	hexane
C=O	Ethanal	$n \rightarrow \pi^*$ $\pi \rightarrow \pi^*$	290 180	15 10,000	hexane hexane
N=O	Nitromethane	$n \rightarrow \pi^*$ $\pi \rightarrow \pi^*$	275 200	17 5,000	ethanol ethanol
C-X    X=Br X=I	Methyl bromide Methyl Iodide	$n \rightarrow \sigma^*$ $n \rightarrow \sigma^*$	205 255	200 360	hexane hexane

Table 3.7 shows the list of some simple chromophores and their light absorption characteristics. The oxygen non-bonding electrons in alcohols and ethers do not give rise to absorption above 160 nm. Molar absorptivities may be very large for strongly absorbing chromophores (>10,000) and very small if absorption is weak (10 to 100).

The magnitude of  $\varepsilon$  reflects both the size of the chromophore and the probability that light of a given wavelength will be absorbed when it strikes the chromophore.

The absorption of light radiation in a sample obeys the Beer-Lambert relationship, which states that the concentration of a substance in a sample is directly proportional to the absorbance,  $A$ . The incident radiation refers to  $I_o$  and the intensity of transmitted radiation refers to  $I$ ,

$$A = \varepsilon bc \quad (3.10)$$

where  $\varepsilon$  is the molar absorptivity constant,  $b$  is the path length and  $c$  is the molar concentration of the absorbance. When monochromatic radiation passes through a homogeneous sample, the intensity of the emitted radiation depends upon the thickness,  $L$  and concentration,  $c$ . The ratio  $I_o/I$ , known as transmittance, is expressed as a percentage and is therefore referred to as % transmittance. The absorbance is related to percent transmittance,  $T$  by the expression:

$$A = \log\left(\frac{I_o}{I}\right) = \log\left(\frac{100}{T}\right) = \varepsilon bc \quad (3.11)$$

Figure 3.16 shows Cary 50 UV-Visible spectrophotometer used for optical characterization of polymer electrolytes. The wavenumber range for this equipment is 180-900 nm, and the wavenumbers considered in this research are within the range of 300 – 600 nm at a scan speed of 60 nm/min. Prior to using ‘UV-Cary50’ software, baseline correction of the spectrophotometer was carried out using tetrahydrofuran (THF) for polymer electrolyte solution. 1 mL of polymer electrolyte was diluted in 10

mL of THF and rinsed in ultrasonic bath with re-distilled deionized water for 10 min. The absorption spectra were recorded at a rate of  $60 \text{ nm min}^{-1}$ , with a spectral resolution of 2 nm at room temperature in a 1 cm optical path quartz cuvette.



Figure 3.16 Cary 50 UV-Visible spectrophotometer

## CHAPTER FOUR

### RESULTS AND DISCUSSION

This chapter presents results of various studies of the properties of nanocomposite solid polymer electrolytes. The particles size and particle size distribution of manganese dioxide ( $\text{MnO}_2$ ) filler were examined by transmission electron microscope (TEM) and the optimum composition of PMMA-PEO- $\text{LiClO}_4$ -EC- $\text{MnO}_2$  nanocomposite were obtained through the electrical, structural, thermal and optical studies.

#### 4.1 Structural Studies

##### 4.1.1 Transmission electron microscope (TEM) analysis of $\text{MnO}_2$ nano-filler

Figure 4.1 represents the TEM image of the  $\text{MnO}_2$  nanoparticles. The figure exhibits non-spherical shape of particles with average size of the particles is within the range of 30 nm. The particle size distribution of  $\text{MnO}_2$  nano-particles is shown in Figure 4.2 with a normal type. The distribution was found to be dependent on sampling technique, sample size and preparation method (Vella *et al.* 2006).

A number of physical phenomena become pronounced as the size of the material in a system approaching nano scale. These include statistical mechanical effects, as well as quantum mechanical effects. The increase in surface area of nanosize filler to volume ratio alters mechanical, thermal and catalytic properties of electrolytes (*Internet reference 16/5/2012*). Additionally, filler in nano-scale provides high specific surface area that is available for interaction with the polymer. This interaction competes with the local lithium-polymer coordination sites which in turn frees up the polymer



segmental motion. However, with increasing filler content, some agglomeration begins to occur which reduces the active surface area available to interact with the polymer (Forsyth *et al*, 2002)

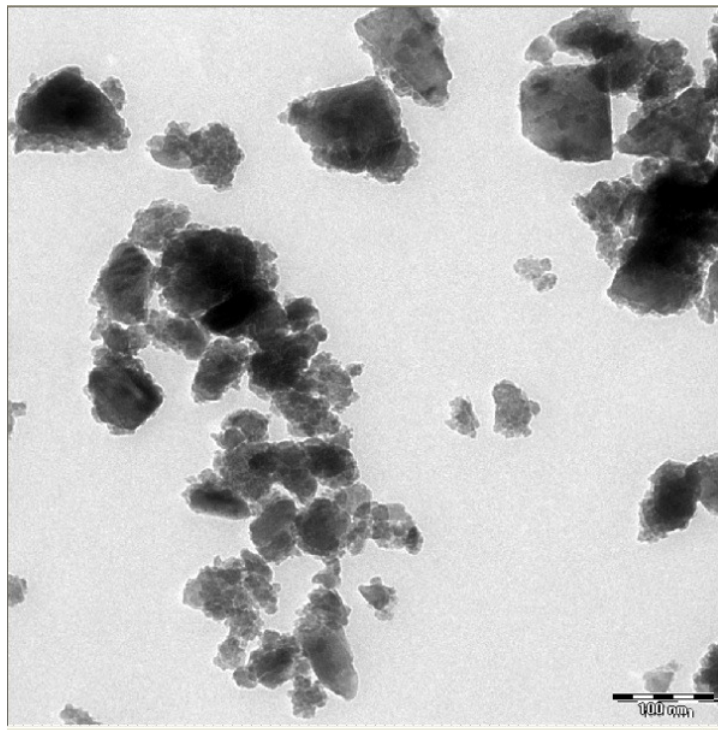
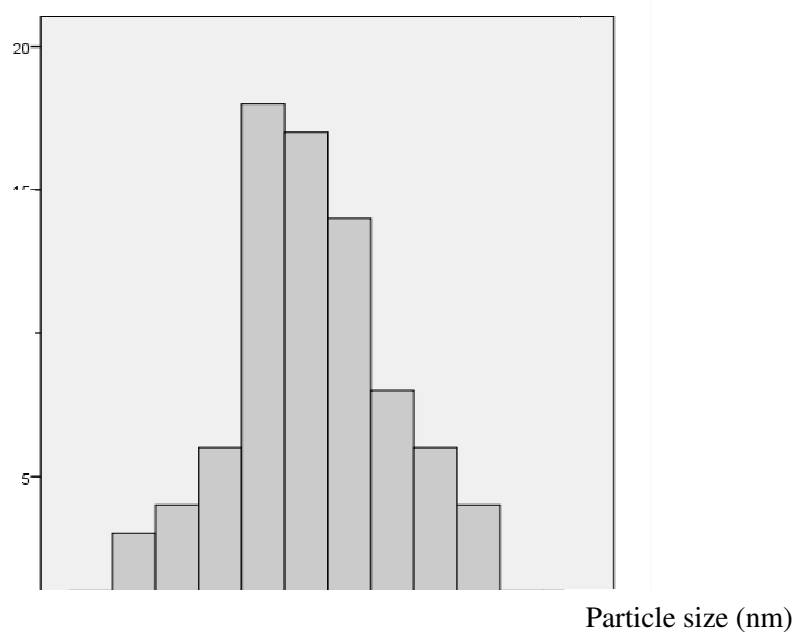


Figure 4.1: TEM image of MnO<sub>2</sub> nanoparticles



MnO<sub>2</sub> nanoparticles

#### 4.1.2 X-ray diffraction (XRD) studies

Figure 4.3 (a) – (b) show the XRD pattern for pure PMMA and PEO. It can be observed that two obvious crystalline peaks occurred at the angle of  $2\Theta = 13.33, 30.51$  in pure PMMA and one single apparent crystalline peak happened at angle of  $2\Theta = 13.77$  in pure PEO. Figures 4.4(a) – (f) show the XRD patterns of PMMA:PEO blend at 90:10, 80:20, 70:30, 60:40, 50:50 and 40:60 weight percent.

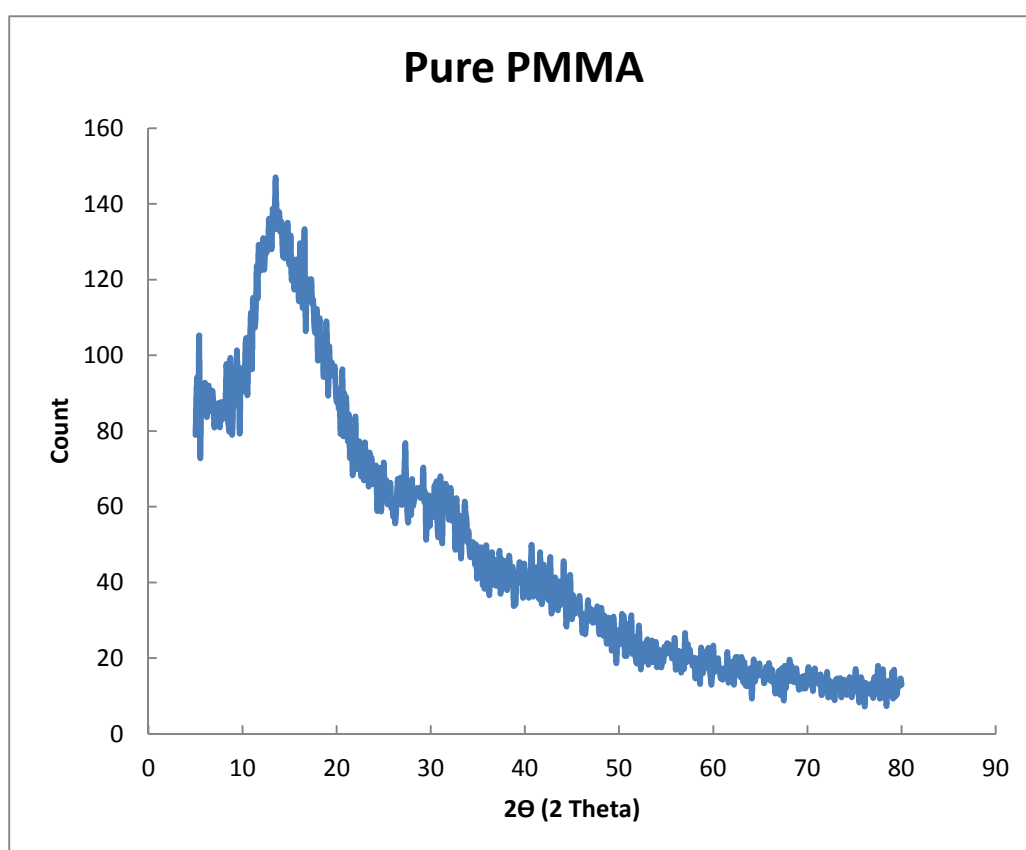


Figure 4.3 (a) shows the XRD pattern for pure PMMA.

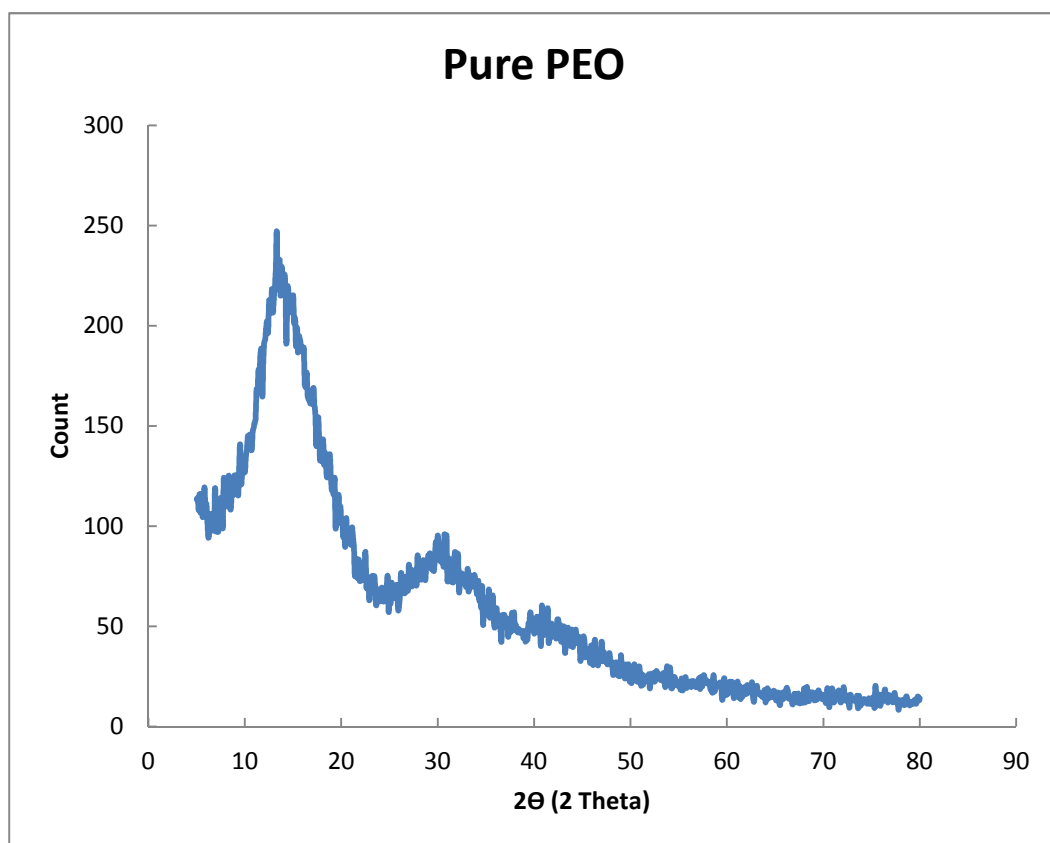


Figure 4.3 (b) shows the XRD pattern for pure PEO.

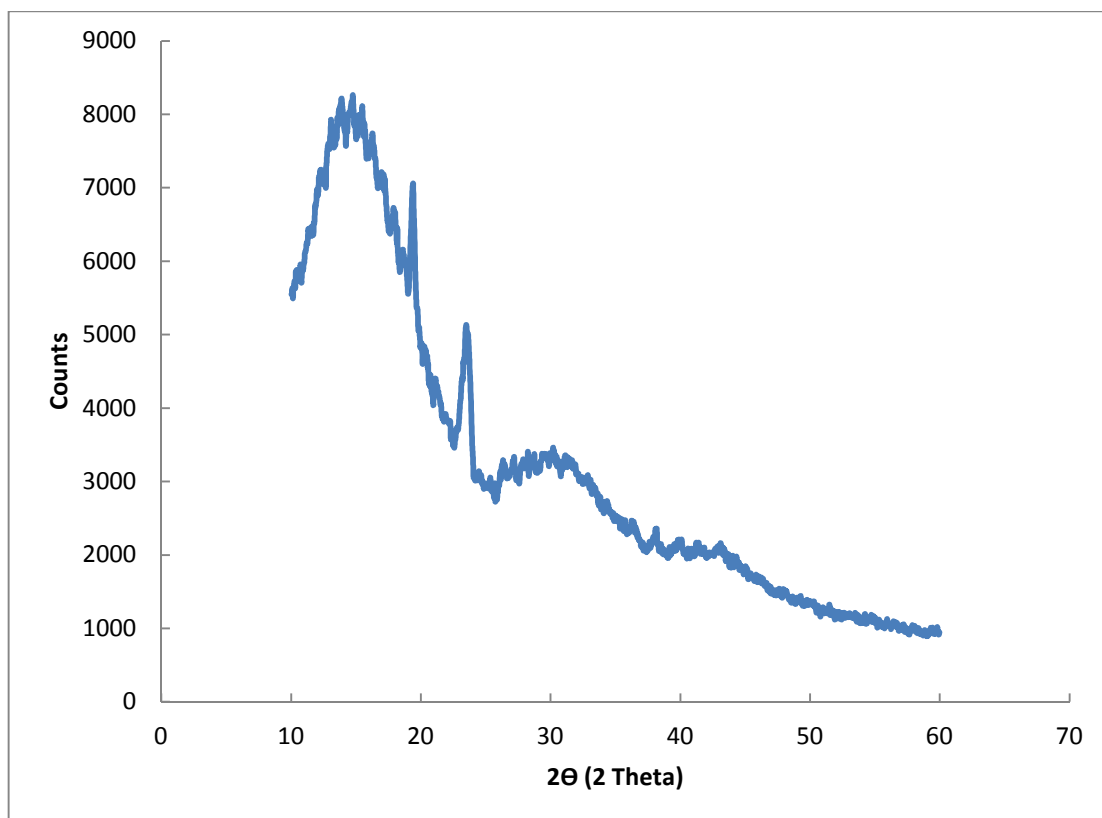


Figure 4.4 (a) XRD pattern for 90:10 wt% of PMMA/PEO blend

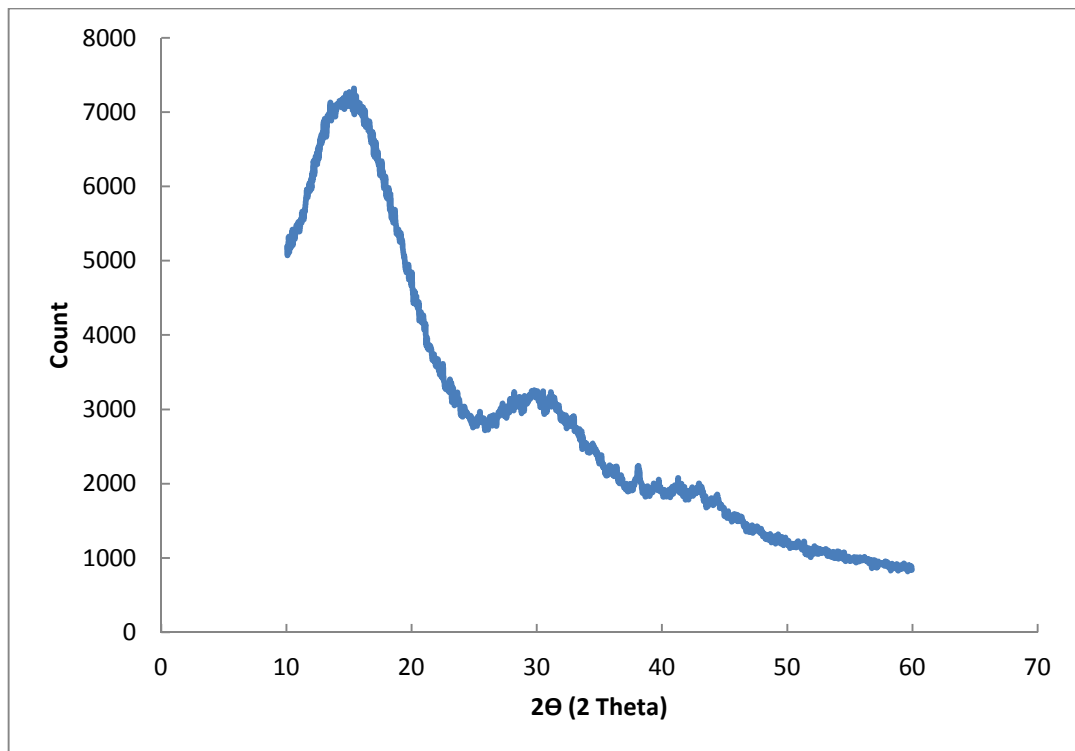


Figure 4.4 (b) XRD pattern for 80:20 wt% of PMMA/PEO blend

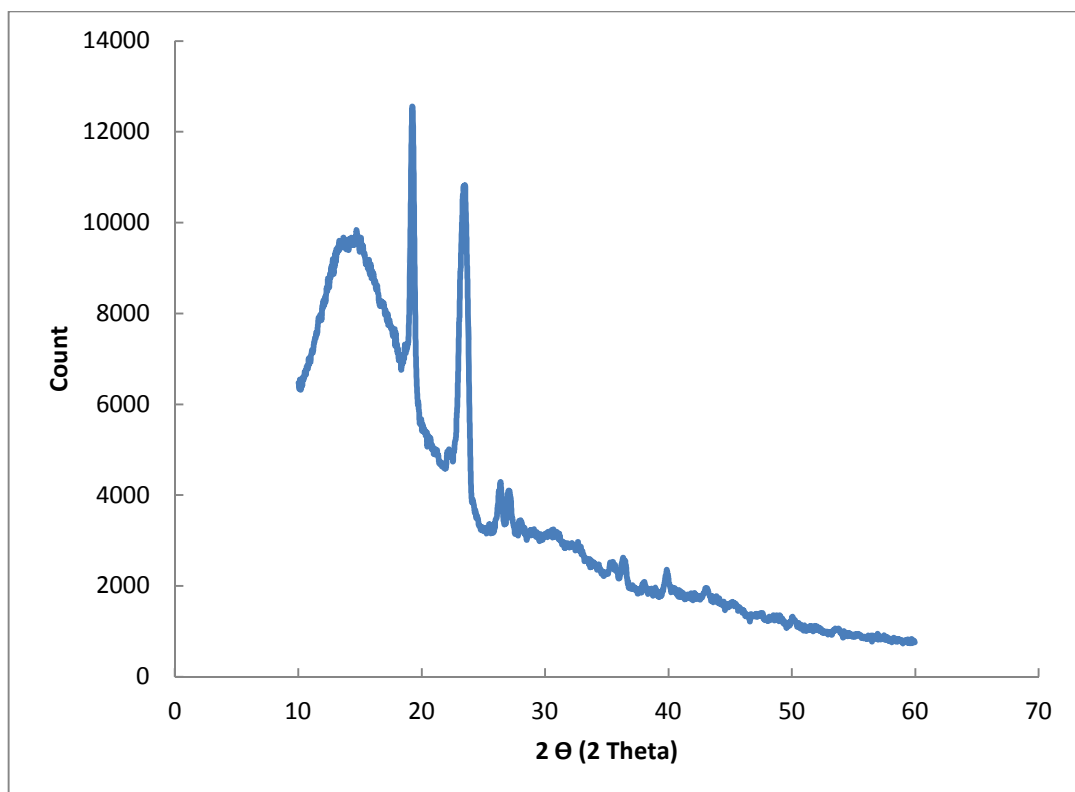


Figure 4.4 (c) XRD pattern for 70:30 wt% of PMMA/PEO blend

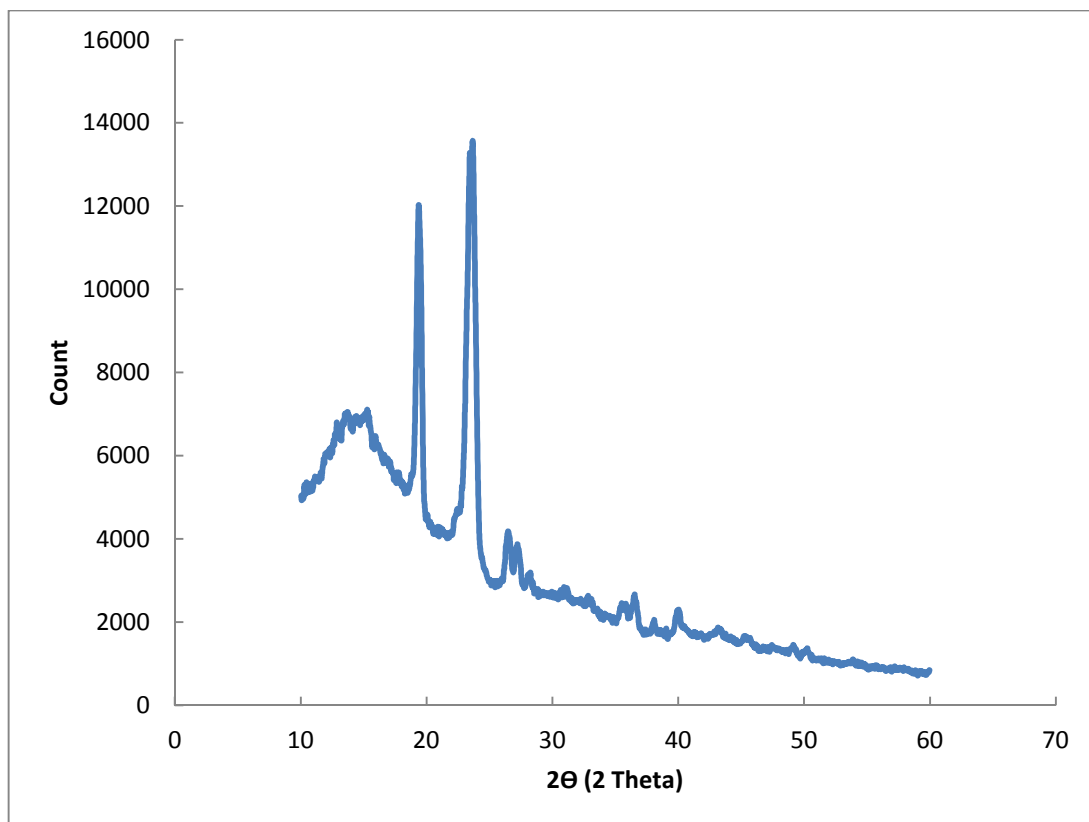


Figure 4.4 (d) XRD pattern for 60:40 wt% of PMMA/PEO blend

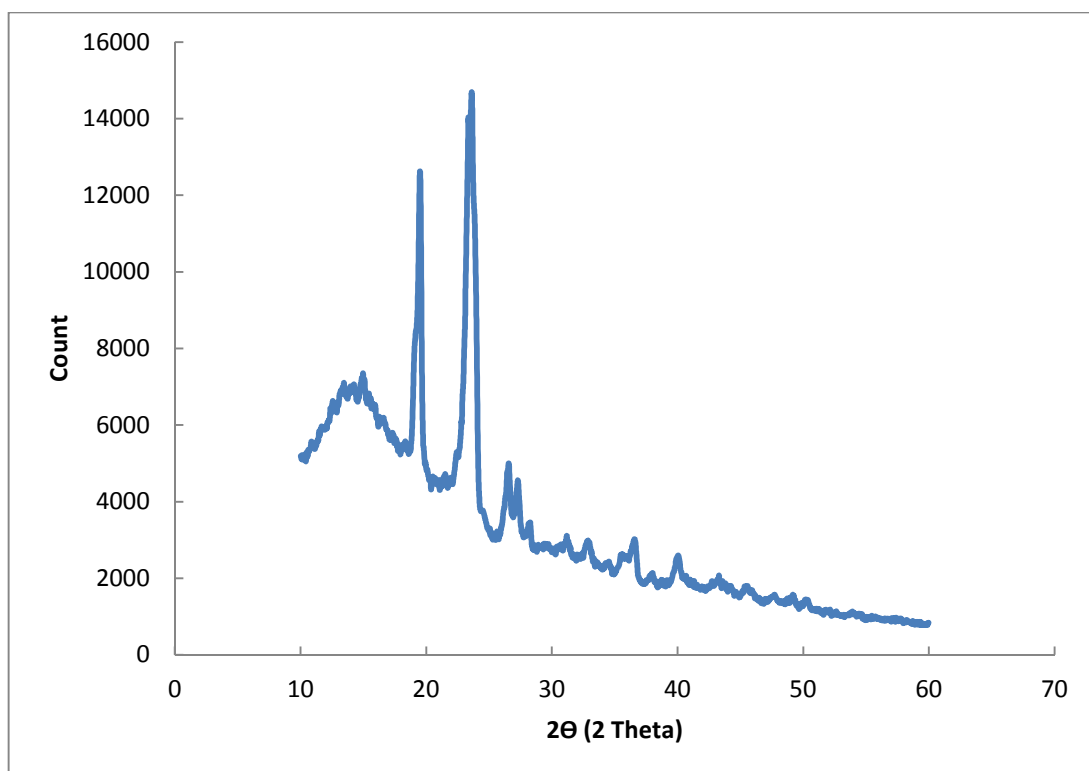


Figure 4.4 (e) XRD pattern for 50:50 wt% of PMMA/PEO blend

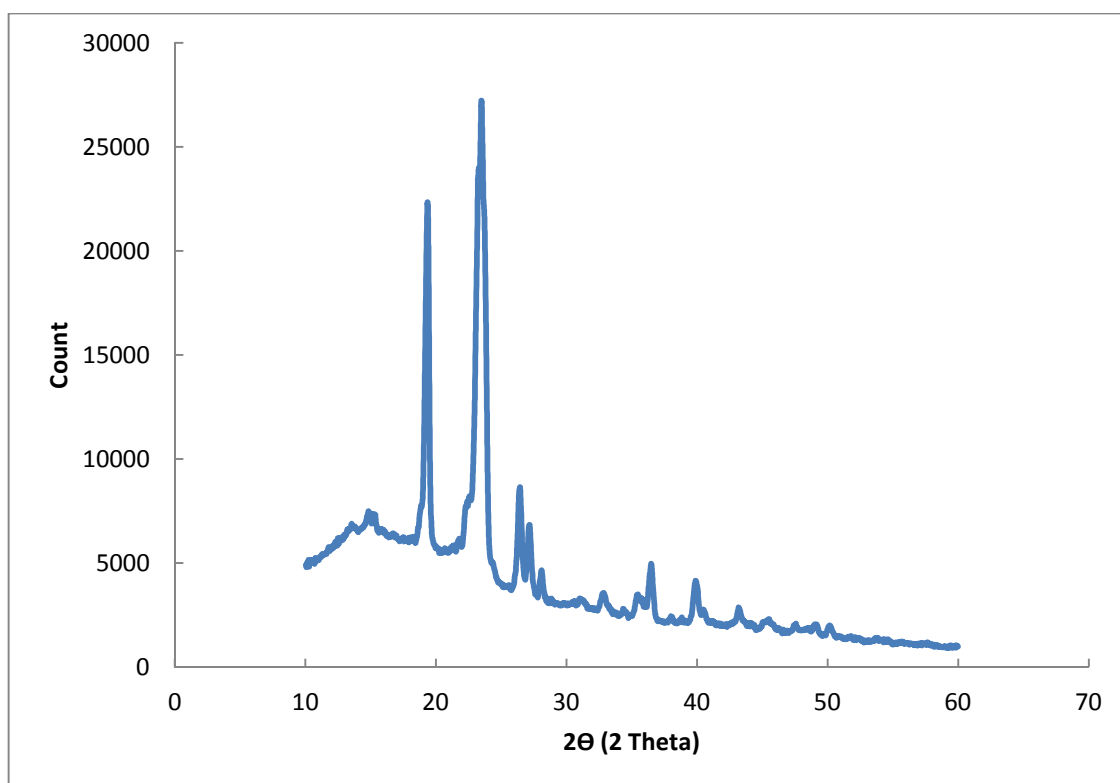


Figure 4.4 (f) XRD pattern for 40:50 wt% of PMMA/PEO blend

The XRD pattern of the pure PMMA shows a semi crystalline nature and two amorphous humps were observed in XRD pattern of pure PEO. Table 4.1 show the crystallite size of pure PEO, pure PMMA and various composition of PMMA/PEO polymer blend system. From table 4.1 we can conclude that the amorphousity of 80PMMA:20PEO is the highest as the system has a smallest crystalline size compare to pure PMMA and pure PEO. There is a wide broadening of crystalline peak observed in Figure 4.4 (b) due to the strain inclusion in the polymer blend electrolyte system that explained the decreasing crystallite size. This indicates the homogeneity of the polymer blend. Apparently, the most suitable composition of polymer matrix as a host was 80:20 weight percent of PMMA/PEO.

Table 4.1 Crystallite size of pure PEO and pure PMMA in comparison with the various composition of PMMA/PEO polymer blend system.

Sample	$2\theta \pm 0.01$ (degree)	d (nm)
pure PMMA	13.33	0.83
	30.51	0.79
pure PEO	13.77	0.68
90PMMA:10PEO	14.11	5.25
	19.15	1.65
	23.22	0.70
80PMMA:20PEO	14.64	0.71
	29.64	0.75
70PMMA:30PEO	15.19	0.96
	19.26	9.67
	23.52	6.09
	27.04	4.09
60PMMA:40PEO	14.44	0.96
	19.26	6.91
	23.52	6.09
	27.04	3.50
50PMMA:50PEO	14.44	0.89
	19.44	6.04
	23.70	4.87
	26.85	3.50
40PMMA:60PEO	15.00	0.96
	19.44	6.04
	23.33	6.08
	26.85	3.50

Figure 4.5 shows the XRD patterns of the polymer electrolytes with various weight percent of MnO<sub>2</sub> filler. Generally, it can be observed that three crystalline peaks occurred at angle of  $2\theta = 28.6^\circ$ ,  $37.4^\circ$ ,  $42.6^\circ$  and  $56.2^\circ$ . The present of these crystalline peaks were due to the presence of polymer side chains. However, the intensities of the crystalline peaks are varies with weight percent of MnO<sub>2</sub> in the polymer electrolyte Table 4.2 show the crystallite size for various composition of filler MnO<sub>2</sub> in plasticized polymer electrolytes.

Table 4.2 Crystallite sizes for various composition of filler MnO<sub>2</sub> in plasticized polymer electrolyte.

Sample	d (nm)			
2θ ± 0.01 (degree)	28.6°	37.4°	42.6°	56.2 °
54.7PMMA:13.4PEO:7.6LiClO <sub>4</sub> :19EC:5MnO <sub>2</sub> ;	0.03	-	-	-
51.9PMMA:13PEO:7.2LiClO <sub>4</sub> :18EC:10MnO <sub>2</sub>	0.07	-	0.04	-
48.9PMMA:12.2PEO:6.8LiClO <sub>4</sub> :17EC:15MnO <sub>2</sub>	0.10	0.03	0.02	0.04
46.1PMMA:11.5PEO:6.4LiClO <sub>4</sub> :16EC:20MnO <sub>2</sub>	0.25	0.07	0.02	0.07
43.2PMMA:10.8PEO:6LiClO <sub>4</sub> :15EC:25MnO <sub>2</sub>	0.11	0.05	0.03	0.05

From Table 4.2, it is observed that the composition of 54.7PMMA:13.4PEO:7.6LiClO<sub>4</sub>:19EC:5MnO<sub>2</sub> (Figure 4.5 (a)) gives the most amorphous state where the crystallite size overall were small compare to other composite electrolyte systems. In other words, this composition is said to be most homogenous composite polymer electrolyte. This implies that the optimum composition of fillers (5 wt% MnO<sub>2</sub>) has prevented the salts from totally recrystallizing out of the polymer electrolytes system and helps to dissociate the salt leading to an increase in the number density of mobile ions and conductivity. At the same time, the presence of optimum composition filler in polymer electrolyte increase the stability and mechanical strength of the polymer electrolyte which allow the fabrication of a free standing



electrolyte system. In Figures 4.5 (b) – (e), it can be observed that several crystalline peaks start to appear at angle of  $2\theta = 37.4^\circ$ ,  $42.6^\circ$  and  $56.2^\circ$ . This can be explained that the amount of filler above 5 wt% start to agglomerate with other ions components and form clustered ions in the polymer electrolyte system. Furthermore, the polymer electrolyte systems in Figures 4.5 (b) - (e) appeared to be brittle and fragile which is not stable as polymer electrolyte systems. Figure 4.6 (a) - (d) shows the XRD pattern for polymer blend, polymer electrolytes, plasticized polymer electrolytes and composite polymer electrolytes. From Figure 4.6, we can observe that the presence of filler in polymer electrolytes further suppress the crystallinity where almost no crystalline peak were observed in composite polymer electrolytes.

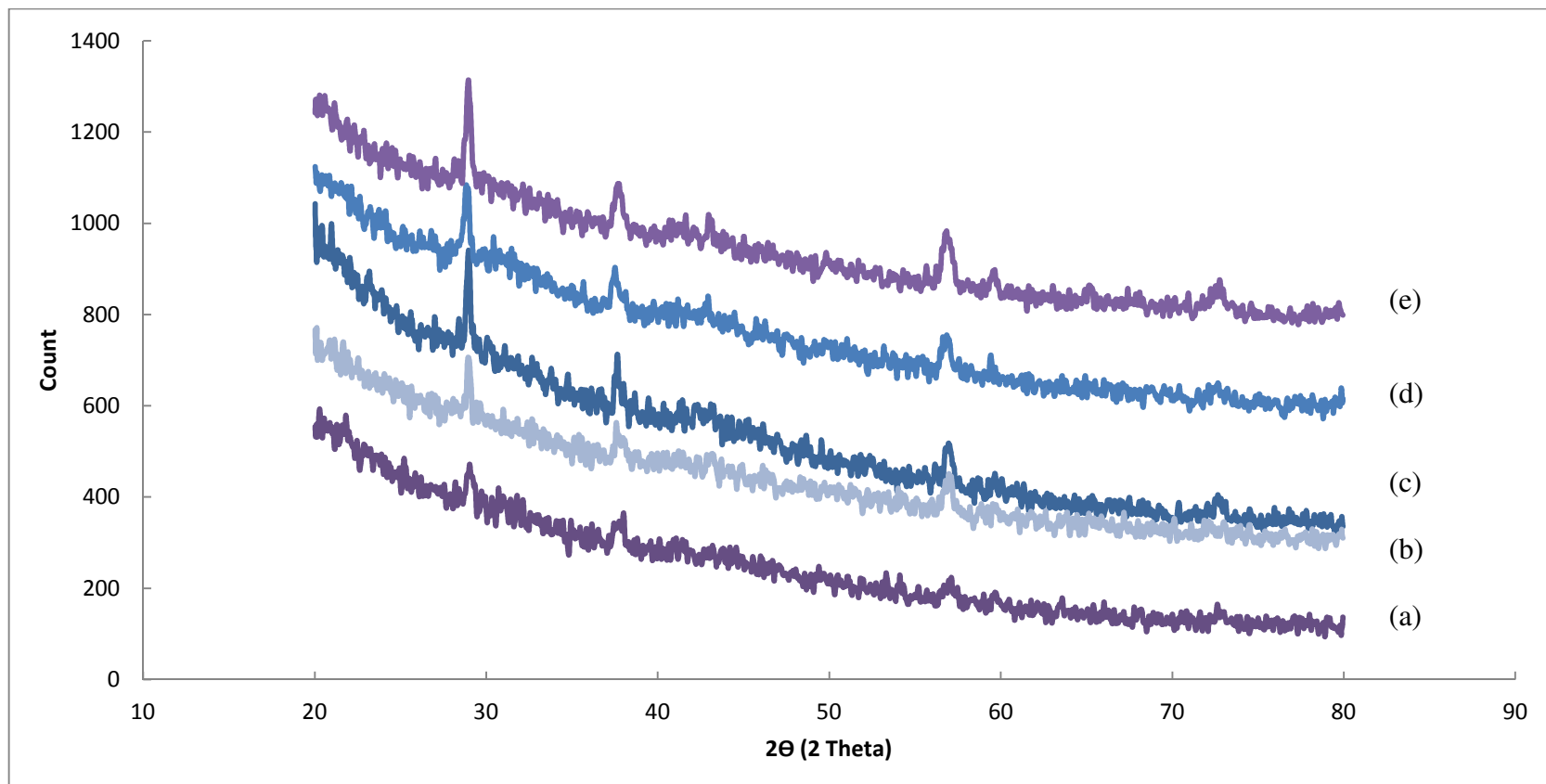


Figure 4.5 XRD patterns for polymer electrolytes with various weight percent of  $\text{MnO}_2$  nanofiller :

a) 54.7PMMA:13.4PEO:7.6LiClO<sub>4</sub>:19EC:5MnO<sub>2</sub>; b) 51.9PMMA:13PEO:7.2LiClO<sub>4</sub>:18EC:10MnO<sub>2</sub> ;

c) 48.9PMMA:12.2PEO:6.8LiClO<sub>4</sub>:17EC:15MnO<sub>2</sub>; d) 46.1PMMA:11.5PEO:6.4LiClO<sub>4</sub>:16EC:20MnO<sub>2</sub>;

e) 43.2PMMA:10.8PEO:6LiClO<sub>4</sub>:15EC:25MnO<sub>2</sub>

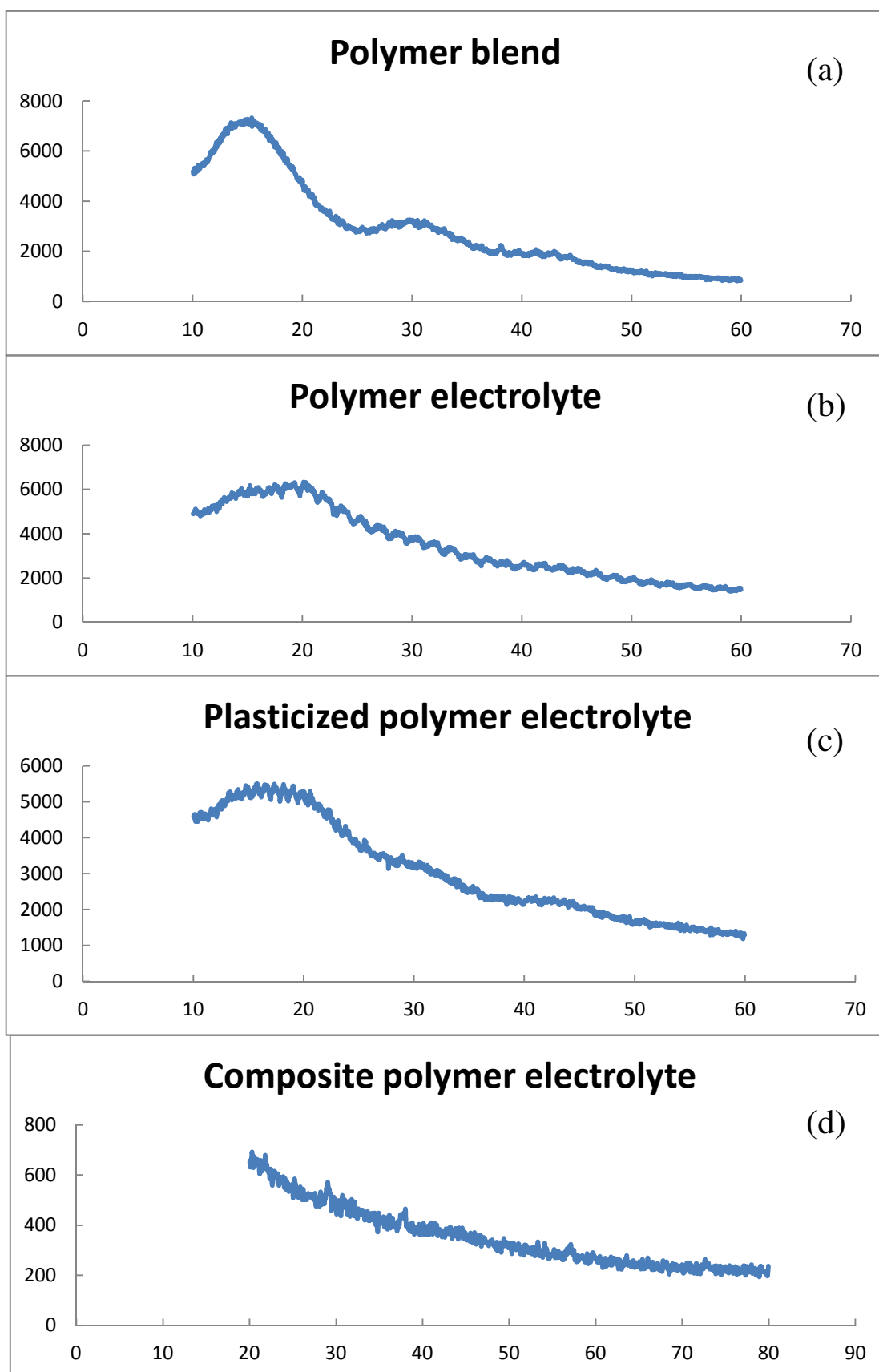
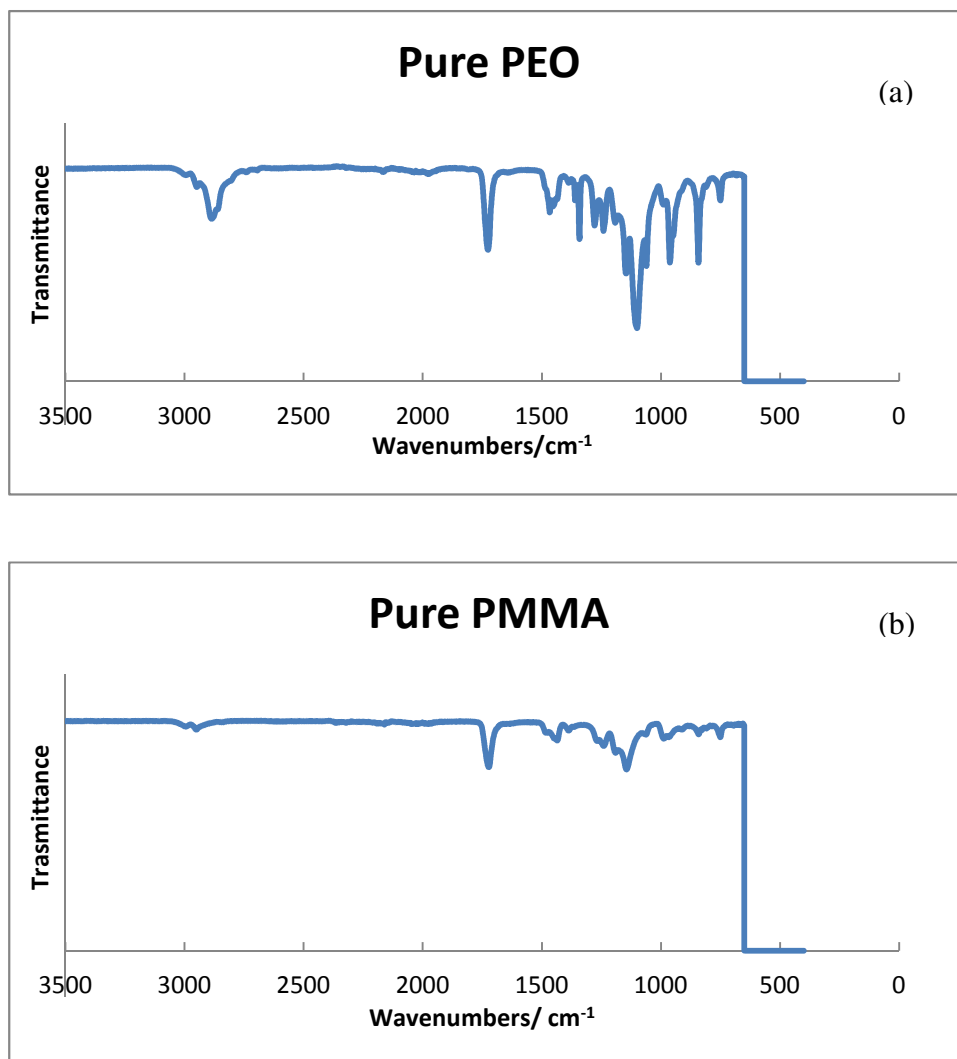


Figure 4.6 XRD pattern for (a) 80PMMA:20PEO (b) 72PMMA:18PEO:10LiClO<sub>4</sub> (c) 57.6PMMA:14.4PEO:8LiClO<sub>4</sub>:20EC (d) 54.7PMMA:13.4PEO:7.6LiClO<sub>4</sub>:19EC:5MnO<sub>2</sub>

### 4.1.3 Fourier transform infrared (FTIR) studies

Figure 4.7(a) - (f) show the FTIR spectra for pure PEO, pure PMMA, polymer blend, polymer electrolyte, plasticized polymer electrolyte and composite polymer electrolytes in the region of  $3500 - 500 \text{ cm}^{-1}$ .



. Figure 4.7 FTIR spectra for (a) pure PEO ; (b) pure PMMA

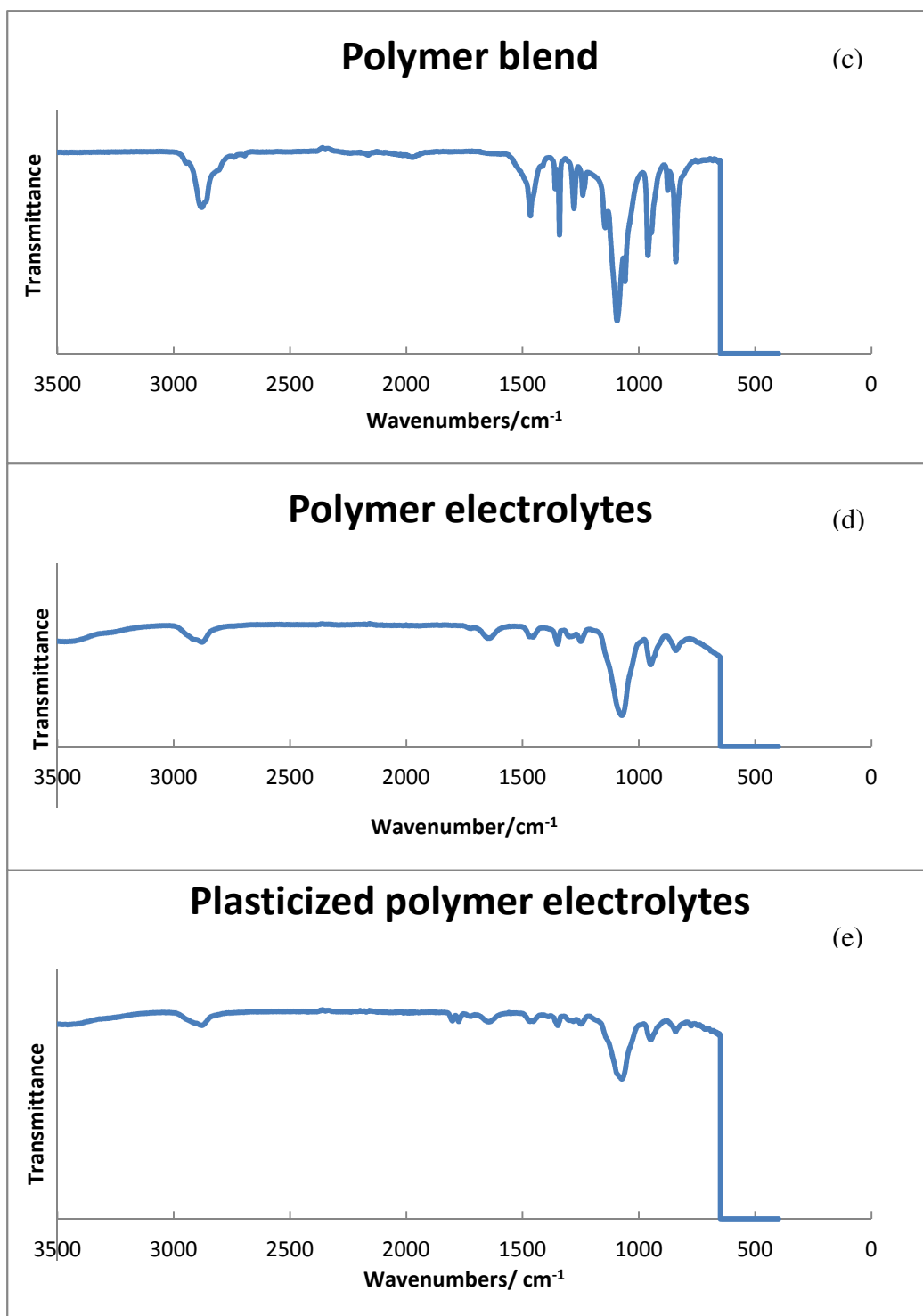


Figure 4.7 FTIR spectra for

(c) 80PMMA:20PEO polymer blend ;

(d) 72PMMA:18PEO:10LiClO<sub>4</sub> polymer electrolyte

(e) 57.6PMMA:14.4PEO:8Li:20EC plasticized polymer electrolyte

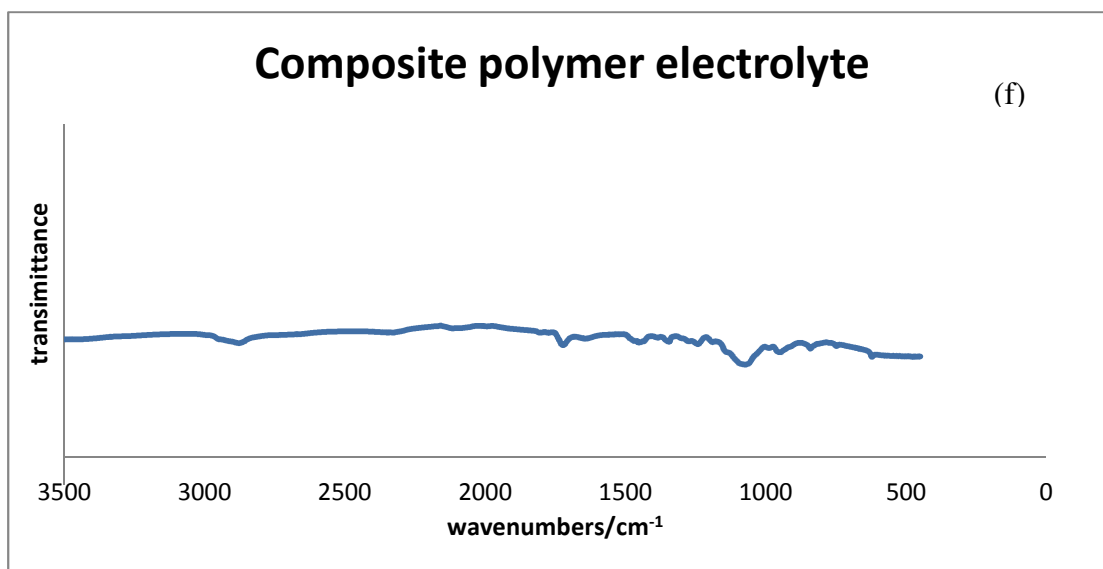


Figure 4.7 (f) FTIR spectra for 54.7PMMA:13.4PEO:7.6LiClO<sub>4</sub>:19EC:5MnO<sub>2</sub> composite polymer electrolyte.

FTIR spectroscopy has been used to identify the functional groups and the interaction between components in a system. Figures 4.7 (a) – (c) show the FTIR spectra for pure PEO, pure PMMA and polymer blend system respectively. For pure PMMA the frequency at  $842\text{ cm}^{-1}$  is assigned to C-H rocking vibrations. The frequencies at  $2950\text{ cm}^{-1}$  and  $1242\text{ cm}^{-1}$  are assigned to CH<sub>2</sub> stretching and O-CH<sub>2</sub> deformation vibrations of pure PMMA. The peaks at  $950\text{ cm}^{-1}$  and  $1240\text{ cm}^{-1}$  may be assigned to CH<sub>2</sub> wagging and CH<sub>2</sub> rocking vibrations respectively in pure PEO. The absorption peaks at  $1454\text{ cm}^{-1}$ ,  $1889\text{ cm}^{-1}$  and  $2889\text{ cm}^{-1}$  are assigned to asymmetric C-H stretching in pure PEO. The peak at  $1736\text{ cm}^{-1}$  corresponding to the stretching frequency of C=O of pure PMMA is shifted to about  $1432\text{ cm}^{-1}$  in the PMMA-PEO polymer blend. The frequency  $1151\text{ cm}^{-1}$  due to the C-C vibration is shifted to  $948\text{ cm}^{-1}$  in the polymer blend. The C-C stretching frequency  $1354\text{ cm}^{-1}$  of pure PEO is shifted to about  $1145\text{ cm}^{-1}$  in the polymer blend. The shifted broad peaks found in the polymer

electrolyte originated from the complex formation between all the components in the polymer electrolyte system. The formation of new peaks along with changes in the existing peaks in the FTIR spectra confirms the complexation. These results suggest that homogeneous polymer complex are formed over all the blend compositions.

On the other hand, Figure 4.7 (d) - (f) show the FTIR spectra for salt added polymer electrolyte, plasticized polymer electrolytes and composite polymer electrolytes. It can also be observed that the intensity of absorption band at most of the peaks are reduced when salt, plasticizer and filler are added. This shows that the complexation has occurred between polymer blend, lithium perchlorate salt, EC plasticizer and MnO<sub>2</sub> fillers. In spite of that, in Figure 4.7 (e) the peak at 928 cm<sup>-1</sup> that assigned to C=O bending band, and slightly shifted to 716 cm<sup>-1</sup> due to the interaction of polymers with the CH<sub>2</sub> bending band at 1480 cm<sup>-1</sup> of pure EC. The band at 1860 cm<sup>-1</sup> is due to C=O stretching of pure EC. The ring breathing of EC at 1803 cm<sup>-1</sup> disappears in the polymer electrolyte system, indicating the occurrence of interactions between the polymers and plasticizer, EC. There is hardly any noticeable shift in peaks of the plasticized polymer electrolytes and composite polymer electrolytes as presented in Figures 4.7 (d) and (e). Hence, it can conclude that filler addition does not interact much with the components in plasticized polymer electrolyte, yet only stabilize the modification of bond in plasticized polymer electrolytes and provide inner driving force in addition to the external driving force of the applied electric field (Rajendra *et al.* 2000).

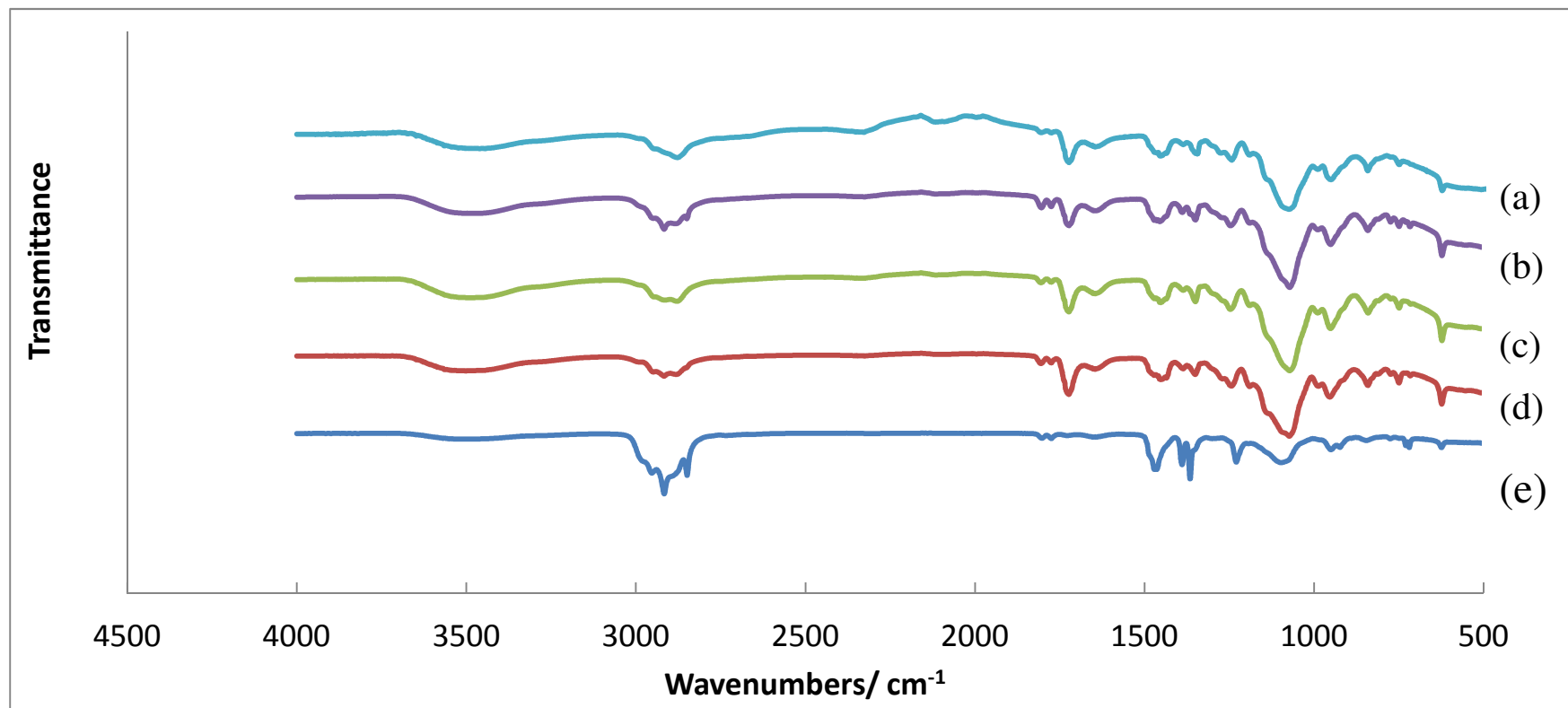


Figure 4.8 FTIR spectra for the optimum concentration of polymer electrolytes with various weight percent of  $\text{MnO}_2$  nanofiller:

- (a) 54.7PMMA:13.4PEO:7.6LiClO<sub>4</sub>:19EC:5MnO<sub>2</sub>
- (b) 51.9PMMA:13PEO:7.2LiClO<sub>4</sub>:18EC:10MnO<sub>2</sub>
- (c) 48.9PMMA:12.2PEO:6.8LiClO<sub>4</sub>:17EC:15MnO<sub>2</sub>
- (d) 46.1PMMA:11.5PEO:6.4LiClO<sub>4</sub>:16EC:20MnO<sub>2</sub>
- (e) 43.2PMMA:10.8PEO:6LiClO<sub>4</sub>:15EC:25MnO<sub>2</sub>

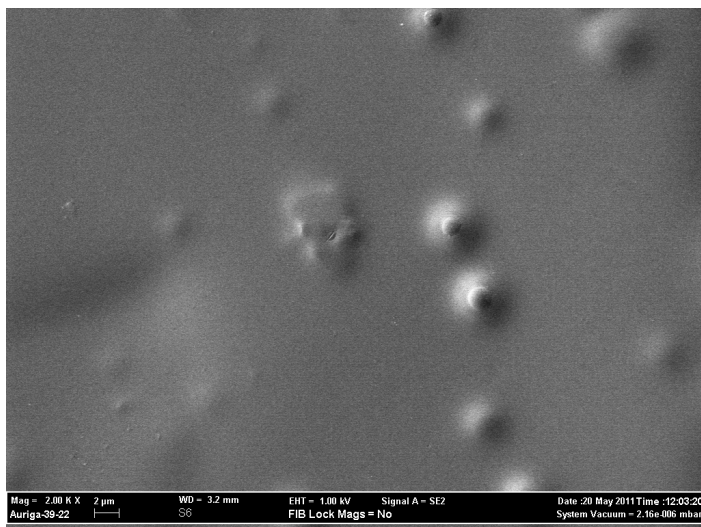


Figure 4.8 show the FTIR spectra for PMMA-PEO-LiClO<sub>4</sub>-EC-MnO<sub>2</sub> polymer electrolytes in region 4500 – 5000 cm<sup>-1</sup>. It can be observed the present of new peaks at 2916 and 2848 cm<sup>-1</sup> for the sample containing 25wt% of MnO<sub>2</sub>.. The interactions between the polymer electrolytes and MnO<sub>2</sub> filler may result in “charge transfer”, whereby the sp<sup>2</sup> carbons in the polymer blend matrix compete with dopant ions and perturb the H-bond, resulting in an increase in the stretching intensity (Rajendra *et al.*, 2000). In the region of 2000 to 3000 cm<sup>-1</sup>, the intensities of the peaks decrease with decreasing filler contents. The ionic conduction is higher due to the contribution of filler which provides an inner driving force in addition to the external driving force of the applied electric field (Rajendra *et al.* 2000). Therefore, it can be concluded that the nanocomposite polymer electrolyte containing the optimum concentration of MnO<sub>2</sub> filler is more sensitive to the external electric fields and is more efficient for the conduction of lithium ions. These observations imply that there are interactions between the components in the polymer electrolyte system. From the above analysis, the complex formation of nanocomposite polymer electrolyte has been confirmed.

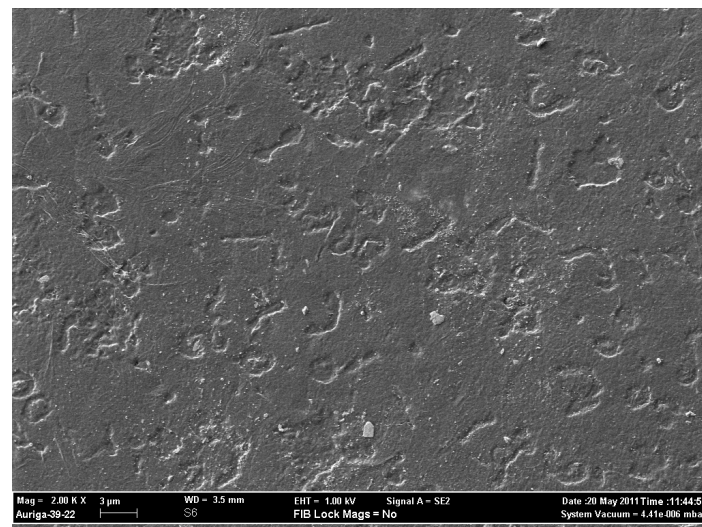
#### 4.1.4 Morphological studies

Figures 4.9 (a) – (d) show the surface morphologies of PMMA-PEO, PMMA-PEO-LiClO<sub>4</sub>, PMMA-PEO-LiClO<sub>4</sub>-EC and PMMA-PEO-LiClO<sub>4</sub>-EC-MnO<sub>2</sub> polymer electrolyte systems. The figures show a marked change in the surface properties on the addition of salts, plasticizer and filler. Prior to the addition of plasticizer, the micrograph of PMMA-PEO and PMMA-PEO-LiClO<sub>4</sub> (Figure 4.9 (a) and Figure 4.9 (b)) show a smooth surface with low crystalline domain. After plasticizer addition (Figure 4.9 (c)), the micrograph of plasticized polymer electrolyte shows the presence of spherulites, which is the characteristic of lamellar structure, with surface roughness that may be related to the crystalline fraction of the material. The boundary between the spherulites is the amorphous phase regions (Dhilip *et al*, 2010). The effect of adding EC, plasticizer is in the highest conducting sample of PMM-PEO-LiClO<sub>4</sub> system has been investigated. It is observed that the samples are softer and less brittle.

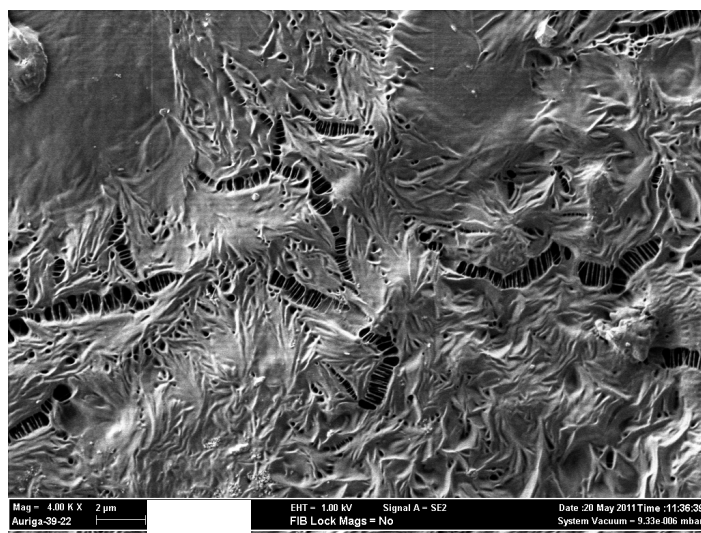
Upon addition of filler, there was a decrease in the spherulite size and hence a substantial increase in the amorphous boundary region. The surface roughness and crystalline texture are decreased ultimately resulted in smooth texture of the surface. Therefore, the filler addition helps in further reducing the crystallinity of the polymer electrolyte films, which is responsible for obtaining higher conductivity. Figure 4.9(d) shows the micrograph image of nanocomposites polymer electrolytes which recorded the highest ionic conductivity. It shows that the MnO<sub>2</sub> nanoparticles are distributed randomly in the polymer host (Mohd Rafie Johan *et al*, 2011). Furthermore, there are no define boundaries for foreign impurities exist which also justify the homogeneity of the mixture.



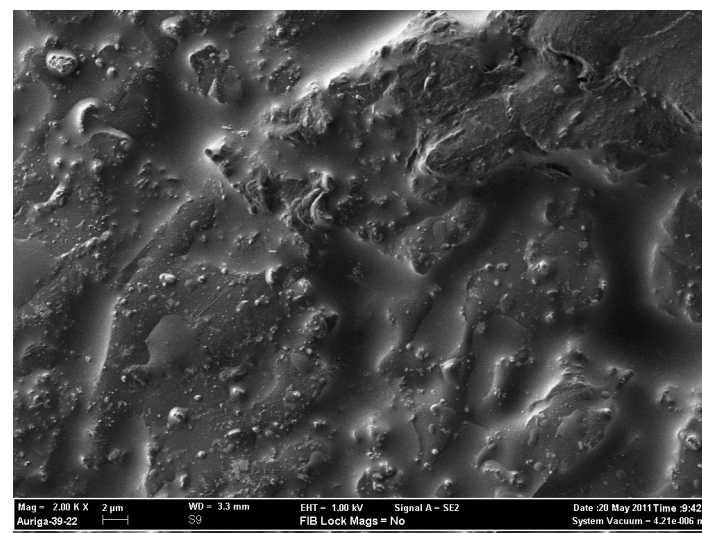
(a)



(b)



(c)



(d)

Figure 4.9 FESEM images for (a) 80 wt% PMMA-20 wt% PEO, (b) 72 wt% PMMA-18 wt% PEO- 10 wt%LiClO<sub>4</sub>, (c) 57.6 wt% PMMA-14.4 wt% PEO-8 wt% LiClO<sub>4</sub>-20 wt% EC, (d) 54.72 wt% PMMA-13.68 wt% PEO-7.6 wt% LiClO<sub>4</sub>-19 wt% EC-5 wt% MnO<sub>2</sub>

## 4.2 Conductivity Studies

Figure 4.10 (a) shows the typical Nyquist plot of PEO-PMMA polymer electrolytes at various weight percent of PMMA. The value of conductivity of the polymer blend is contributed by the presence of mobile ions in the air and surrounding. The typical Nyquist plot of PEO-PMMA comprises of a broadened semicircle which attributed to the due to the parallel combination of bulk resistance (due to the migration of ions) and bulk capacitance (due to the immobile polymer chains). The frequency response of the polymer electrolyte could be represented by an equivalent circuit consisting of a parallel combination of resistance and capacitance (Macdonald, 1987). The presence of the depressed semicircle reveals the non-Debye nature of the sample due to the potential well for each site, through which the ion transport takes place, not being equal (Lanfredi *et al*, 2002). The intercept of the semicircle with the real axis ( $Z_{\text{real}}$ ) at low frequency give rise to the bulk resistance ( $R_b$ ) of the materials. It is evident from the plot that 80:20 weight percent of PMMA/PEO has the smallest diameter of impedance arc. This indicate that this composition of electrolyte possess highest ionic conductivity.

Figure 4.10 (b) shows the variation of ionic conductivity for different weight percent of PMMA-PEO. It is notable that the ionic conductivity of the polymer blend composition of 80 wt% of PMMA and 20wt% of PEO showed the highest value at room temperature which is  $2.02 \times 10^{-8}$  S/cm. A small decrease in conductivity is observed for a composition beyond 80 wt% of PMMA due to viscosity in the polymer blend which later was further justified by DSC.

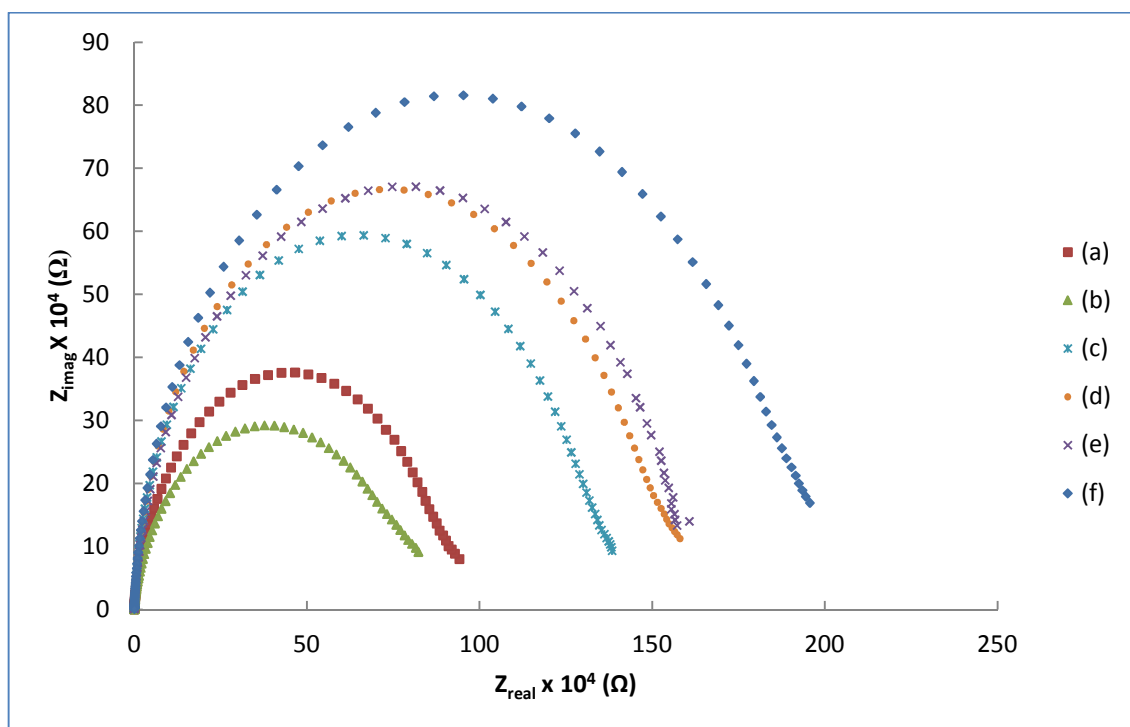


Figure 4.10 (a) Complex impedance spectra of polymer electrolytes at various weight percent of PMMA/PEO blend: (a) 90:10 (b) 80:20 (c) 70:30 (d) 60:40 (e) 50:50 (f) 40:60

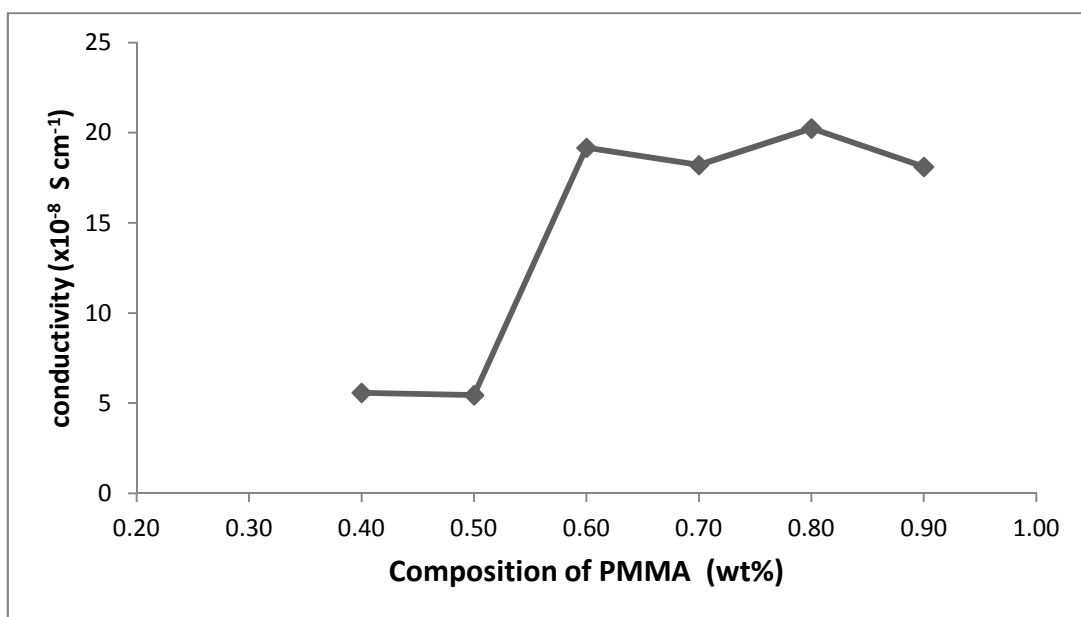


Figure 4.10 (b) Variation of conductivity for different weight percent of PMMA/PEO

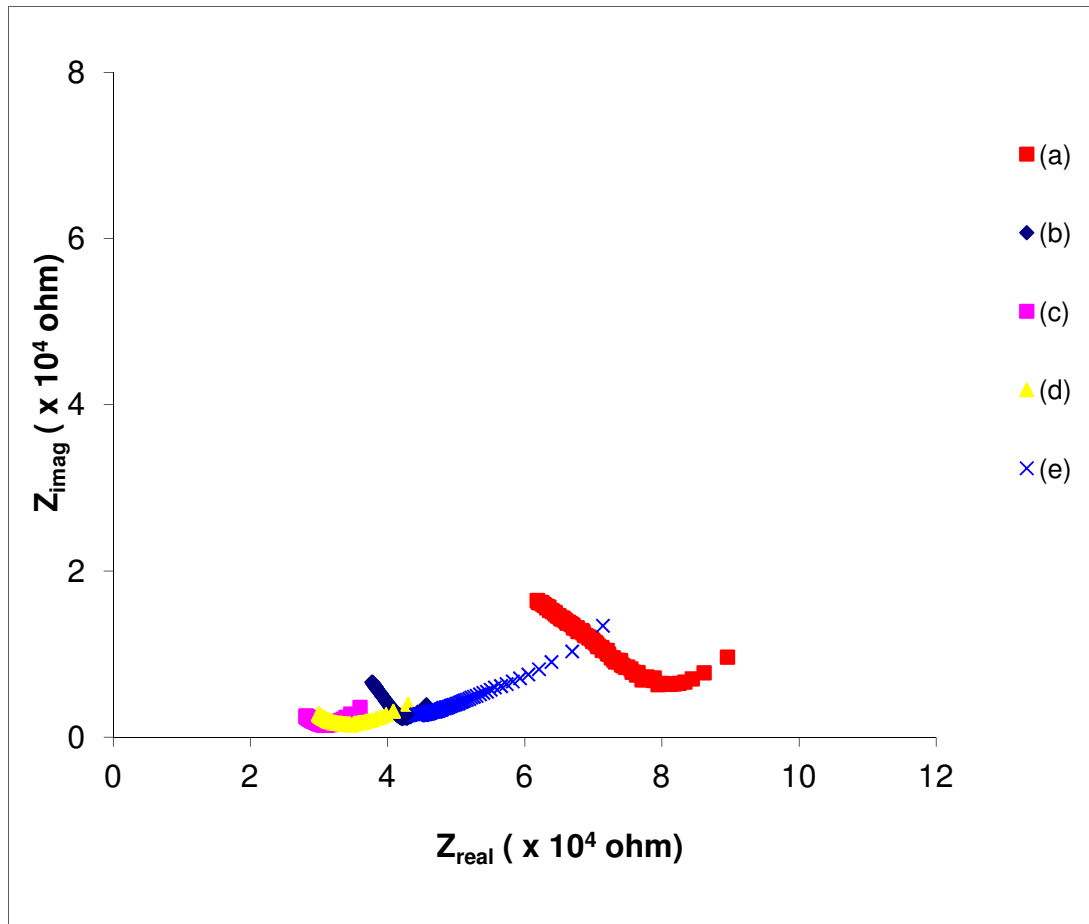


Figure 4.11 (a) Complex impedance spectra of polymer electrolytes 80:20 wt% of PMMA/PEO at various  $\text{LiClO}_4$ : (a) 2.5 wt%; (b) 5 wt%; (c) 7.5 wt%; (d) 10 wt% (e) 12.5 wt%

Figure 4.11(a) shows the complex impedance spectra of 80:20 wt% of PMMA/PEO blend at various  $\text{LiClO}_4$ . The absence of symmetrical semicircle observed at high frequencies suggests that the presence of electrical processes in the material with a spread of relaxation time. The relaxation process might be due to the presence of immobile species/electrons at low temperature and defects/vacancies at higher temperature. The present of inclined spike at low frequency represents the formation of double layer capacitance at the electrode–electrolyte interface due to the migration of ions. The electrode double layer at each interface possesses increasing impedance against ion transfer with decrease in frequency (Bohnke *et al*, 1993). Furthermore the

inclination of the spike at an angle less than  $90^\circ$  to the real axis is due to the roughness of the electrode–electrolyte interface (Ressy *et al*,2007).

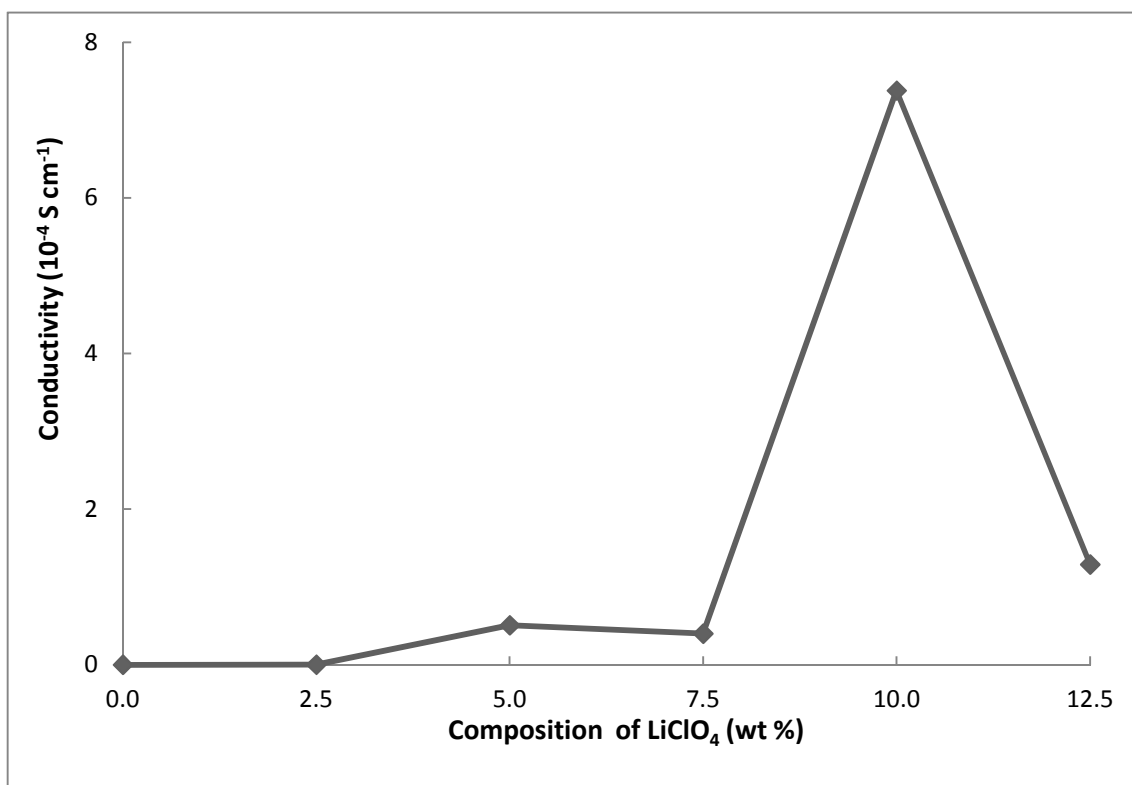


Figure 4.11 (b) Variation of conductivity for 80:20 wt% PMMA-PEO with different wt % of LiClO<sub>4</sub>

Figure 4.11 (b) shows the impedance spectra of PEO-PMMA blend at various weight percent of LiClO<sub>4</sub> salts. It can be observed that the conductivity of the polymer blend increases with the increase in salt content. The highest value of conductivity is  $7.38 \times 10^{-4} \text{ S cm}^{-1}$  for 10wt% of LiClO<sub>4</sub>. As the salt content increases, the number of free mobile ions increases and thus increases the ionic conductivity,  $\sigma$ . However, for system with salt content beyond 10 wt% of LiClO<sub>4</sub>, the conductivity decreases because ions start to agglomerate and decrease the number of free mobile ions.

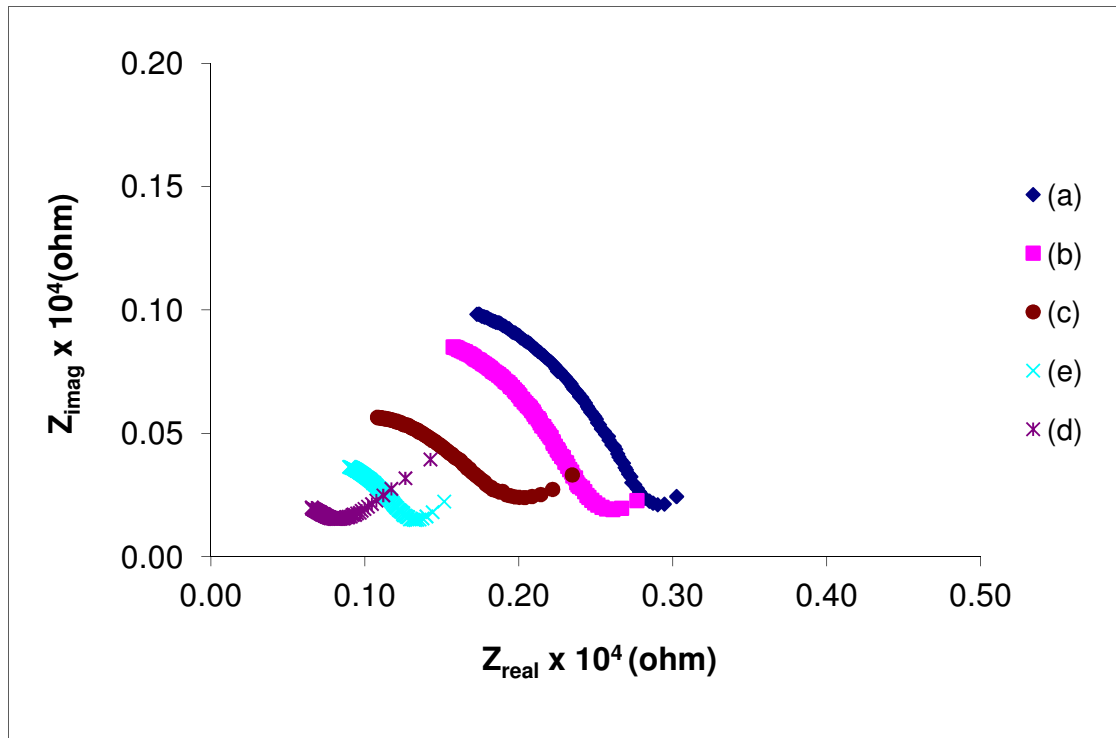


Figure 4.12 (a) Complex impedance spectra for PMMA/PEO/LiClO<sub>4</sub> polymer electrolytes at various EC plasticizer: (a) 5 wt% (b) 10 wt% (c) 15 wt% (d) 20 wt% (e) 25 wt%

Figure 4.12 (a) shows the impedance spectra of Complex impedance spectra of PMMA/PEO/LiClO<sub>4</sub> polymer electrolytes at various wt% EC plasticizers. The presence of asymmetric semicircle in the higher frequency region is due to bulk and grain boundary resistance of the electrolyte. The inclined straight line at lower frequency region with the real axis can be attributed due to the capacitance of electrolyte/electrode double layer. The diameter within the semi-circle of the Nyquist plots decreases with increasing the concentration of plasticizer. This may be associated with the substantial decrease in grain boundary resistance of the materials when the concentration of plasticizer is increased (Wang *et al*, 2005). As a result, the movement of Li<sup>+</sup> ion through the polymer chain becomes easier. This provide the evidence that plasticizer plays an important role in influencing the ionic conductivity of polymer electrolyte system.



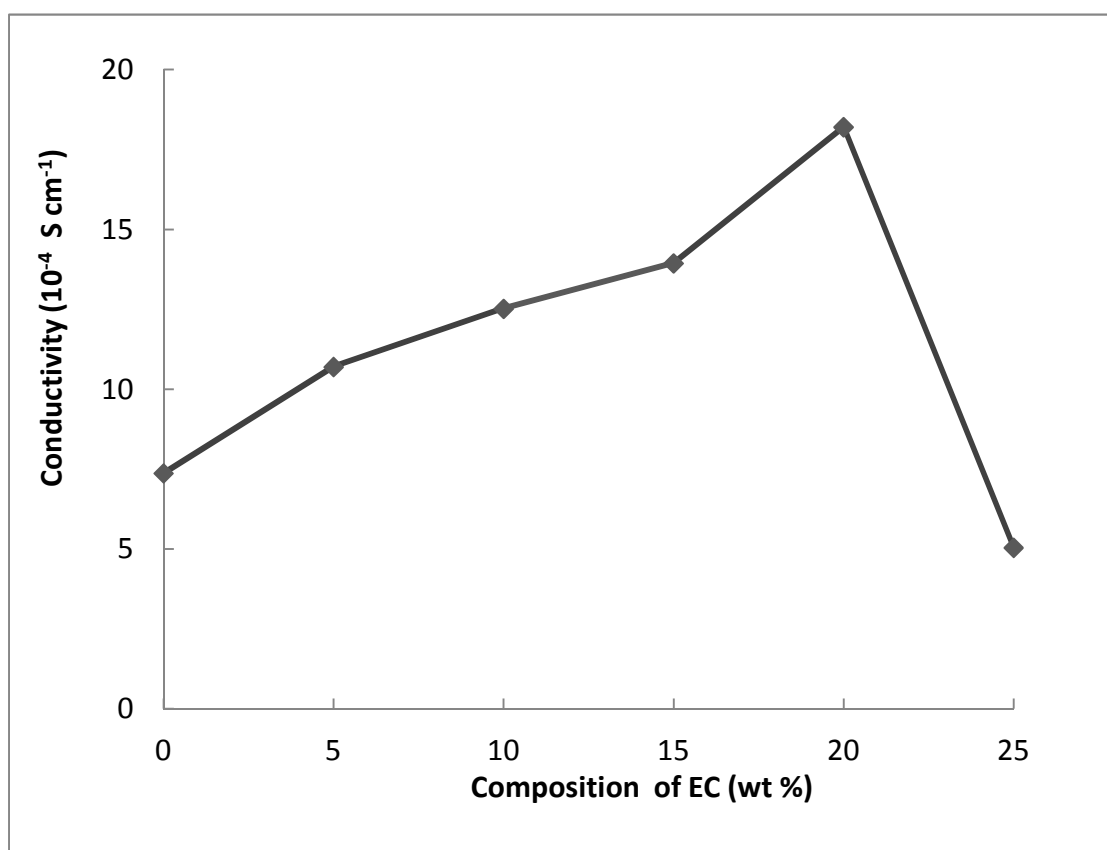


Figure 4.12 (b) Variation of ionic conductivity for PMMA/PEO/LiClO<sub>4</sub> with different weight percent of EC.

Figure 4.12 (b) shows the effect of EC on the conductivity of the highest conducting PMMA-PEO-LiClO<sub>4</sub> sample. It is observed that the ionic conductivity of the salted polymer blend electrolyte is increased upon the addition of EC plasticizer. EC possess the properties of low viscosity and high dielectric constant, which facilitates to dissociate more salts into ions and increases the ionic conductivity. The maximum conductivity value of  $1.82 \times 10^{-3} \text{ S cm}^{-1}$  is obtained at 20 wt% of the plasticizer content and decrease again at EC content of 25 wt%. This decrease in conductivity could be due to ion aggregation. This is because ion aggregation decreases the available number of charge carriers.

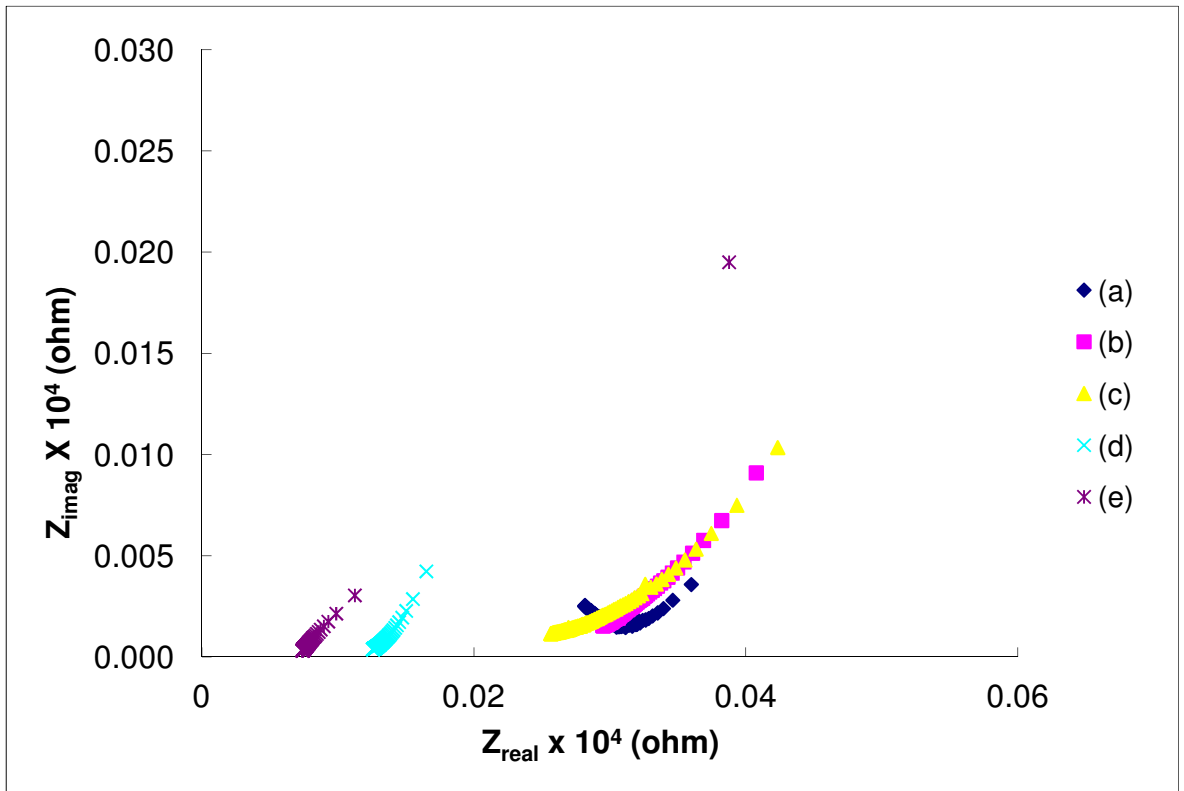


Figure 4.13 (a) Complex impedance spectra for 80:20:10:20 wt% of PMMA/PEO/LiClO<sub>4</sub>/EC polymer electrolytes at various MnO<sub>2</sub> filler: (a) 5 wt% (b) 10 wt% (c) 15 wt% (d) 20 wt% (e) 25 wt%

Figure 4.13 (a) shows the impedance spectra of 80:20:10:20 weight percent of PMMA/PEO/LiClO<sub>4</sub>/EC polymer electrolytes at various wt% of MnO<sub>2</sub> filler. It is noted that the semicircle observed at high frequencies completely disappears when nano-fillers MnO<sub>2</sub> were added into the plasticized polymer electrolyte. This result suggests that, only the resistive component of polymer electrolyte prevails (Kim *et al*, 1998). In the low frequency response region, the appearance of the non-vertical spike is attributed to the additional capacitance and resistance contribution arising out of dielectric relaxation and ion trapping in the polymer electrolyte network (Wright *et al*, 1982).

Figure 4.13 (b) shows the effect of  $\text{MnO}_2$  nano-filler on the conductivity of the highest conducting PMMA-PEO- $\text{LiClO}_4$ -EC sample. It is observed that the conductivity increases upon the addition of  $\text{MnO}_2$  filler with a maximum value of  $5.02 \times 10^{-3} \text{ S cm}^{-1}$  at room temperature. The addition of nano-filler retards the recrystallization of polymer chains. Since the size of filler is too small compared to the polymer host, the filler is able to penetrate into the polymer matrix and promotes an interaction between filler, plasticizer and polymer chain molecules. Consequently, the cohesive force between the polymer chains is reduced and provides a more flexible chain segmental motion (Uma *et al*, 2004).

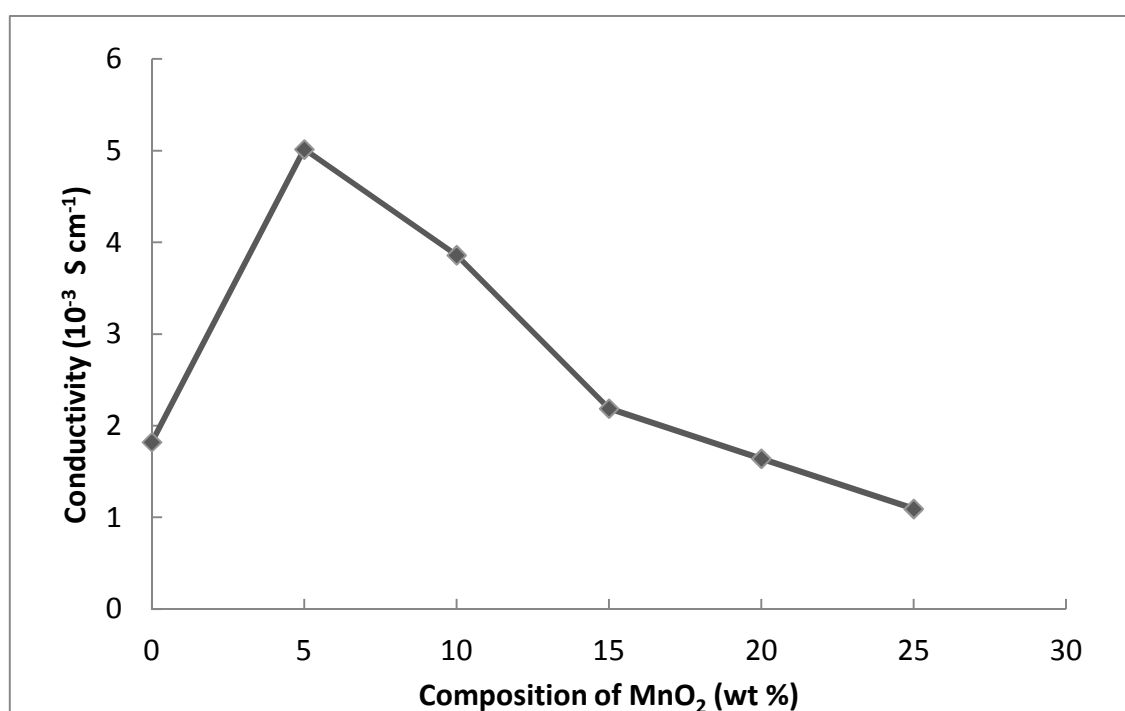


Figure 4.13 (b) Variation of ionic conductivity 80:20:10:20 wt% of PMMA/PEO/ $\text{LiClO}_4$ /EC polymer electrolyte with respect to filler content at room temperature

Figure 4.14 (a) – (d) show the temperature dependence of ionic conductivity for various polymer electrolyte systems. All the curves display similar behaviour, i.e. a combination of VTF and Arrhenius behaviour. Arrhenius region is noticed in low temperature regime while VTF nature is exhibited at higher temperature. The effect of temperature (T) on conductivity is not governed by the classical theory that is the dependence of conductivity on temperature does not follow only the Arrhenius law where the activation energy for the ion's motion in polymer matrix is dominant. When ion transport is facilitated by the mobility of the polymer, the conductivity may obey the Vogel-Tammann-Fulcher (VTF) relation at higher temperature around melting temperature of the polymer electrolytes. (Appetecchi *et al*, 1998).

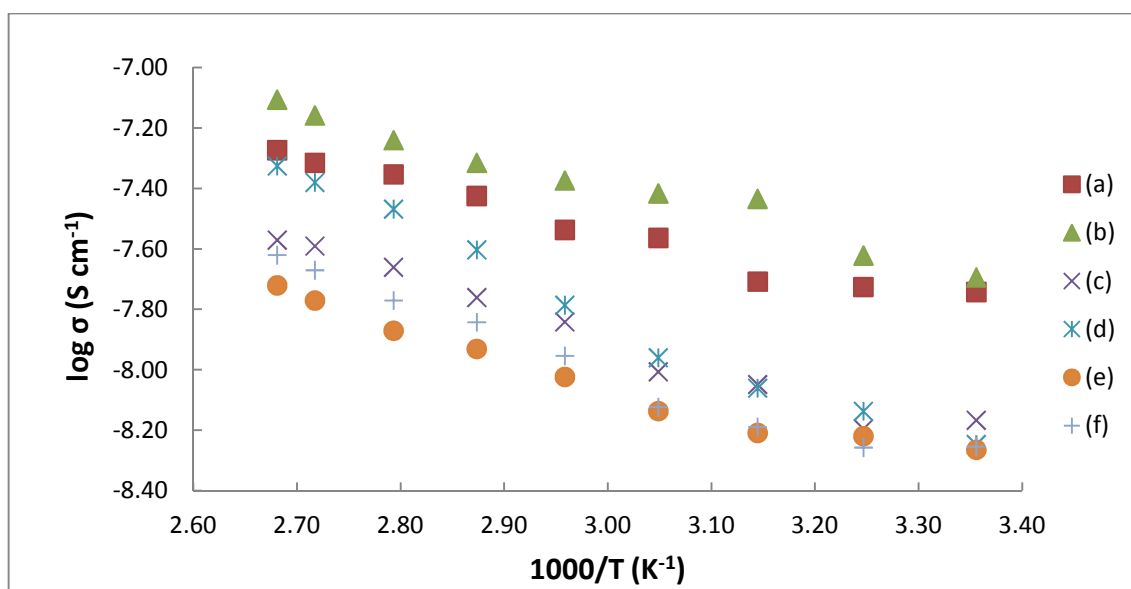


Figure 4.14 (a) Temperature dependence of ionic conductivity for various weight percent of PMMA: PEO blend polymer electrolyte systems: 90:10; (b) 80:20; (c) 50:50; (d) 60:40; (e) 50:50; (f) 40:60

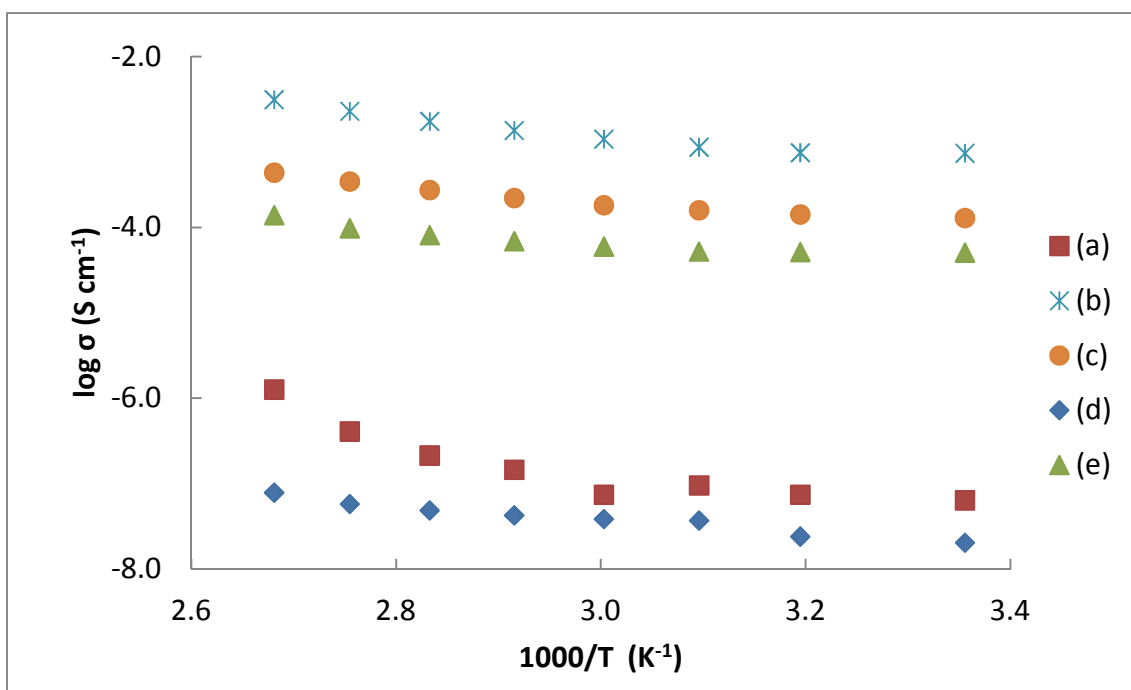


Figure 4.14 (b) Temperature dependence of ionic conductivity for PMMA/PEO blend at various weight percent of LiClO<sub>4</sub> salt: (a) 2.5 wt% (b) 5 wt% (c) 7.5 wt% (d) 10 wt% (e) 12.5 wt%

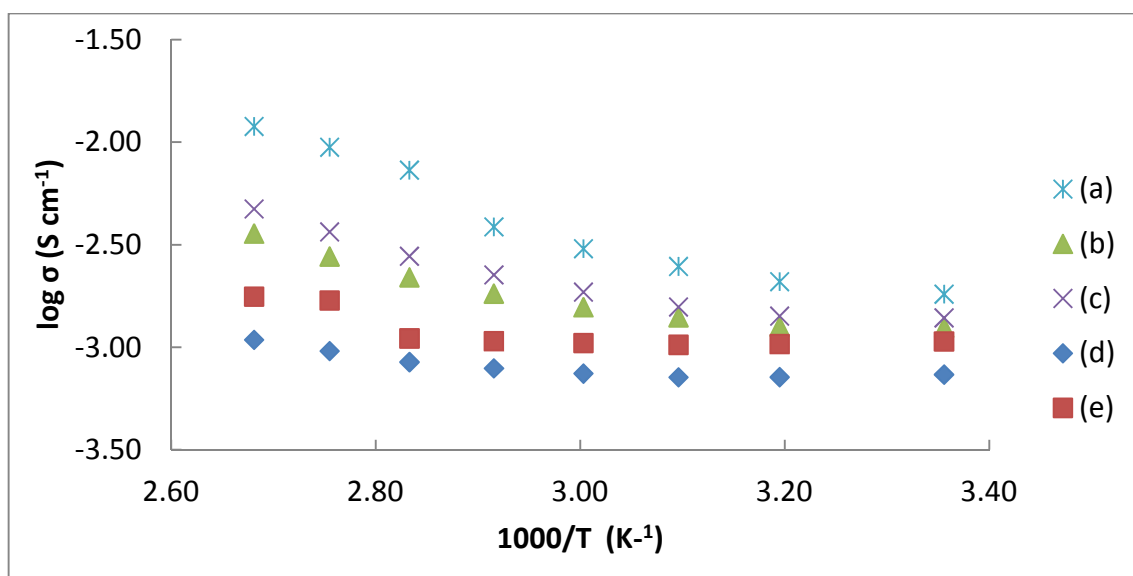


Figure 4.14 (c) Temperature dependence of ionic conductivity for PMMA/PEO/LiClO<sub>4</sub> at various weight percent of EC plasticizer: (a) 5 wt% (b) 10 wt% (c) 15 wt% (d) 20 wt% (e) 25 wt%

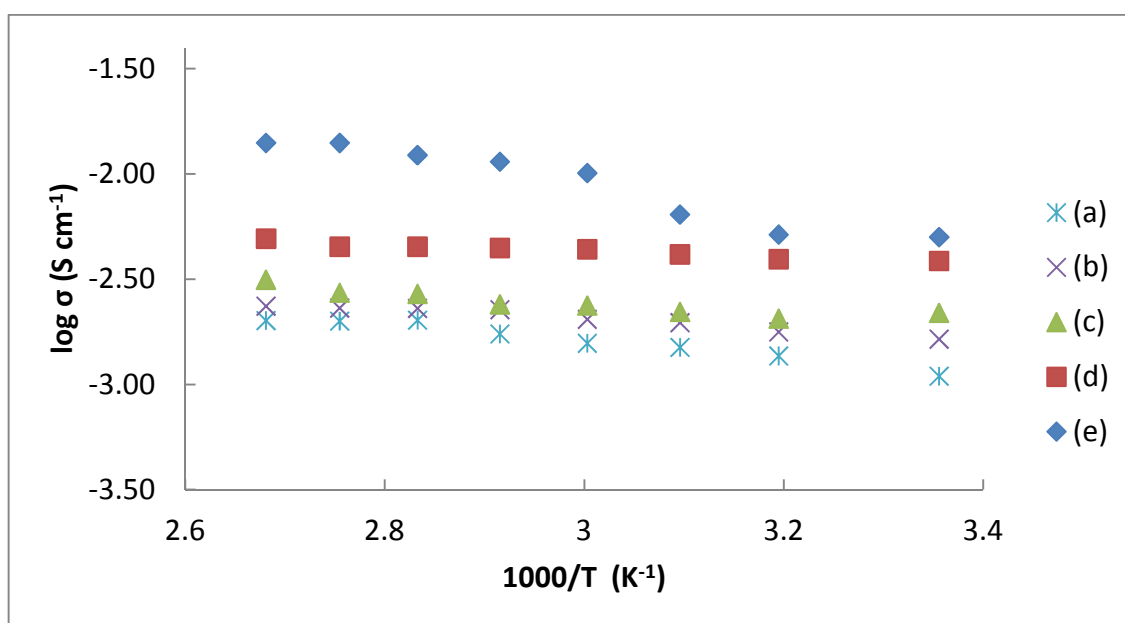


Figure 4.14 (d) Temperature dependence of ionic conductivity for PMMA/PEO/LiClO<sub>4</sub>/EC at various weight percent of MnO<sub>2</sub> filler: (a) 5 wt% (b) 10 wt% (c) 15 wt% (d) 20 wt% (e) 25 wt%

### 4.3 Dielectric Studies

Figures 4.15 – 4.16 show the frequency dependence of real and imaginary parts of the dielectric relaxation curves for 80:20 wt% of PMMA/PEO, 80:20:10 wt% of PMMA/PEO/LiClO<sub>4</sub>, 80:20:10:20 wt% of PMMA/PEO/LiClO<sub>4</sub>/EC and 80:20:10:20:5 wt% of PMMA/PEO/LiClO<sub>4</sub>/EC/MnO<sub>2</sub> polymer electrolyte system. Both real and imaginary parts of the dielectric constant rise sharply towards low frequencies. However the rise is displaced to higher frequencies upon addition of salts, plasticizer and filler into the polymer electrolyte systems. The periodic reversal of the electric field occurs extremely fast at high frequencies and that there is no excess of ion diffusion in the direction of the field. The polarization due to the charge accumulation decreases, leading to the decrease in the value of the real and imaginary part of dielectric constant (Ramesh *et. al.*, 2001)

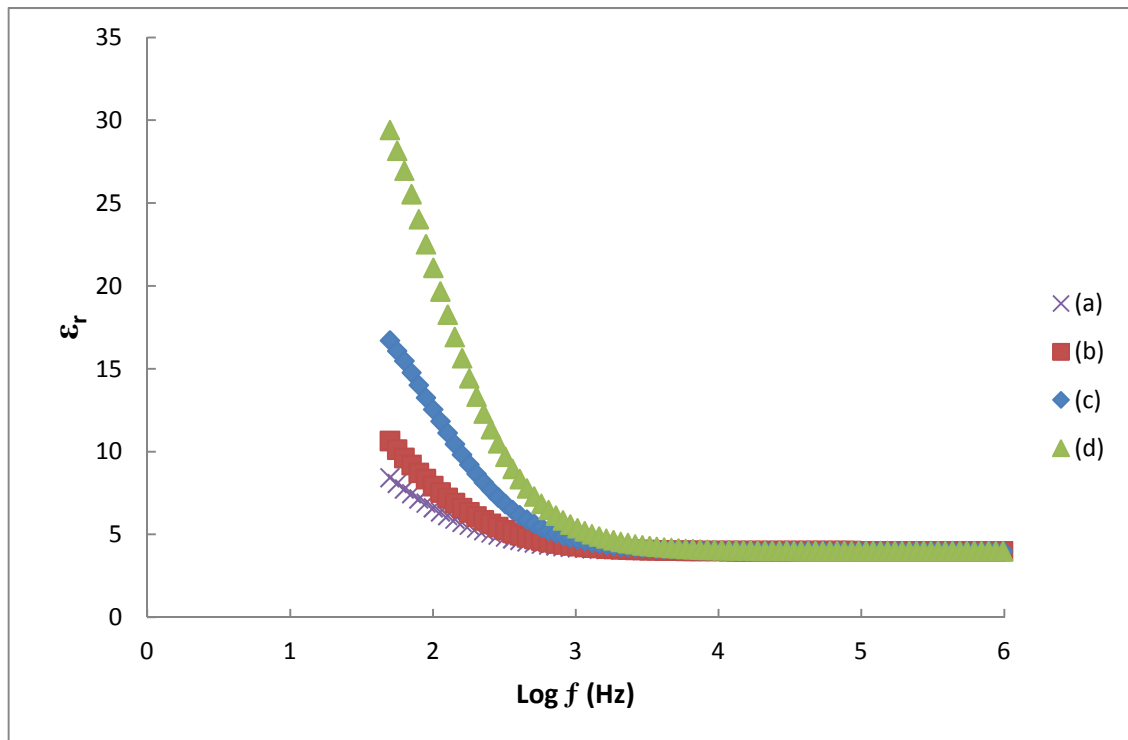


Figure 4.15 Variation of real part of dielectric constant of (a) PMMA-PEO, (b) PMMA-PEO-LiClO<sub>4</sub>, (c) PMMA-PEO-LiClO<sub>4</sub>-EC and (d) PMMA-PEO-LiClO<sub>4</sub>-EC-MnO<sub>2</sub> at room temperature.

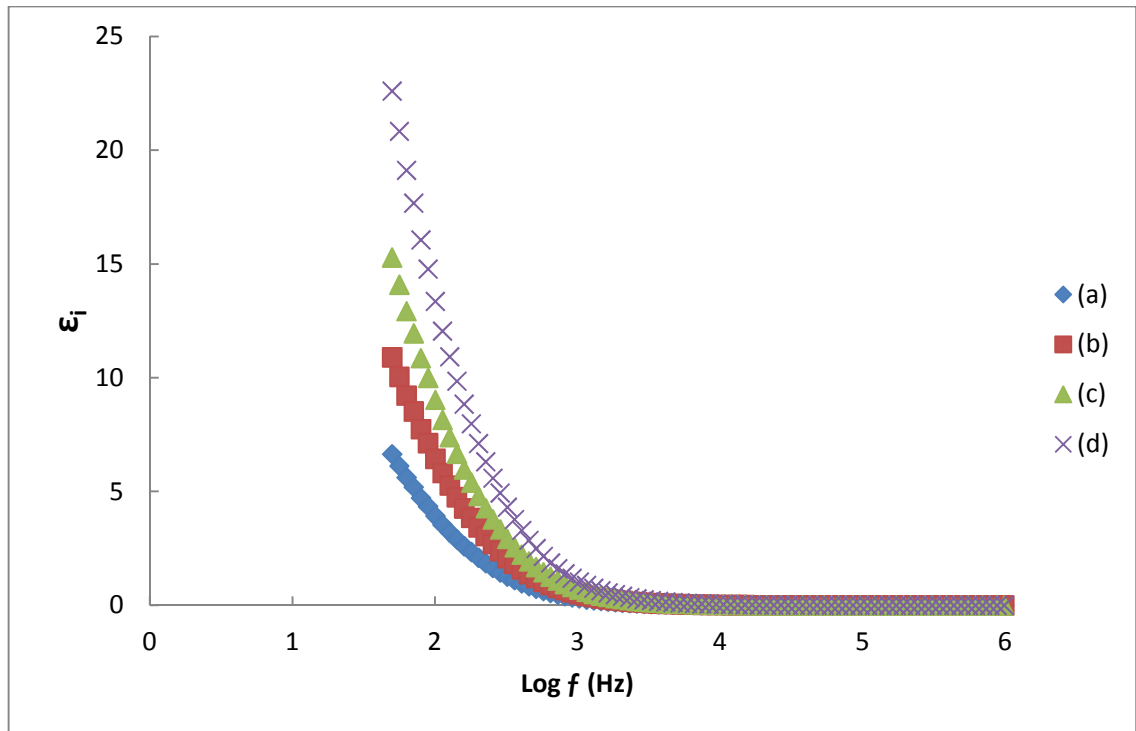


Figure 4.16 Variation of imaginary part of dielectric constant of (a) PMMA-PEO, (b) PMMA-PEO-LiClO<sub>4</sub>, (c) PMMA-PEO-LiClO<sub>4</sub>-EC and (d) PMMA-PEO-LiClO<sub>4</sub>-EC-MnO<sub>2</sub> at room temperature.

When LiClO<sub>4</sub> salt was added into the PMMA-PEO electrolyte system, the dielectric constant rose sharply at low frequencies. This behaviour indicates that the electrode polarization and space charge effects were occurred (Tambelli, 2002). The cation of salts forms transient cross-links with the chain segment by coordination with oxygen atom on the PEO backbone and thus leads to the polymer-salt interaction. Thereby, it causes steric hindrance in rotation of the dipoles as a results of cross-linking. The results tend to increase the dielectric constant value but with a sharp fall as the frequency increases.

The dielectric constant  $\epsilon_r$  increase with decreasing frequency after the addition of plasticizer EC. This is attributed to the high concentration of charge accumulation at



the electrode-electrolyte interface (Baskaran *et al*, 2004). However, a rapid decrease in dielectric constant was observed within the frequency range of 1-10 kHz. This may attributed to the tendency of dipoles in macromolecules to orient themselves in the direction of the applied field in the low frequency range.

Apparently, it can be observed that a large increase of  $\epsilon_r$  and  $\epsilon_i$  upon the addition of MnO<sub>2</sub> fillers due to dipolar and free charge contributions. Further increase of the molecular mobility is reflected both by the increase of free charge mobility and the shifting of peak towards the higher frequency side. Some changes are expected in the dipole moment when nano sized MnO<sub>2</sub> fillers are added, which raise the dielectric constant in the system. Since MnO<sub>2</sub> filler has a high dielectric constant (*Internet reference 01/12/2011*), it contributes to the conduction of lithium ions by providing an inner driving force in addition to the external driving force of the applied electric field. It can therefore be concluded that the composite electrolyte, which contains the inorganic filler, is more sensitive to external electric fields and more efficient for the conduction of lithium ions.

This behaviour would make the dipole moments more changeable and polarized under the electric charge and discharge processes. Therefore, the changeable dipole momentum acts as one type of vibration and can give some activation energy and more chance for ion conduction, which accordingly results in the increase of ionic conductivity.

Fig. 4.17 shows the variation of tangent  $\delta$  with frequency of polymer electrolyte system at room temperatures. The loss spectra characterized by peak appearing at a characteristic frequency suggest the presence of relaxing dipoles in all samples. The tangent  $\delta$  peaks shift towards the higher frequency side on the addition of salts, plasticizer and fillers.

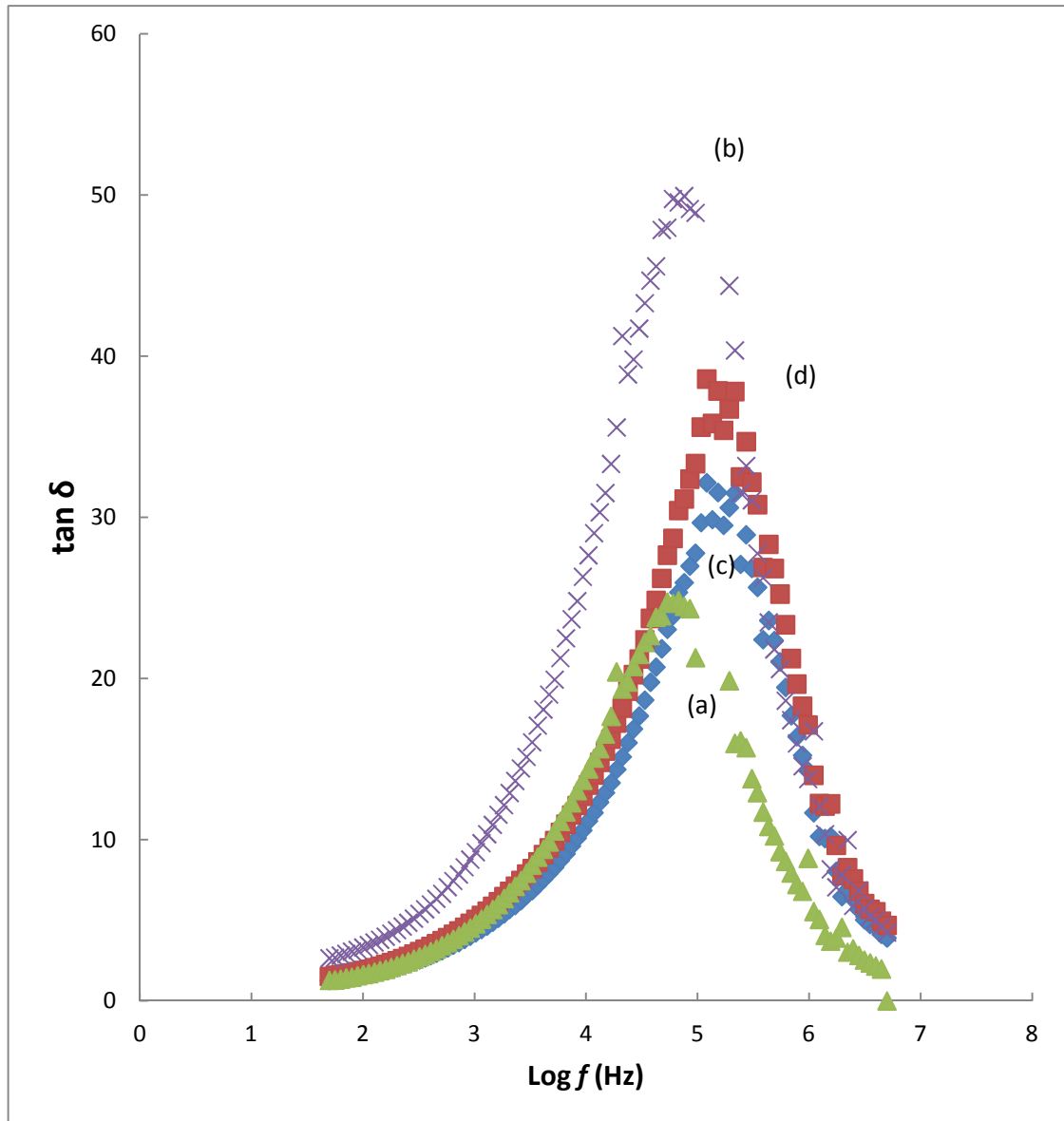


Figure 4.17 Variation of  $\tan \delta$  for (a) PMMA-PEO, (b) PMMA-PEO-LiClO<sub>4</sub>, (c) PMMA-PEO-LiClO<sub>4</sub>-EC and (d) PMMA-PEO-LiClO<sub>4</sub>-EC-MnO<sub>2</sub> at room temperature.

The addition of  $\text{LiClO}_4$  salt into the polymer electrolyte system had a profound effect on the relaxation rate of PMMA-PEO polymer electrolyte system. This relaxation could be attributed to the addition of free moving ions of lithium that coordinated with polymer chain segments (Bergman *et al*, 1995). However, the process of dielectric loss can be assigned to the relaxation phenomena due to glass transition of the amorphous component of the polymer (Havriliak and Negami, 1995). It is observed that the peak frequency is shifting towards the higher frequency side with addition of plasticizer EC.

However, there is an increase in the amorphous content in the materials when  $\text{MnO}_2$  fillers were added into the polymer electrolyte system. These further speed up the segmental motion by increasing the available free volume. It is evidenced by the peak shifting towards higher frequency side, thereby reducing the relaxation time. The relatively fast segmental motion coupled with mobile ions enhances the transport properties on plasticization. The loss peak is shifting towards the higher frequency side on addition of filler.

## 4.4 Thermal Studies

### 4.3.1 Differential Scanning Calorimeter (DSC) analysis

DSC was used to measure the glass transition and crystallization temperature of the polymer electrolyte system within temperature range of -100 to 200 °C at a scanning rate of 5°C per min. The preparation of polymer electrolyte with a low glass transition temperature ( $T_g$ ) is one of the important factors for increasing conductivity. Figures 4.18 – 4.21 show the DSC curves of different polymer electrolyte systems. In Figure 4.18, DSC curves of different ratios of PMMA and PEO on melting and crystallinity behavior of the blend system was shown. Generally, two well-separate peaks were obtained on DSC thermogram as shown due to incompatibility between PMMA and PEO. Only for blend ratio (80:20), a single peak is observed which indicate the miscibility between PMMA and PEO. Apparently, this indicates the formation of an intermolecular interaction between the polymers components. Table 4.3 summarizes the DSC results.

Table 4.3 Thermal properties of PMMA/PEO blends

wt% PEO	wt% PMMA	$T_g$ (°C)	$T_m$ (°C)	$\Delta H_m$ (J/g)	$X_c$ (%)
10	90	-54.84	58.98	54.84	60.01
20	80	-60.00	52.13	53.15	16.18
30	70	-55.54	52.34	232.40	27.48
40	60	-56.54	54.05	386.38	37.33
50	50	-58.84	59.77	424.50	46.11
60	40	-52.65	58.24	376.40	54.42

The degree of crystallinity  $X_c(\%)$  is calculated, according to the equation  $\chi_c = \Delta H_m / 203 \text{ J g}^{-1}$  (where  $\chi_c$  is the relative percentage of crystallinity of the PEO-based blender, and  $203 \text{ J g}^{-1}$  is the  $\Delta H_m$  of 100% crystalline PEO) (Hu *et al*, 2007). It can be seen that the composition of 80wt % PMMA and 20wt% PEO shows the lowest  $T_g$  and  $T_m$  which is around  $-60^\circ\text{C}$  and  $52.13^\circ\text{C}$  respectively. This manifested that the high miscibility level between PMMA and PEO at the composition of 80wt% PMMA and 20wt% PEO. In addition, the decrease of crystallinity,  $\chi_c$  increased the amorphous phase in the polymer blend which collaborate the proof of miscibility again. Figure 4.19 show the DSC thermogram of 80:20 wt% of PMMA/PEO blend at various wt% of  $\text{LiClO}_4$ . From Table 4.4, it can be observed that the melting temperature and crystallinity decreases with salt addition, as usually observed for polymer electrolytes (Armand, 1994). A significant decrease in  $T_g$  with increasing  $\text{LiClO}_4$  concentration is observed. This can be interpreted on the basis of chain flexibility, which is reflected by  $T_g$ . The salt effect is related to a weakening of the dipole–dipole interactions between the PEO-PMMA polymer blend chains due to the presence of salt (Umadevi *et al*, 2002). The low glass transition temperature causes the higher segmental motion of the polymer electrolyte, which enables the easy flow of ions through polymer chains network when there is an applied electric field.

Table 4.4 Thermal properties of PMMA/PEO/ $\text{LiClO}_4$  polymer electrolyte systems

% $\text{LiClO}_4$	$T_g$ ( $^\circ\text{C}$ )	$T_m$ ( $^\circ\text{C}$ )	$\Delta H_m$ (J/g)	$X_c$ (%)
2.5	-60.71	51.98	67.45	28.58
5.0	-61.12	50.93	15.15	27.32
7.5	-67.54	50.34	9.40	24.54
10.0	-70.54	49.05	11.38	12.50
12.5	-	49.77	4.50	22.17

The effect of plasticizer addition on the properties of composite polymer electrolyte is clearly visible in Figure 4.20. It was observed that the plasticized polymer electrolyte systems showed a phase transition in the range of -70 °C to -60 °C, which was attributed to the glass transition temperature ( $T_g$ ) and a melting process located between 60°C and 70°C, related to a crystalline phase. Further, it appears that the glass transition temperature  $T_g$  decreases with increasing EC concentration. Since the glass transition temperature is related to the flexibility in the polymeric segments, the result may be related to a possible enhancement in the flexibility of polymeric chains of the electrolyte systems on addition of plasticizer. It appears that there is a significant reduction in crystallinity of the polymer electrolyte systems on plasticizer addition. This observation is consistent with the line-broadening effect in the XRD pattern with increasing concentration of plasticizer. However, at the concentration above 20 wt% EC, the polymer electrolyte systems are no longer flexible and self-standing, and their  $\text{Li}^+$  conductivities are low and thermally unstable.

Table 4.5 Thermal properties of PMMA/PEO/LiClO<sub>4</sub>/EC polymer electrolyte system

Wt% EC	$T_g$ (°C)	$T_m$ (°C)	$\Delta H_m$ (J/g)	$X_c$ (%)
5	-61.42	61.98	199.81	56.53
10	-63.54	64.13	201.01	47.11
15	-67.71	63.34	16.47	37.96
20	-69.44	69.05	11.40	25.51
25	-64.91	70.00	378.15	62.68

Figure 4.21 shows the effect of MnO<sub>2</sub> nano filler on thermal transitions of PEO-PMMA-LiClO<sub>4</sub>-EC polymer electrolyte system. It is observed that all filler added polymer electrolytes system shows an endothermic peaks temperature around 80 °C attributed to the melting of the crystalline phases of polymer electrolyte. It is observed that with the decreasing of filler concentration, both the T<sub>g</sub> and T<sub>m</sub> decreases. This implies a complete transformation of polymer matrix from semi-crystalline to amorphous phase. The change in morphology is attributed to the filler concentration, which may result from the increased mobility and dissociation effect evidenced by the dielectric constants for increased concentration of charge carriers. This argument supports our observation from the FT-IR studies. When above concentration of 5 wt%, fillers are overloaded and form ions segregation.

Table 4.6 Thermal properties of PMMA/PEO/LiClO<sub>4</sub>/EC/MnO<sub>2</sub> polymer electrolyte system

Wt% MnO <sub>2</sub>	T <sub>g</sub> (°C)	T <sub>m</sub> (°C)	ΔH <sub>m</sub> (J/g)	X <sub>c</sub> (%)
5	-76.42	69.13	16.54	17.99
10	-73.54	74.47	103.65	50.07
15	-70.71	67.34	98.40	57.54
20	-67.44	71.25	216.37	64.53
25	-60.91	73.77	529.01	71.56

Table 4.6 shows the thermal properties of PMMA/PEO/LiClO<sub>4</sub>/EC/MnO<sub>2</sub> polymer electrolyte system .As seen from the table, the degree of crystallinity increases dramatically with increasing of filler content which indicate that the filler is overloaded in the polymer matrix and form ion segregation which conspire with the FTIR and XRD results. The smallest crystallinity,  $\chi_c$  achieved by 80 wt% PMMA- 20 wt% PEO -10 wt%

$\text{LiClO}_4$  – 20 wt% EC - 5wt%  $\text{MnO}_2$  justify the amorphous phase in the polymer electrolyte system which collaborate the proof of miscibility again.

In general, a low glass transition temperature of the polymer electrolyte system is essential to obtain high ionic conductivity at room temperature (Fonseca *et al*, 2002). The  $T_g$  of all the solid polymer electrolytes systems are found to be well below room temperature, which satisfies one of the major prerequisites of a material to behave as a solid polymer electrolyte system at ambient temperatures. The lowest glass transition temperature is achieved when 5wt % of  $\text{MnO}_2$  filler is incorporated into the 80 wt% PMMA -20 wt% PEO -10wt%  $\text{LiClO}_4$  – 20wt% EC polymer electrolyte system which attributed to the disruption of the ordered domains in the polymer matrix.



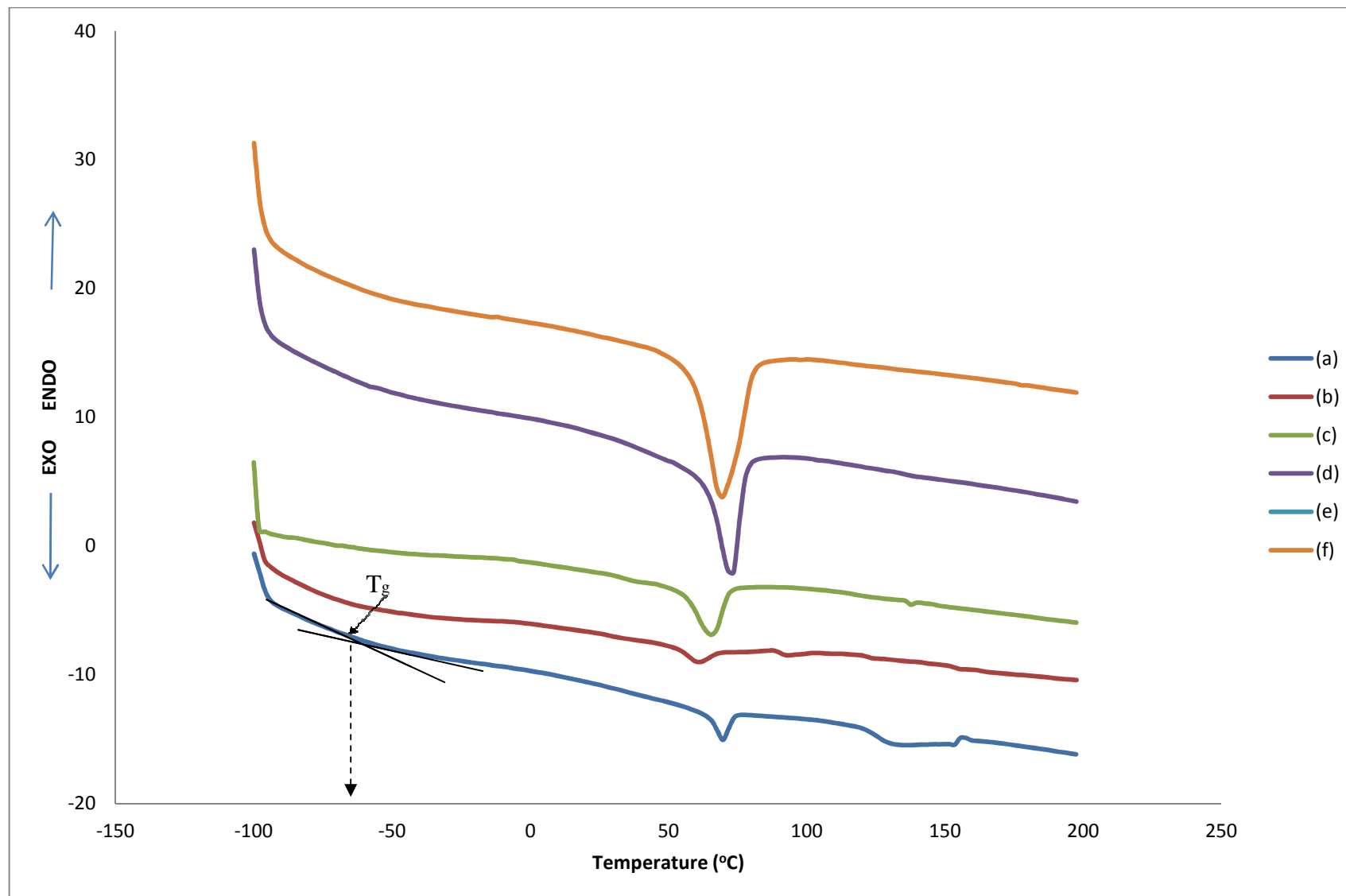


Figure 4.18 DSC thermograms for PMMA/PEO blend at various weight percent: (a) 90:10; (b) 80:20 ; (c) 70:30; (d) 60:40; (e) 50:50; (f) 40:60

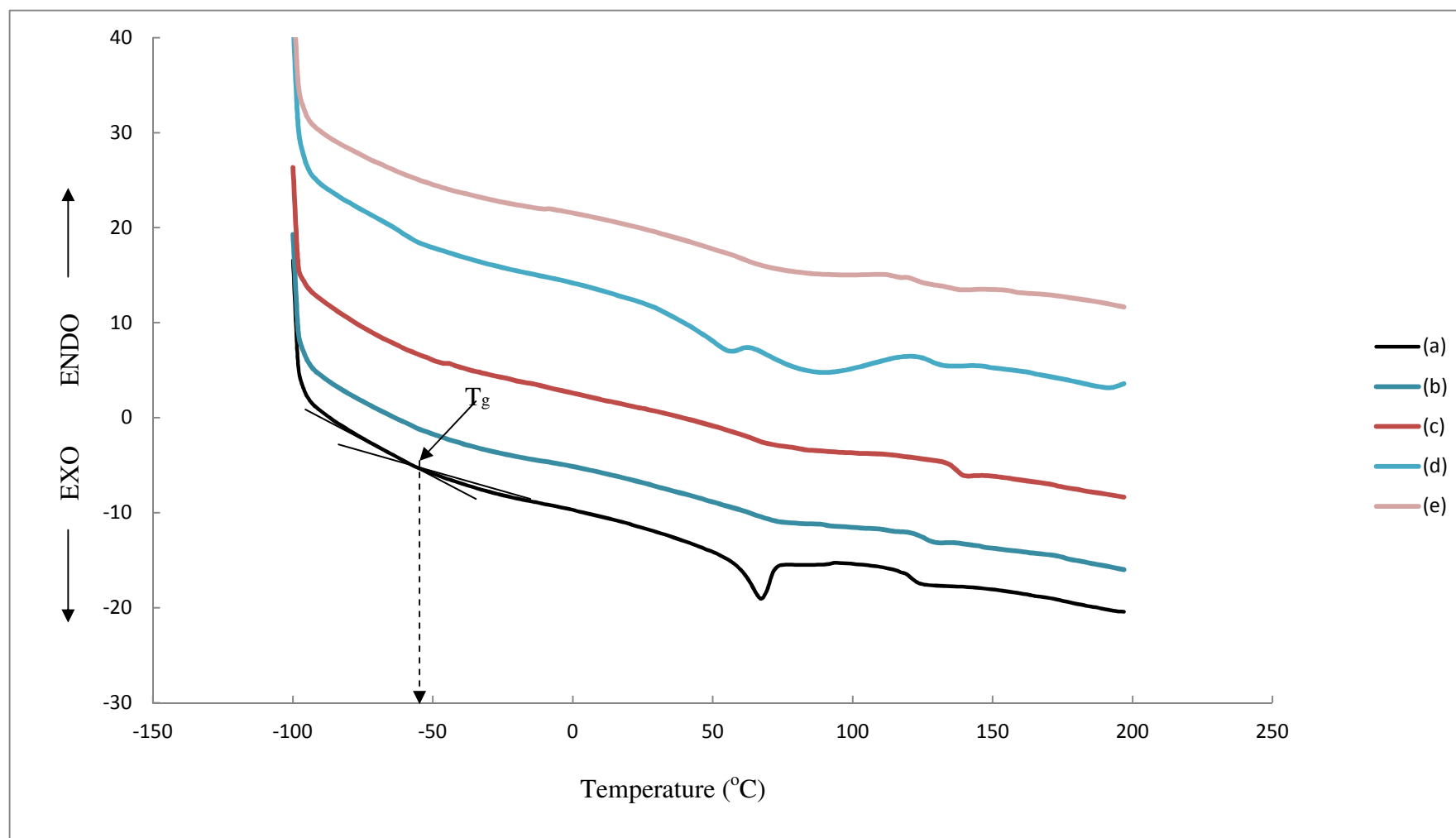


Figure 4.19 DSC thermograms for PMMA/PEO polymer electrolyte system at various weight percent of LiClO<sub>4</sub> : (a) 2.5 wt% ; (b) 5 wt% ; (c) 7.5 wt% ; (d) 10 wt% ; (e) 12.5 wt%

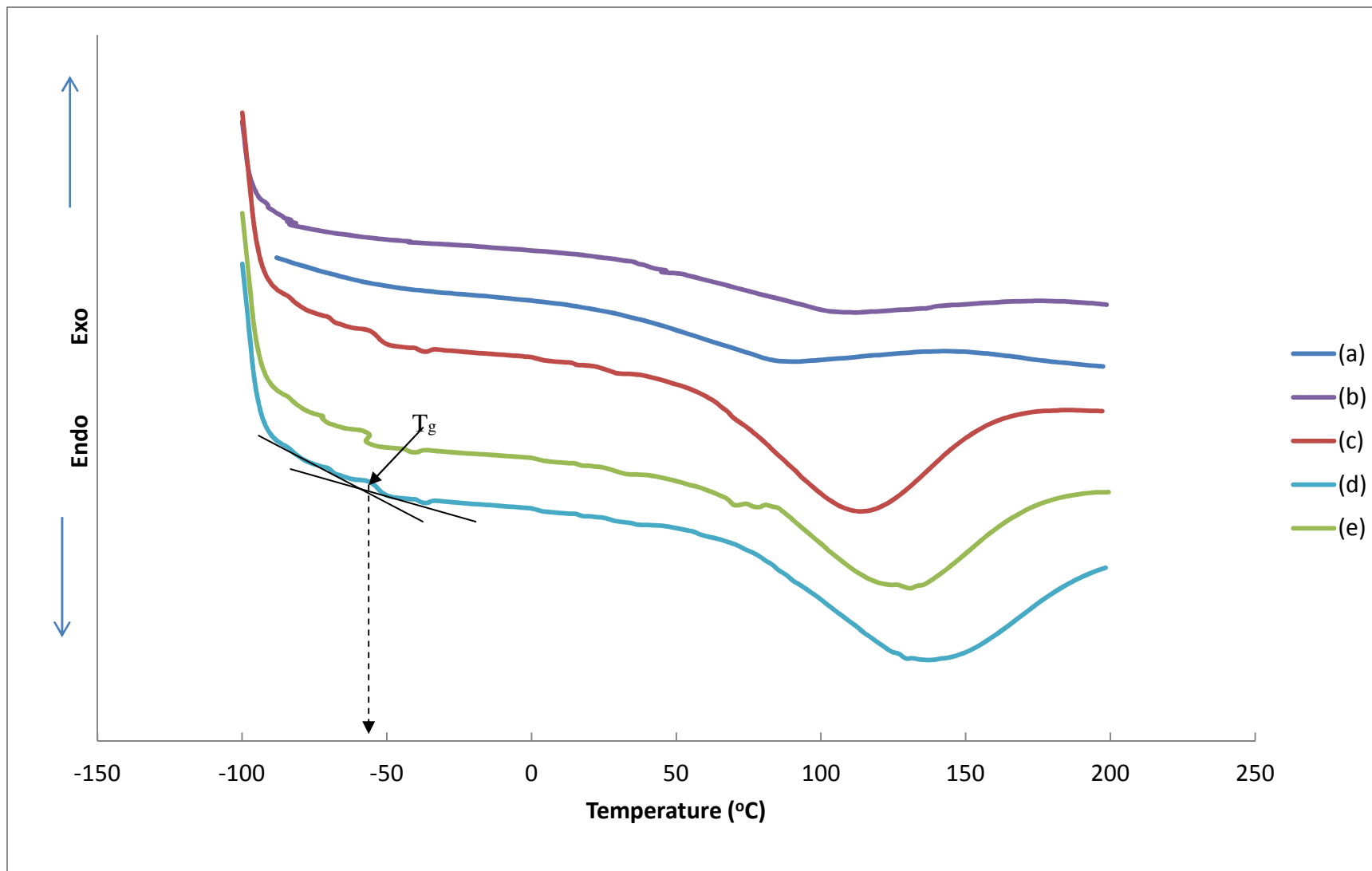


Figure 4.20 DSC thermograms for PMMA/PEO/LiClO<sub>4</sub> polymer electrolyte system at various weight percent of EC : (a) 5 wt% ; (b) 10 wt% ; (c) 15 wt%; (d) 20 wt%; (e) 25 wt%

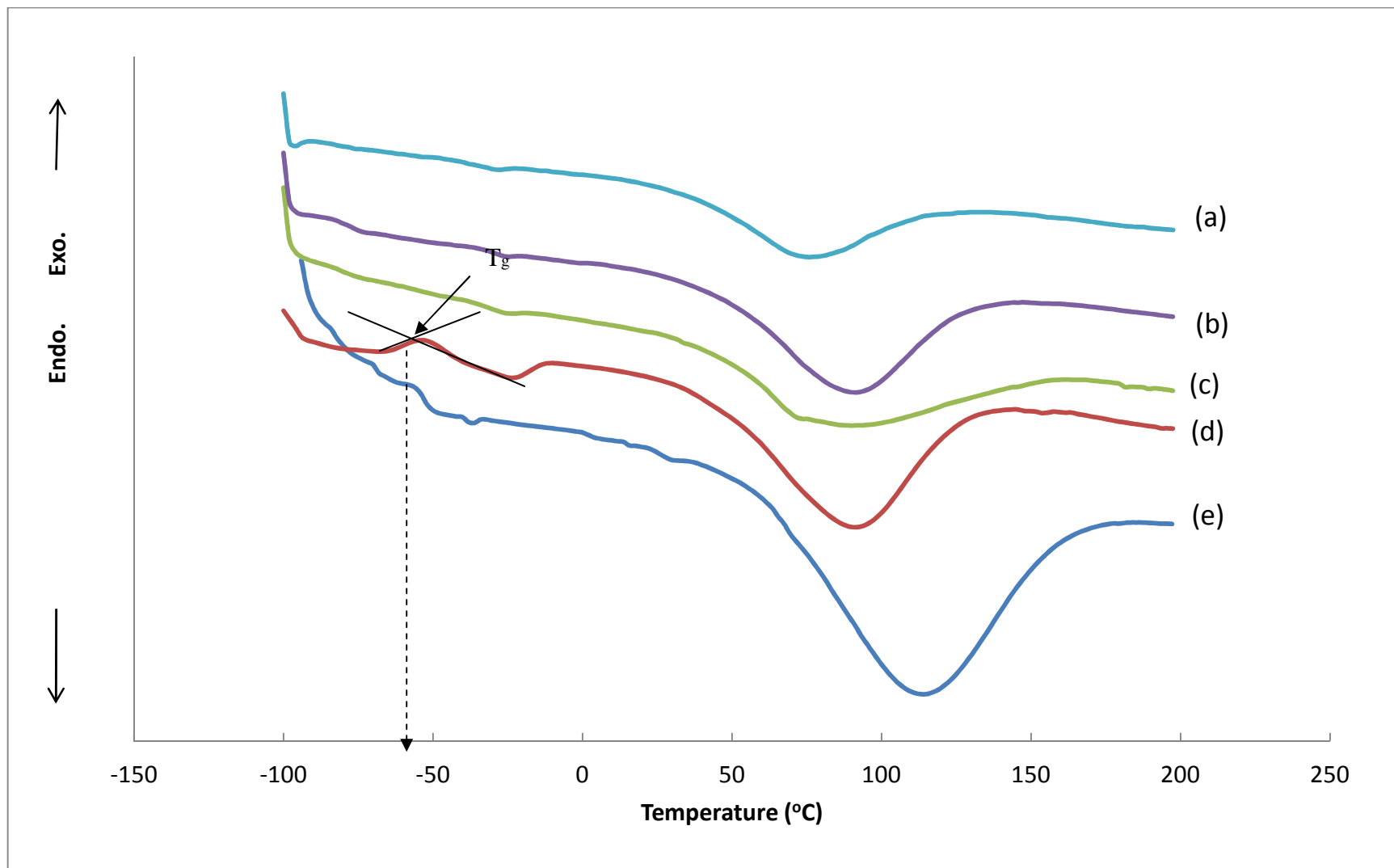


Figure.4.21 DSC thermograms for PMMA/PEO/LiClO<sub>4</sub>/EC polymer electrolyte system at various weight percent of MnO<sub>2</sub> filler: (a) 5 wt% MnO<sub>2</sub> (b) 10 wt% MnO<sub>2</sub> (c) 15 wt% MnO<sub>2</sub> (d) 20 wt% MnO<sub>2</sub> (e) 25 wt% MnO<sub>2</sub>

### 4.3.2 Thermogravimetric (TGA) Analysis

In order to ascertain the thermal stability, the polymer electrolytes systems were subjected to TGA and DTG analysis. Figures 4.22 - 4.25 presented the thermogravimetry (TG) and derivative thermogravimetry (DTG) profiles of polymer electrolytes system at a heating rate of  $10\text{ }^{\circ}\text{C min}^{-1}$ . In Figure 4.22, the polymer blend appears to be quite dry since its weight is almost constant up to  $45\text{ }^{\circ}\text{C}$ . Above  $45\text{ }^{\circ}\text{C}$ , after complete dehydration, no further weight loss is observed until an irreversible decomposition commenced at  $370^{\circ}\text{C}$  and shows a weight loss of 92.13%. It indicates that the polymer blend is stable up to  $45\text{ }^{\circ}\text{C}$ . The loss may be due to decomposition of polymer blend occurred (Stephen *et al*, 2005)

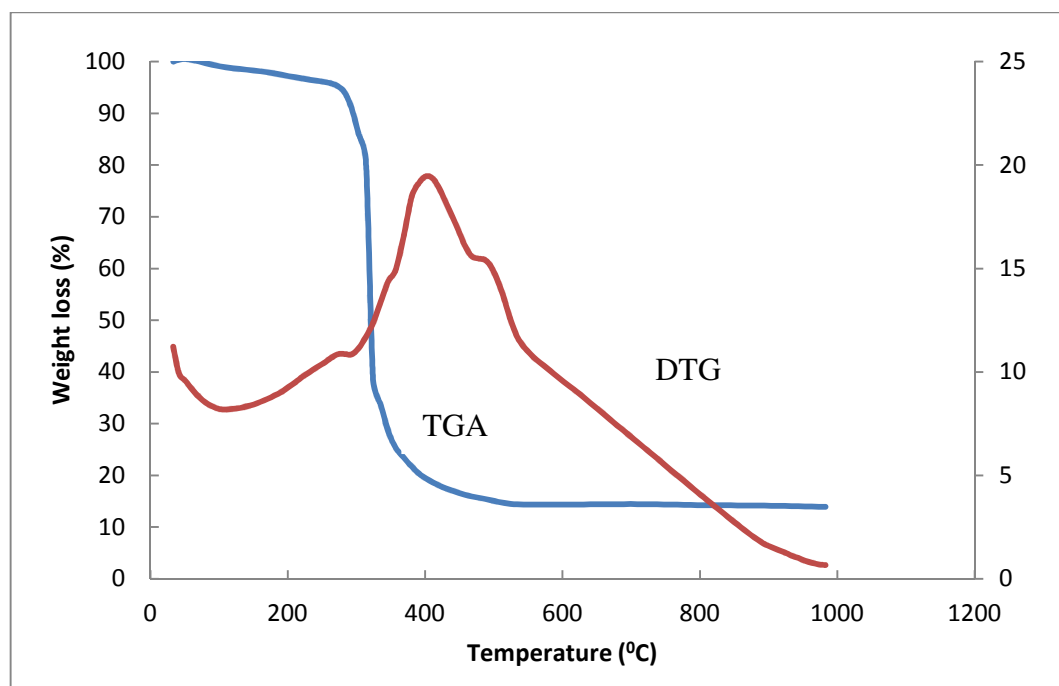


Figure 4.22 TGA-DTG curves for 80:20 wt% of PMMA/PEO blend

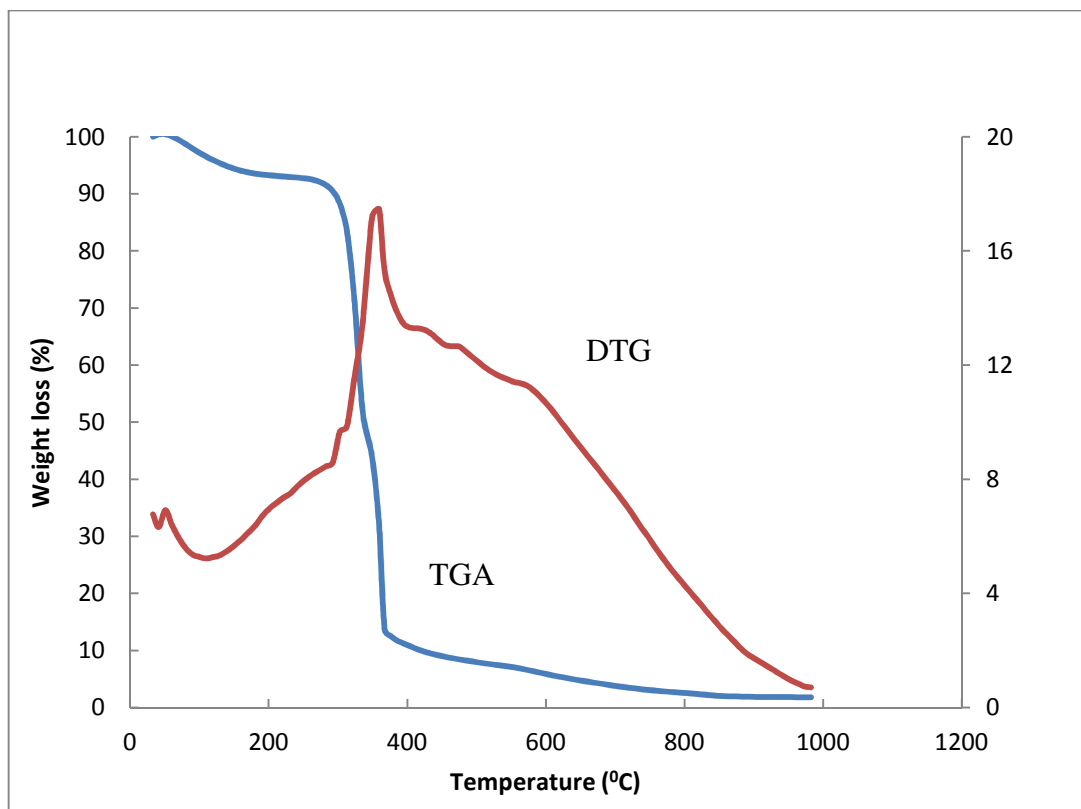


Figure 4.23 TGA-DTG curves for 72PMMA:18PEO:10Li polymer electrolytes

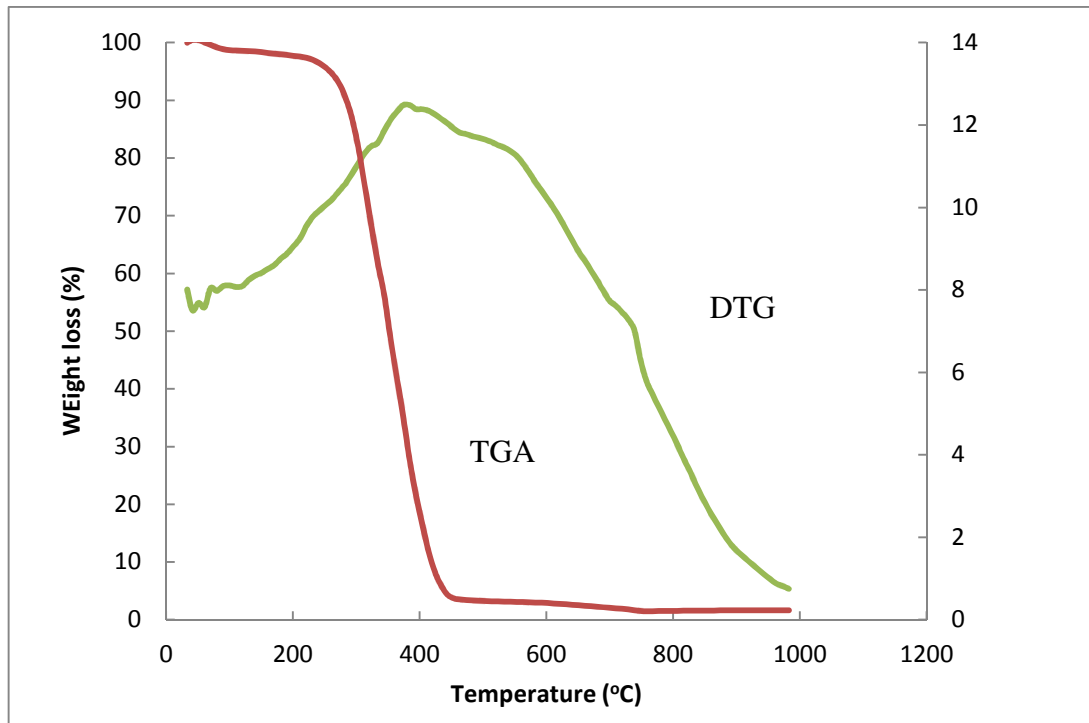


Figure 4.24 TGA-DTG curves for 57.6PMMA:14.4PEO:8Li:20EC polymer electrolytes

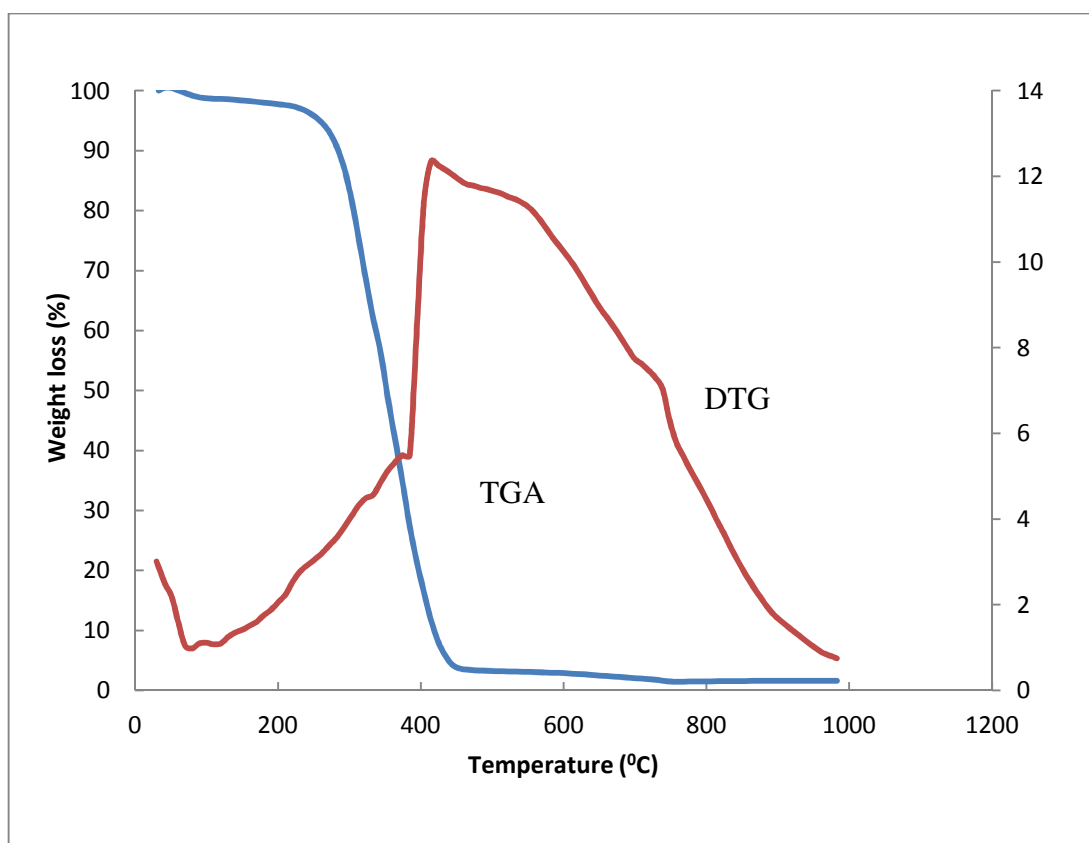


Figure 4.25 TGA-DTG curves for 54.7PMMA:13.4PEO:7.6LiClO<sub>4</sub>:19EC:5MnO<sub>2</sub> polymer electrolytes

Figure 4.23 show the TGA-DTG curve for 72PMMA:18PEO:10Li polymer electrolytes. A weight loss about 4.45% at 85°C is observed due to the removal of moisture in LiClO<sub>4</sub> salt in the electrolyte (Uma *et al*, 2004). The second decomposition occurred at 380 °C which showed weight loss of 85.37%. Obviously, this indicates that 72PMMA:18PEO:10Li polymer electrolyte is stable up to 85°C. Figure 4.24 show the TGA- DTG curves for 57.6PMMA:14.4PEO:8Li:20EC polymer electrolytes. At temperature around 101 °C, a small amount of weight loss is observed. This is considered as the result of loss of solvent and moisture from the electrolytes as mentioned earlier. This first decomposition occurred at temperature 101°C which suffered weight loss from 2.21%. In Figure 4.25, the initial weight loss temperature happened at 110 °C which suffered a weight loss of 0.98%. this shows that thermal stability increase with

the addition of  $\text{MnO}_4$  filler as TGA-DTG curves for 54.7PMMA: 13.4PEO: 7.6 $\text{LiClO}_4$ : 19EC: 5 $\text{MnO}_2$  polymer electrolytes in Figure 4.25 have the first decomposition at higher temperature bearing a lower weight loss. Table 4.7 show the initial and decomposition temperatures and percentage of total weight loss for various solid polymer electrolyte systems

Table 4.7 Initial and decomposition temperatures and percentage of total weight loss for various solid polymer electrolyte systems

Sample	Initial Weight Loss Temperature (°C)	Weight Loss (%)	Decomposition Temperature (°C)	Weight Loss (%)	Total Weight Loss (%)
PMMA-PEO	45	1.28	370	92.13	93.41
PMMA-PEO- $\text{LiClO}_4$	85	4.45	380	85.37	89.82
PMMA-PEO- $\text{LiClO}_4$ - EC	101	2.21	420	96.12	98.33
PMMA-PEO- $\text{LiClO}_4$ - EC- $\text{MnO}_2$	110	0.98	430	89.37	90.35



#### 4.4 Optical Studies

Figure 4.26 shows the optical absorption spectra for the optimum polymer electrolytes within the region of 230-290 nm. It is observed that there is a peak at around 230 nm representing the  $\pi$ - $\pi^*$  electron orbital transition along the backbone of the polymer matrix PMMA-PEO chain (Harold *et al*, 2005). The absorption intensity varies when salts, plasticizer and fillers are added into the polymer electrolyte system. This shows the occurrence of electronic transition between the bonds. The shift in absorption edge towards higher wavelengths indicates the formation of inter/intra bonds between each component in the polymer electrolyte system, which is consistent with the FTIR results. These bonds reflect the variation of energy bandgap which arises due to the variation in crystallinity within the polymer matrix (Yahya, 2000)

Figures 4.27 – 4.28 show the Tauc's plot with variation of  $(\alpha h\nu)^{1/2}$  and  $(\alpha h\nu)^2$  with  $h\nu$ . Optical band gap  $E_g$  can be determined by the extrapolation of best fit line between  $(\alpha h\nu)^{1/2}$  and  $(\alpha h\nu)^2$  intercept the x-axis. The variation of optical band gap with different polymer electrolyte system are summarized in Table 4.8.

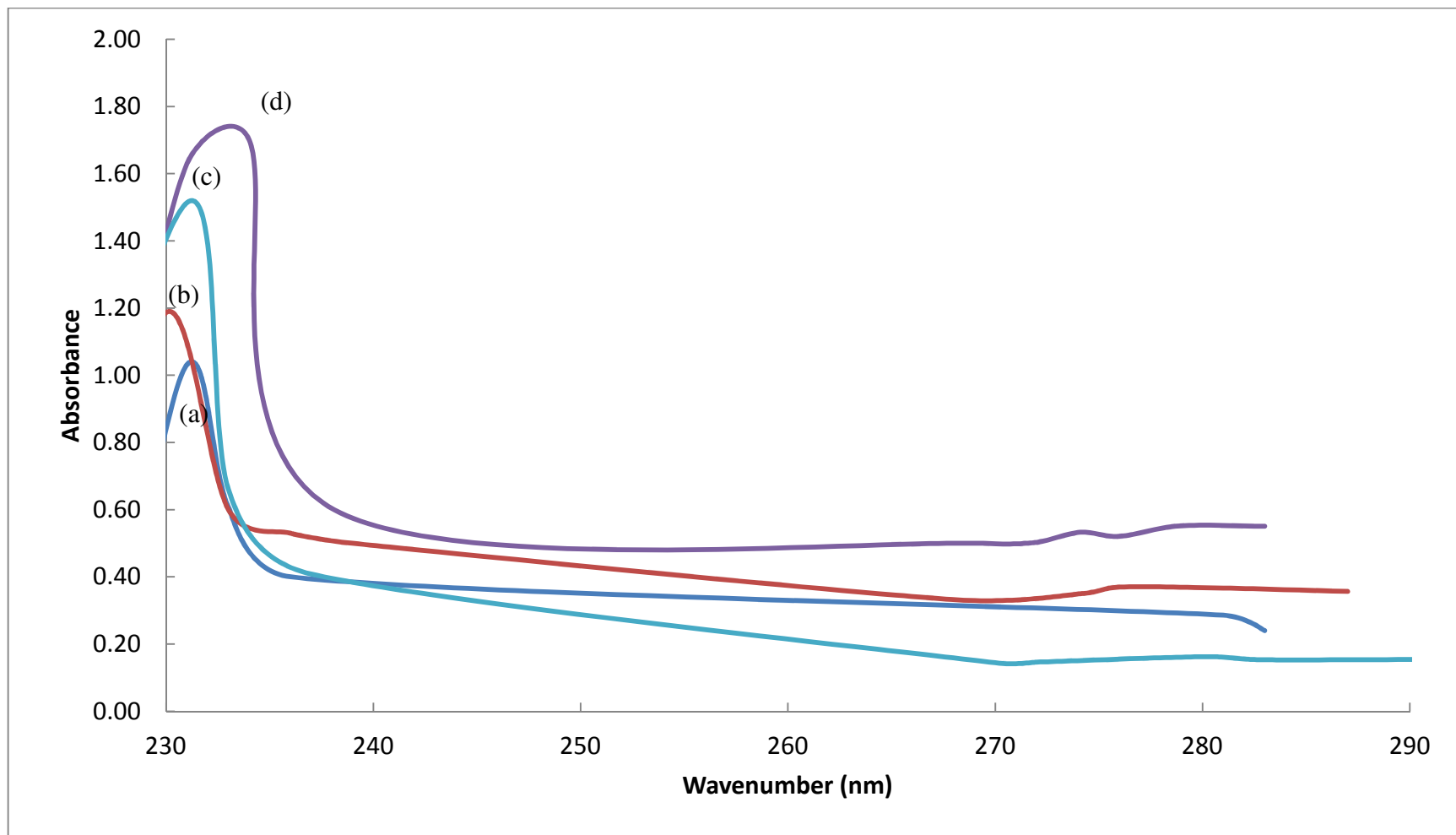


Figure 4.26 Optical absorption spectra for optimum polymer electrolytes: a) PEO- PMMA b) PEO-PMMA-LiClO<sub>4</sub> c) PEO-PMMA-LiClO<sub>4</sub>-EC d) PEO-PMMA-LiClO<sub>4</sub>-EC MnO<sub>2</sub>

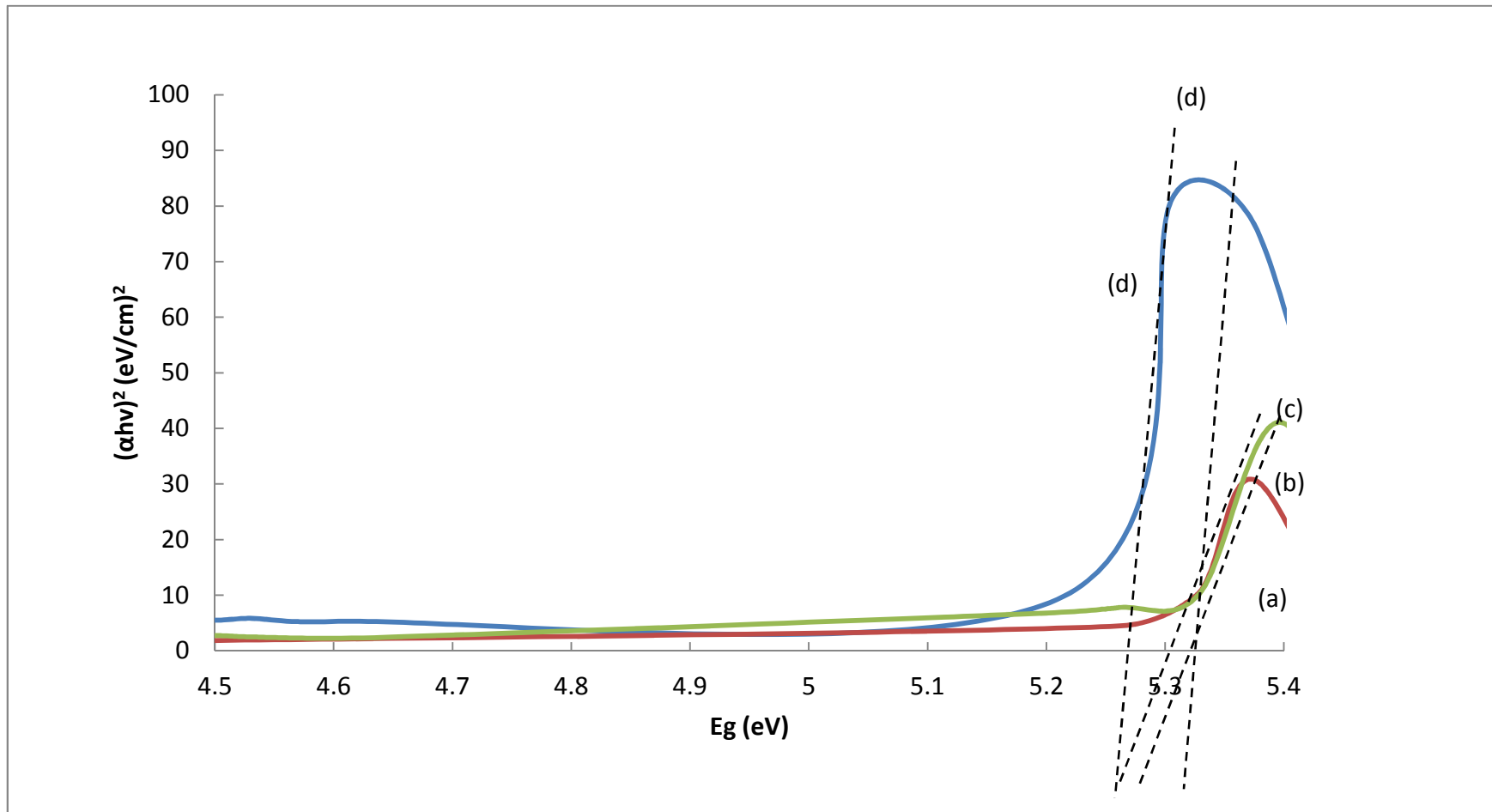


Figure 4.27 Plot of  $(\alpha h\nu)^2$  against  $E_g$  (photon energy) for the optimum polymer electrolytes : a) PEO- PMMA b) PEO-PMMA-LiClO<sub>4</sub> c) PEO-PMMA-LiClO<sub>4</sub>-EC d) PEO-PMMA-LiClO<sub>4</sub>-EC- MnO<sub>2</sub>

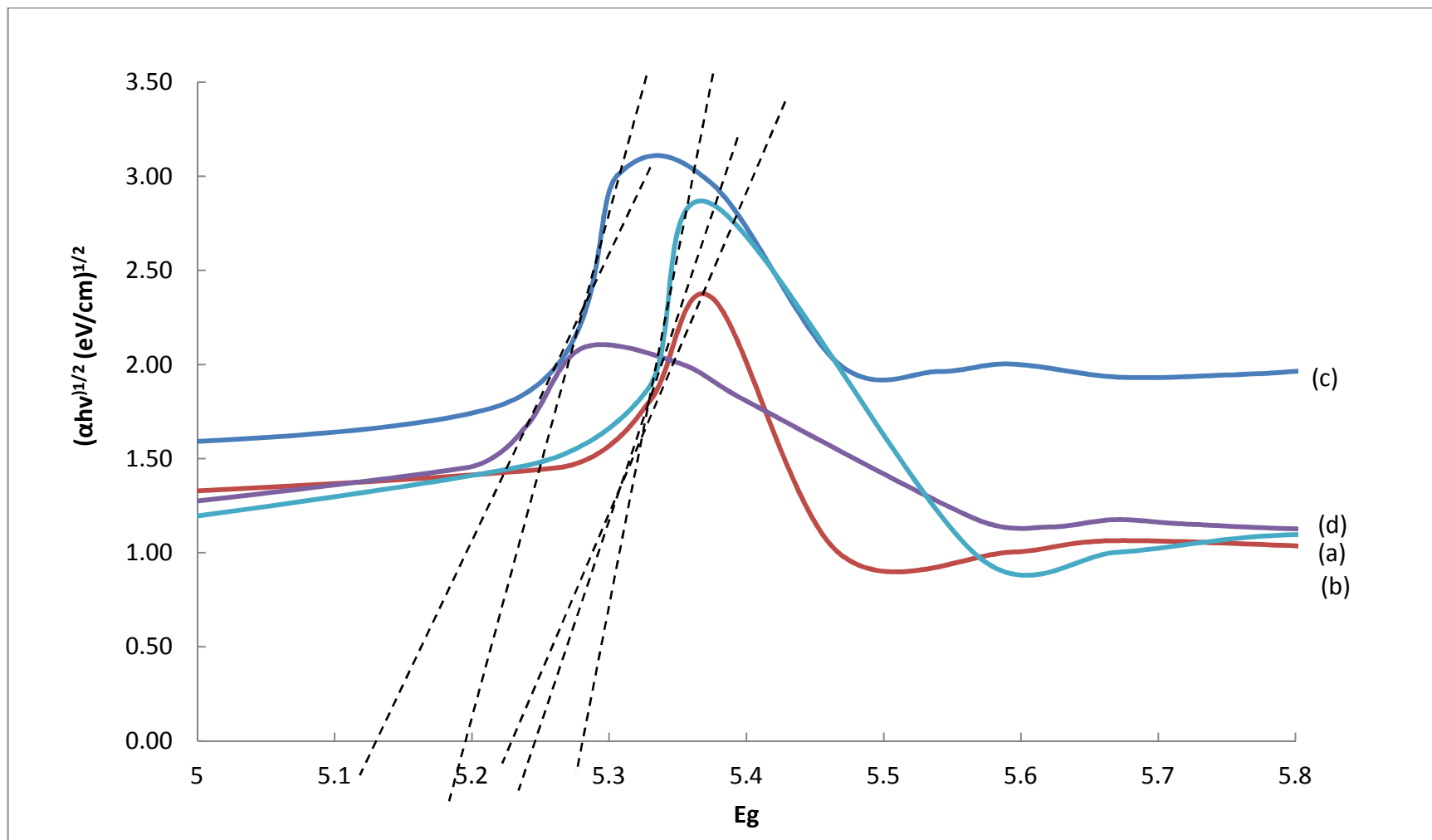


Figure 4.28 Plots of  $(\alpha h\nu)^{1/2}$  against  $E_g$  (photon energy) for the optimum polymer electrolytes: a) PEO- PMMA b) PEO-PMMA-LiClO<sub>4</sub> c) PEO-PMMA-LiClO<sub>4</sub>-EC d) PEO-PMMA-LiClO<sub>4</sub>-EC MnO<sub>2</sub>

Figures 4.27 - 4.28 show that there is a decrease in optical band gap due to the alloying effect, namely a compositional change in the host material (Kitao *et al.*, 1981). This effect is due to the change in bond angles and/or bond lengths. This shows that the addition of fillers will further induce the structural modifications in the matrix and increase the amorphous content in polymer electrolyte system. The complexation between LiClO<sub>4</sub> salts, EC plasticizer and MnO<sub>2</sub> fillers in PMMA –PEO matrix produce localized states in optical band gap which decreases the energy band gap of the polymer electrolyte system. In other words, the decrease in the optical gap results in an increase in the degree of disorder that explained the increase in ionic conductivity of composite polymer electrolyte. These results are in agreement with those obtained from XRD, FTIR and conductivity studies.

Table 4.8 Optical band gap for both direct and indirect of different polymer electrolyte systems

Polymer electrolyte	Band gap (eV)	
	Direct	Indirect
PEO-PMMA	5.305	5.289
PEO-PMMA-LiClO <sub>4</sub>	5.284	5.219
PEO-PMMA-LiClO <sub>4</sub> -EC	5.254	5.216
PEO- PMMA-LiClO <sub>4</sub> -EC MnO <sub>2</sub>	5.213	5.143

## CHAPTER FIVE

### CONCLUSION AND FUTURE RECOMMENDATIONS

In this work, PMMA, PEO, LiClO<sub>4</sub>, EC and MnO<sub>2</sub> were mixed in appropriate amounts to form film by the solution casting technique and subjected to a detailed structural characterization, ionic conductivity studies and optical studies.

#### 5.1 Conclusion

Mechanical milling of MnO<sub>2</sub> powders produces homogenously sized nano-particles with particle size range of 30 nm. High dispersion and narrow size distribution of MnO<sub>2</sub> nano-particles has been successfully prepared. TEM result justify the particles size range.

The ionic conductivity of PMMA-PEO polymer blend was found to be  $2.02 \times 10^{-8} \text{ S cm}^{-1}$ . Upon addition of 12 wt% salt, the ionic conductivity was increased to  $7.38 \times 10^{-4} \text{ S cm}^{-1}$ . Further enhancement in the ionic conductivity of PMMA-PEO- LiClO<sub>4</sub> system has been found on plasticization. The highest room temperature of conductivity achieved for the PMMA-PEO- LiClO<sub>4</sub> system with 25 wt% EC is  $1.82 \times 10^{-3} \text{ Scm}^{-1}$ . The presence of the filler has shown the conductivity enhancement of the polymer electrolyte where the addition of 5 wt% MnO<sub>2</sub> slightly increases the conductivity up to  $5.02 \times 10^{-3} \text{ S cm}^{-1}$  at room temperature.

The increase in conductivity can be attributed to:

- (i) Increase amorphicity of the samples. This is reflected in the values of percentage of crystallinity. Sample with more amorphous structure exhibits higher conductivity.
- (ii) Increase in the number of ions in the PMMA-PEO-LiClO<sub>4</sub> system due to dissociation of salt.
- (iii) Plasticization effect. Plasticizer increases the degree of salt dissociation (or number of ions) and serves as a diffusion pathway for the lithium ions. The plasticizer seems to play a catalytic role in dissociating the salt and increasing the carrier concentration.
- (iv) The ceramic particle acting as nucleation centers for the minute crystallites. The ceramic filler aiding in the formation of disordered phases in the polymer electrolyte. The addition of filler forms a new kinetic path via polymer-ceramic boundaries.
- (v) The temperature-dependent ionic conductivity plots of the electrolyte films seem to obey the Arrhenius relationship at low temperature region and VTF relationship at high temperature region.

The structure and complexation of the polymeric material in the electrolyte system has been ascertained by the XRD, FESEM, and FTIR analysis. The XRD and FTIR studies revealed that the optimum filler concentration provide large amount of amorphous volume due to the complexation of components within the polymer electrolyte system, which produced greater ionic diffusivity. The optical band gaps results further proved that a composition of 80 wt% PMMA, 20 wt% PEO, 10 wt% LiClO<sub>4</sub>, 20 wt% EC- 5 wt% MnO<sub>2</sub> is the best candidate for electrochemical device applications. Thermal studies which include DSC, TGA and DTG were carried out to

determine the thermal stability of the electrolyte system. It was found that the polymer electrolyte system of 580 wt% PMMA, 20 wt% PEO, 10 wt% LiClO<sub>4</sub>, 20 wt% EC- 5 wt% MnO<sub>2</sub> possess T<sub>g</sub> within the range of 50 – 60 °C were obtained.

## 5.2 Suggestion for future work

Work should be continued to enhance the conductivity of the electrolyte to as high as 10<sup>-3</sup> or 10<sup>-2</sup> S cm<sup>-1</sup> since electrolytes synthesized based on nanocomposite polymers show superior properties as compared to conventional polymer electrolytes. This may be achieved by:

- (i) Introducing a second or third plasticizer. Using a combination of suitable plasticizer to help dissociate the ions and low viscosity to increase mobility of system.
- (ii) Future studies should be emphasize on the battery fabrication because the polymer electrolyte systems studied in this research are quite promising and possess the potential of substituting the liquid electrolyte in batteries.
- (iii) Trapping the liquid organic electrolyte solution in an appropriate polymer matrix to form the so called hybrid polymer electrolytes



## References

- Abraham K. M., Alamgir M. *Solid State Ionics*, 311, 70 (1994)
- Ajji, A., *Polymer Engineering & Science*, 35, 64 (1995)
- Ali, A. M. M., Yahya M. Z. A., Bahron H., Subban R. H.Y., Harun, M. K., *Materials Letters*. 61, 2026 (2006)
- Albinsson I., Mellander E. & Stevens J.R.. *Journal of Chemical Physics*, 96, 681 (1992)
- Alias Y., Ling I., Kumatha K., *Ionics*, 11, 472 (2006)
- Allen N. S., Ortega A., Sandoval G., Liao C. M., *Polymer*, 85, 927 (2004)
- Althues H, Henle J, Kaskel S. *Chemical Society*, 36, 145 (2007)
- Armand M. B., Chabagno J. M., Duclot M., *Ionics*, 12, 131 (1979)
- Armand. M. *Solid State Ionics*, **69**, **309** (1994)
- Ashcroft A. T., Cheetham A. K., Harris P. J. F., Jones R.H., Natarajan S., Sankar G., Stedman N. J., Thomas J .M. *Catalysis Letters*, 24, 47 (1994)
- Bergman R., Brodin A., Engberg D., Lu Q., Angell C.A. and Torell L.M. *Electrochimica Acta* **40**, **2049** (1995)
- Bohnke O, Frand G, Resrazi M, Rousselet C. and Truche C., *Solid State Ionics*, 66, 97 (1993)
- Bruce P. G., *Electrochimica Acta*, **40**, 207 (1995)
- Brummer S. B., Koch V. R., *Materials for Advanced Batteries*, 78, 128 (1978)

- Brus L. E. *Journal of Chemical Physics*, 80, 440 (1984)
- Capiglia C., Mustarelli P., Quartarone E., Tomasi C., Magistri A., *Solid State Ionics*, **118**, 73 (1999)
- Caseri W., *Chemical Engineering Communication*, 196, 549 (2009)
- Caseri W. *Macromolecular Rapid Communication*, 21, 70522 (2000)
- Chandra S., Sekhon S. S., Arora N. *Ionics*, 6, 112 (2000)
- Colomban P. J. *Physics and Chemistry of Solids*, 45, 981 (1984)
- Cohen M.H., & Turnbull D., *Journal of Chemical Physics*, 31, 1164 (1959)
- Cosaert K., Eeckhout E., Goethals E., Prez FD, Guegan P, Cheradame H., *Polymer*, 51, 1231 (2002)
- Croce F., Persi L., Scrosati B. *Solid State Ionics*, 69, 320 (2001)
- Davis D.S., Shalliday T.S., *Physical Review Letters* **118**, 1020 (1960)
- Dillip K. Pradha, Samantaray B. K., Choudhary R. N. P., Karan N. K., Reji Thomas, *Ionics* 17, 127 (2011)
- Fenton, D. E. Parker, J. M. & Wright, *Polymer*, 14, 589 (1973).
- Forsyth M., MacFarlane D.R., Best A., Adebahr J., Jacobsson P., Hill A.J., *Solid State Ionics* **147**, 203 (2002)
- KatiharDickerson R.R., Kondragunta S., Stenchikov G., Civerolo K.L., Doddridge B.G., Holben B.N. *Science*, 278, 82730 (1997)

- Elliott W. Report No 1, Contract NAS 3-6015 (1964)
- Ericson H, Svanberg C, Brodin A, Grillone A M, Panero S & Scrosati B *Electrochimica Acta* 45, 1409 (2000)
- Fan L., Dang Z., Nan C.W., *Electrochimica Acta*, **48**, 205 (2002)
- Faubl H., Quinn M.H. *International Contact Lens Clinic*, 27, 6574 (2000)
- Fenton D.E., Parker J.M., Wright P.V., *Polymer*, **14**, 589 (1973)
- Feuillade G., Perche P. *J. Appl. Electrochimica* 5, 63 (1975)
- Fonseca C.P., Cezare T.T., Neves S. *J. Power Sources*, **112**, 395 (2002)
- Fontenella J.J., Wintergill M.C., Calame J.P. , Andeen C.G., *Solid State Ionics*, 8, 333 (1983)
- Gray F.M., *Polymer electrolytes, Advance Material*, Weinheim, Germany (1997)
- Gray F.M. Fundamentals and Technological Applications, *Advance Material*, Weinheim, Germany (1991)
- Harold, G., John, W., Eldridge, M. *The Definitive Processing Guide and Handbook*, New Jersey (2005)
- Hashimi, S.A., Thakur, A.K., Upadhyaya, H.M., *European Polymer Journal*, 34, 1227 (1998)
- Havriliak S. and Negami S. *Polymer*, **8**, 161 (1967)
- Heffels W, Friedrich J, Darribe`re C, Teisen J, Interewicz K, Bastiaansen C, *Polymer*, 2, 14356 (1997)

- H.M.J.C. Pitawala, M.A.K.L. Dissanayake , V.A. Seneviratne. *Solid State Ionics*. 178, 885 (2007)
- Huang X.D., Goh S.H., *Polymer*, **43**, 583 (2000)
- Hui Yang, Xiao-Dong Shen, *Journal of Power Sources*, 67, 515 (2007)
- Hung C.H., Whang W.T. *Journal of Material Science*, 15, 26774 (2005)
- Jayathilaka P.A.R.D., Dissanayake M.A.K.L., Albinsson I., Mellander B.E., *Electrochimica. Acta*, **47**, 3257 (2002)
- Julien C.M. *Solid State Ionics*, 177, 11 (2006)
- Kerr J.B., Han Y.B., Liu G., Reeder C., Xie J., Sun X., *Electrochimica Acta*, **50**, 234 (2004)
- Kim D.W., Kim Y.R., J.K. Park, Moon S.I. *Solid State Ionics*, 106, 329 (1998)
- Kim D.W., Noh K.A., Min H.S., Kang D.W., Sun Y.K., *Solid State*, **5**, 63 (2002)
- Kim H.S., Shin J.H., Moon S.I., Kim S.P., *Electrochimica Acta*, **48**, 1573 (2003)
- Kim K.T., Kim K.B., Kim S.W., Park J.K., *Electrochimica Acta*, **45**, 4001 (2000)
- Kitao M., Akao H., Ishikawa T., Yamada S. *Physica Status Solidi (a)*. 64, 493 (1981).
- Kumar B., Scanlon L.G., Spry R.J. *Journal of Power Sources*, **96**, 337 (2001)
- Lanfredi S., Saia P.S. & Lebullenger R. *Solid State Ion*, 146, 329 (2002)
- Lee, L. H., Park, J. K. & Kim ,*Journal of Polymer Science*, 34, 1427 (1996).
- Leo C.J., Rao G.V.S., Chowdari B.V.R.. *Solid State Ionics*, **148**, 159 (2002)

LEO Preparation and Characterization of Solid Polymer Electrolyte System, Thesis, University of Malaya (2005)

Leo C.J., Subba Rao G.V. & Chowdari B.V.R. *Solid State Ionics*, 148, 159 (2002)

Li Z. H., Zhang H. P., Zhang P., *The Journal of Applied Electrochemistry*, 38, 109 (2004)

Linford R.G., Scrosati B., *Applications of Electroactive Polymers*, London (1993)

MacCallum, J.R., Smith M.J., Vincent C.A. *Solid State Ionics*, 11, 307 (1984)

MacCallum J.R. & Vincent C.A., *Polymer Electrolyte Review* 1, Elsevier, London (1987)

Macdonald J R, *Impedance spectroscopy, Emphasizing Solid Materials and Systems*. Wiley, New York (1987)

Mano V., Felisberti, M.I., Paoli, *Macromolecules*, 30, 3026 (1997)

Martinez-Pardo, Cardoso J., Vazquez H. & Aquilar M., *Nuclear Instrument and Method*, 140, 325 (1998)

Mastragostino, M., Soavi, F., Zanelli, A., *Journal of Power Sources*, 81, 72 (1995)

Masui T, Yamamoto M, Sakata T, Mori H, Adachi G., *Journal of Material Chemistry*, 10, 3537 (2000)

Mathis U., Kaegi R., Mohr M., Zenobi R., *Atmospheric Environment*, 38, 4347 (2004)

Meneghetti, P., Qutubuddin, S., Webber A. *Electrochimica Acta*, 49, 4923 (2004)

- Michael M.S., Jacob M.M.E., Prabakaran S.R.S., Radhakrishna S. *Solid State Ionics*, 98, 167 (1997)
- Mishra S., Perumal G.B., Naik J.B. *Polymer-plastics Technology and Engineering*, 36, 489 (1997)
- Mohamed N.S., Subban R.H.Y., Arof A.K., *Journal of Power Sources*, 56, 153 (1995)
- Mohd Rafie Johan, Oon Hooi Shy, Suriani Ibrahim, Siti Mariah Mohd Yassin, Tay Yin Hui, *Solid State Ionics*, 196, 41 (2011)
- Monroe C., Matsukevich D. N., Maunz P., Moehring D. L., Olmschenk S., *Physical Review Letters*, 100, 150404 (2008)
- Morishita K, Takarada T. *Journal of Materials Science*. 34, 1169 (1999).
- Nan C. E. W., Fan L., Lin Y., and Cai Q., *Physical Review Letters*, 91, 2661041 (2003)
- Osada Y., Kajiwaru K., *Gels handbook*, San Diego (1995)
- Othman, L., Chew, K.W., Osman, Z., *Ionics*, 10, 1007 (2007)
- Osman Z., Arof A.K., *Electrochimica Acta*. 48, 993 (2003)
- Owen J., Booth C., Price C., Editors Comprehensive polymer science, *Pergamon Press*, Oxford, 2, 669 (1989)
- Perpechko, *Low Temperature Properties of Polymers*, MIR Publishers, Moscow (1997)
- Periasamy P., Tatsumi K., Shikano M., Fujieda T., Saito T., Mizuhata M., Kajinami A., Deki S., *Journal of Power Sources*, 88, 269 (2000)

- Puri B.R., Sharma L.R., Panthania M.S. Principles of Physical Chemistry, *Prentice Hall*, 3 (1998)
- Qian X., Gu N., Cheng Z., Yang X., Wang E., and Dong S., *Materials Chemistry and Physics*, 74, 98 , (2002)
- Ramesh S., Arof A. K., *Science Engineering*, 85, 11 (2001)
- Rajendra S., Mahalingam T., Kanna R., *Solid State Ionic*, 130, 143 (2000)
- Rajendran S., Sivakumar M., Subadevi, *Materials Letters*, 58, 641 (2004)
- Ratner M.A., *Polymer Electrolytes Review*, 23, 173 (1987)
- Reddy M.J., Chu P.P., *Journal of Power Sources*, 135, 1 (2004)
- Ressy V.S., Zhu Q.Y., Miang L.Q., *Solid State Electrochemistry*, 11, 542 (2007)
- Rhoo H.J., Kim H.T., Park J.K., Hwang T.S., *Electrochimica Acta*, 42, 1571 (1997)
- Rhoo H.J., Kim H.T., Park J.K., Hwang T.S.. *Electrochimica Acta*, **42**, 1571 (1997)
- Ries G, Heller W, Puchta H, Sandermann H, Seidlitz HK, Hohn B. *Nature*, 406, 98101 (2000)
- Sekhon S. S., Singh H. P. *Solid State Ionics*, 152, 167 (2002)
- Sekhon S. S., Pradeep, Agnihotry S. A. *Solid State Ionics*, 24, 217 (1998)
- Shriver D.F., Bruce P.G. *Solid state electrochemistry*, 21, 95 (1995)
- Sim L.H., Gan S.N., Chan C.H., Yahya R. *Spectrochimica Acta Part A: Molecular and Biomolecular Spectroscopy*, 76, 287 (2010)

- Singh, Nilam Singh & K.P. Singh, *Bulletin of Material Science*, 28, 599 (2005)
- Song J. J., Wang Y. Y. , Wan C. C. , *Journal of Power Sources*, 77, 183 (1999)
- Song L., Chen Y., Evans J.W., *Journal of Electrochemical Society*, **144**, 3797 (1997)
- Sperling L.H., *Introduction to Physical Polymer Science*, Wiley, New York (1993)
- Stephan A.M., Kataoka H., Saito Y., *Macromolecules* **34**, 695 (2001)
- Stephan A.M., Kumar T.P., Karan R.T., Renganathan N.G., Pitchumani S., Muniyandi N., *Journal of Power Sources*, 83, 80(2004)
- Stephan A.M., Renganathan N.G., Gopukumar S., *Chemistry Physics*, 85, 6 (2004)
- Surinder Singh, *Nuclear Instrument and Method*, 244, 252 (2006)
- Tambelli C.C., Bloise A.C., Rosario A.V., Magon C.J., Donoso J.P. *Electrochimica Acta*, **47**, 1677 (2002)
- Tarascon J.M., Gozdz A.S., Schmutz C., Chmutz F., Shokoohi F., Warren P.C., *Solid State Ionics*, 49, **86** (1996)
- Thutupalli G.M., Tomlin S.G., *Applied Physics*, **9**, 1639 (1976)
- Uma T., Mahailngam T., Stimming U., *Material Chemistry Physics*, 85, 131 (2004)
- Umadevi C., Sharma A.K. & Rao V.V.R.N. *Journal of Material Letter*, 56, 167 (2002)
- Watanabe M., Ogata N., *Polymer Electrolyte Review* (1987)
- Wright P.V. & Lee C.C. *Polymer* , 23, 681 (1982)



Wu X. *Novel Polymer Electrolyte for Lithium Rechargeable Battery*, PhD Thesis, NUS (1999)

Xiong M, Gu G, You B, Wu L. *Journal of Applied Polymer Science*, 90, 192331 (2003)

Yahya Al-Ramadin, *Optical Material*, 14, 287 (2000)

Yuwono A.H., Liu B., Xue J., Wang J., Elim H.I., Ji W., *Journal of Materials Chemistry* 14, 297 (2004)

Zhang J, Luo S, Gui L. *Journal of Materials Science*, 32, 146972 (1997)

Zheng J, Siegel R.W., Toney C.G., *Journal of Polymer Science Polymer Physics*, 41, 103350 (2003)

# **Appendix**